A COMBINATORIAL STUDY ON HYDROGEN SEPARATION MEMBRANES

A THESIS SUBMITTED TO
THE GRADUATE SCHOOL OF NATURAL AND APPLIED SCIENCES
OF
MIDDLE EAST TECHNICAL UNIVERSITY

BY

FATİH PİŞKİN

IN PARTIAL FULFILLMENT OF THE REQUIREMENTS
FOR
THE DEGREE OF DOCTOR OF PHILOSOPHY
IN
METALLURGICAL AND MATERIALS ENGINEERING

APRIL 2018

Approval of the thesis:

A COMBINATORIAL STUDY ON HYDROGEN SEPARATION MEMBRANES

submitted by **FATİH PİŞKİN** in partial fulfillment of the requirements for the degree of **Doctor of Philosophy in Metallurgical and Materials Engineering Department, Middle East Technical University** by,

Prof. Dr. Halil KALIPÇILAR
Dean, Graduate School of **Natural and Applied Sciences** ________________

Prof. Dr. C. Hakan GÜR
Head of Department,
Metallurgical and Materials Engineering Dept. ________________

Prof. Dr. Tayfur ÖZTÜRK
Supervisor,
Metallurgical and Materials Engineering Dept., METU
____

Examining Committee Members:

Prof. Dr. M. Kadri AYDINOL
Metallurgical and Materials Engineering Dept., METU ________________

Prof. Dr. Tayfur ÖZTÜRK
Metallurgical and Materials Engineering Dept., METU ________________

Prof. Dr. Ali Arslan KAYA
Metallurgical and Materials Engineering Dept.,
Muğla Sıtkı Koçman University ________________

Prof. Dr. Ender SUVACI
Materials Science and Engineering Dept.,
Anadolu University ________________

Assoc. Prof. Dr. Y. Eren KALAY
Metallurgical and Materials Engineering Dept., METU ________________

Date: 30.04.2018

I hereby declare that all information in this document has been obtained and presented in accordance with academic rules and ethical conduct. I also declare that, as required by these rules and conduct, I have fully cited and referenced all material and results that are not original to this work.

Name, Last name: Fatih, Pişkin

Signature :

ABSTRACT

A COMBINATORIAL STUDY ON HYDROGEN SEPARATION MEMBRANES

Pişkin, Fatih
Ph.D., Department of Metallurgical and Materials Engineering
Supervisor : Prof. Dr. Tayfur Öztürk

April 2018, 128 pages

Metallic membranes among the hydrogen separation membranes are quite attractive due to their very high hydrogen selectivity and hydrogen permeability. The efforts in metallic membranes generally concentrate on to identify membrane compositions which have a high hydrogen permeability with a reduced cost. Among the metallic membranes, Pd and Pd alloys, i.e. f.c.c. membranes are quite common as separation membranes. However, the high cost of Pd limits its widespread use in industrial applications. The efforts to address such problems have concentrated on two main approaches. One is reducing the Pd content of the membranes by alloying and producing membranes in the form of thin films. Another approach is to develop new alternative membrane compositions which are Pd-free.

Of the Pd-free membranes, Nb, V, Ta and their alloys, i.e. b.c.c. membranes are particularly attractive due to their orders of magnitude higher hydrogen permeability as compared to Pd-based membranes. However, the b.c.c. membranes have an insufficient catalytic activity to dissociate hydrogen molecules into its atomic form, which is essential for hydrogen separation. The excessive hydrogen solubility resulting in embrittlement is another drawback for b.c.c. membranes. For this reason, the efforts on b.c.c. membranes have focused on identifying the alloying elements that would reduce the level of hydrogen solubility while maintaining a reasonable hydrogen permeability.

However, developing alternative alloy compositions by alloying or finding completely new membrane compositions via traditional methods such as synthesizing one membrane composition at a time and testing it for the purpose are not always successful. These also require extended coordinated efforts that are time-consuming as well. Therefore, a combinatorial method that would allow the production of multiple material compositions in a single experiment and which may then be evaluated by an effective screening technique is a highly useful approach to develop new membrane compositions.

The present work is an outcome of an effort to develop low-cost hydrogen separation membranes on the basis of combinatorial materials science. For this purpose, a total of three ternary systems, i.e. Nb-Pd-Ti, Pd-Ag-Ti, and Pd-Ag-Ni were investigated by a combinatorial method. Nb-Pd-Ti was selected aiming to produce dominantly b.c.c. membranes, while the Pd-Ag-Ti and the Pd-Ag-Ni ternary alloys were chosen to yield f.c.c. membranes. A total of 21 thin films, each with a different composition, covering a large compositional field in the ternary diagram were deposited in a single experiment via magnetron sputtering. The thin films were then screened by a four-probe resistivity measurement in terms of a reactivity index. The compositions identified as candidates as a hydrogen separation membrane were fabricated in the form of foils and then tested for the hydrogen permeability.

The present work demonstrates that the adopted approach is a quite effective way of finding the suitable compositions for low-cost hydrogen separation membranes.

Keywords: Hydrogen separation membrane; combinatorial approach; resistivity-based screening; Pd-based membranes; Nb-based membranes.

ÖZ

ÇOĞULCU YAKLAŞIMLA HİDROJEN AYIRICI MEMBRANLARIN GELİŞTİRİLMESİ

Pişkin, Fatih
Doktora, Metalurji ve Malzeme Mühendisliği Bölümü
Tez Yöneticisi: Prof. Dr. Tayfur Öztürk

Nisan 2018, 128 sayfa

Hidrojen ayırma membranları arasından metalik membranlar sahip oldukları çok yüksek hidrojen seçicilikleri ve hidrojen geçirgenlikleri nedeniyle oldukça ilgi çekicidirler. Metalik membranlar üzerindeki çalışmalar, genellikle bu membranlar için mümkün olduğunca düşük maliyetli ve yüksek geçirgenliğe sahip bileşimlerin belirlenmesi üzerine yoğunlaşmaktadır. Metalik membranlar arasından, Pd ve Pd alaşımları, yani f.c.c. membranlar, bir ayırma membranı olarak oldukça yaygın olarak kullanılmaktadır. Fakat Pd'nin yüksek maliyeti, endüstriyel uygulamalardaki geniş kullanımını sınırlandırmaktadır. Bu tarz sorunların aşılmasına yönelik çabalar iki yaklaşımda odaklanmıştır. Bunlardan biri membranların Pd içeriğini, alaşımlama veya ince film membran üretimiyle azaltmaya yöneliktir. Diğer bir yaklaşım da Pd içermeyen alternatif yeni membranların geliştirilmesidir.

Pd-içermeyen membranlar arasından Nb, V, Ta ve bunların alaşımları, yani b.c.c. membranlar, Pd esaslı membranlarla karşılaştırıldığında daha yüksek hidrojen geçirgenliğine sahip oldukları için ilgi çekicidirler. Bununla birlikte, b.c.c. membranlar hidrojen geçirgenliği için kritik olan hidrojen moleküllerini ayrıştırılması noktasında yetersiz bir katalitik özelliğe sahiptirler. Bir diğer önemli problem de, kırılganlıkla sonuçlanan aşırı hidrojen çözünürlüğüne sahip olmalarıdır.

Bu nedenle, b.c.c. membranlar özelindeki çalışmalar, makul bir hidrojen geçirgenliğini muhafaza ederken, yüksek hidrojen çözünürlüğünün seviyesini düşürecek alaşım elementlerinin belirlenmesi üzerine yoğunlaşmıştır.

Fakat alaşımlama ile alternatif kompozisyonların geliştirilmesi veya tamamen yeni membran kompozisyonlarının bulunması, tek seferde bir kompozisyonun üretilmesi ve amaç için test edilmesi gibi geleneksel yöntemlerle her zaman başarılı olmamaktadır. Ayrıca, bu tarz yaklaşımlar zaman alıcı kapsamlı çalışmalar gerektirmektedir. Bu nedenle, tek bir deneyde çoklu malzeme kompozisyonlarının üretilmesine ve daha sonra etkin bir tarama tekniği ile bu kompozisyonların değerlendirilmesine imkan sağlayacak çoğulcu bir yaklaşım, yeni membran bileşimleri geliştirmek için son derece yararlı bir yöntem olarak öne çıkmaktadır.

Mevcut çalışma, benimsenen çoğulcu bir yaklaşım temelinde düşük maliyetli hidrojen ayırma membranlarının geliştirilmesine yönelik yürütülen bir çalışmayı kapsamaktadır. Bu kapsamda Nb-Pd-Ti, Pd-Ag-Ti ve Pd-Ag-Ni üçlü alaşım sistemleri kombinatoryal bir yöntem ile üretilmiştir. Nb-Pd-Ti alaşımı ağırlıklı olarak b.c.c., Pd-Ag-Ti ve Pd-Ag-Ni üçlü alaşımları da çoğunlukla f.c.c. membranlar üretebilmek için tercih edilmiştir. Seçilen her bir sistem için üçlü diyagramda geniş bir kompozisyon alanını kapsayan, her biri farklı kompozisyona sahip toplam 21 membran manyetik sıçratma yöntemiyle tek bir deneyde üretilmiştir. Membranlar daha sonra dört uçlu direnç yöntemi ile reaktivite indeksleri açısından taranmıştır. Hidrojen ayırma membranı için aday olarak saptanan bileşimlerden uygun olan alaşımlar folyo halinde üretilmiş ve takiben hidrojen geçirgenliği açısından test edilmiştir.

Mevcut çalışma, benimsenen yaklaşımın, düşük maliyetli hidrojen ayırma membranları için uygun bileşimlerin belirlenmesinde oldukça etkili bir yöntem olduğunu göstermektedir.

Anahtar Kelimeler: Hidrojen ayırma membranı; çoğulcu yaklaşım; direnç esaslı tarama; Pd esaslı membranlar; Nb esaslı membranlar.

To
Berke Pişkin
and my family

ACKNOWLEDGEMENTS

I would like to express my gratitude to my supervisor, Prof. Dr. Tayfur Öztürk for his guidance, advice, support, encouragement and valuable suggestions throughout the course of the studies. It has always been a privilege to work with such a special person.

Thanks are to all my friends at the Department of Metallurgical and Materials Engineering, METU for their support in the completion of the thesis. Thanks are also to Serkan Yılmaz for his patience and support during the electron microscopy studies.

I would especially like to thank my family for all the love, trust, support, worries and encouragement they have shown throughout my life.

My special thanks to Berke Pişkin, for her endless love, encouragement, patience, advice, and support during my thesis studies.

Finally, I would also like to thank Prof. Bilge Yıldız for giving an opportunity to work in her research group, Laboratory for Electrochemical Interfaces at the Massachusetts Institute of Technology (MIT) and also her guidance and support during the research.

This study was supported by TUBITAK (The Scientific and Technological Research Council of Turkey) with a scholarship under 2211-C Domestic Doctoral Scholarship Programme Intended for Priority Areas, Grant No: 1649B031501200 and 2214-A International Doctoral Research Fellowship Programme, Grant No; 1059B141501191.

TABLE OF CONTENTS

CHAPTERS

APPENDICES

LIST OF TABLES

TABLES

LIST OF FIGURES

FIGURES

CHAPTER 1

INTRODUCTION

Hydrogen can be produced from a variety of resources such as fossil fuels, biomass, and water. However, a very large share of the current hydrogen production is only based on the fossil fuels. Two major hydrogen production methods rely on the fossil fuels are coal gasification and steam reforming of hydrocarbons. Currently, the dominant technology for hydrogen production is the steam reforming of hydrocarbons, e.g. natural gas or methane, with a share of 90%. However, any of the hydrogen production method involved yields hydrogen in a gas mixture with a variety of other species such as CO, CO_2, and H_2S instead of pure H_2. Therefore, there is a need to separate the hydrogen from these gas mixtures in order to obtain it in a pure form. This is especially critical for the applications that require high purity hydrogen such as proton exchange membrane fuel cells.

Hydrogen separation membranes allow extraction of hydrogen from the mixed gases. This mixture could be a syngas generated from the reformation of hydrocarbons or coal gasification or biomass gasification. Currently, gas-grid is based on pure methane but there are signs that hydrogen, as well as other combustible gases, might be injected into this system. Thus the sources from which hydrogen could be separated might include gas-network as well. Hydrogen separated in this way could be used in fuel cells to generate electricity. All these require the use of efficient separation membranes with a low cost.

Among the hydrogen separation membranes, metallic membranes are quite attractive due to their very high hydrogen selectivity (theoretically infinite), and high hydrogen permeability. Efforts in metallic membranes have concentrated on to identify compositions with as high permeability as possible with reduced cost. Of the metallic membranes, Pd and Pd alloys, i.e. f.c.c. membranes are quite common as a separation membrane and they are commercially available. However, the hydrogen embrittlement and the high cost of Pd restricts their wide range use in industrial applications. The efforts to address these problems are concentrated on two approaches. One is reducing the Pd content of the membranes by alloying, which would also improve the embrittlement resistance. This can also be achieved by producing the membranes in the form of thin film. Second is to find new alternatives which are free of Pd.

Hydrogen embrittlement of Pd membranes is a result of α-β phase transformation which results in pronounced volume change in the lattice. This simply leads the formation of microcracks resulting in the membrane failure. This structural transformation can be avoided with alloying. One of the well-known alloy systems is Pd-Ag. The addition of 20-30 at.% Ag is quite effective in avoiding this phase transition. Alloying with Ag also improves the hydrogen permeability by a factor of 1.7-2.0 compared to pure Pd. Alloying with Ag also help reduce the cost of the membrane and there are Pd-Ag commercial alloys, e.g. Pd77Ag23. Similar results could also be obtained with different alloying elements such as Cu, Y, Au, and Ni.

Nb, V, Ta and their alloys, i.e. b.c.c. membranes are particularly attractive due to their orders of magnitude faster hydrogen permeability compared to Pd-based membranes. However, b.c.c. membranes have an insufficient catalytic activity to split hydrogen molecules into atomic form in order to initiate hydrogen permeation. Thus, b.c.c. based membranes require a secondary catalytic layer, e.g. Pd, to address this problem. The major drawback of b.c.c. membranes is the excessive hydrogen solubility which results in embrittlement. To produce mechanically durable membranes, the studies have concentrated on identifying alloying elements that would reduce the level of hydrogen solubility in b.c.c. membranes, while maintaining the reasonable hydrogen permeability.

Another alternative approach in membranes is to aim for amorphous alloys. They usually have an open crystal structure that provides higher hydrogen solubility. Due to this open structure, hydrogen permeation occurs with a lower risk of embrittlement. These alloys are usually composed of multi-component elements and Ni-Nb-Zr is the most common alloy system for such membranes. However, the metastable nature of amorphous alloys and their tendency to crystallization, causing lower permeability, still are the main concerns. Additionally, the membrane surface is not as active as the f.c.c. membranes, so they also require a secondary catalytic layer, as in b.c.c. membranes.

Different membrane types summarized above all concentrate on identifying compositions having a reasonable hydrogen permeability, especially with a reduced cost. There are mainly two approaches so as to produce membranes with a low cost. The first one is the alloying of the precious metals with less expensive counterparts as explained above. The second one is the fabrication of the membranes in the form of thin film, which reduces the use of elements. Thus, thin film production methods have been taking growing attention in recent years.

However, finding an alternative composition by alloying or developing a new membrane composition is not always successful via traditional production methods such as synthesizing one membrane composition at a time and testing it for the purpose. This also requires extended coordinated efforts that are time-consuming as well. Therefore, a combinatorial method that would allow the synthesis of multiple material compositions in a single experiment and which may then be evaluated by a screening technique is a highly useful approach to develop new membrane compositions.

The current work is an outcome of an effort to develop low-cost hydrogen separation membranes on the basis of combinatorial materials science. The method described was applied to Nb-Pd-Ti, Pd-Ag-Ti, and Pd-Ag-Ni ternary alloys. Nb-Pd-Ti alloy was chosen aiming to yield dominantly b.c.c. membranes, while the Pd-Ag-Ti and the Pd-Ag-Ni ternary alloys were chosen to yield f.c.c. membranes. A magnetron sputtering unit was used to create a thin film material library for each ternary alloy. A total of 21 membranes, each with a different composition, covering a wide compositional field in the ternary diagram were deposited in a single experiment. The membranes were then screened by a four probe resistivity measurement in terms of a reactivity index, defined as the ratio of resistivity under hydrogen to that under argon in the same conditions. The compositions were also screened due to their lattice volume as well, as a requirement for b.c.c. membranes. The compositions determined as a candidate for hydrogen separation membrane were fabricated in the form of a foil. The foils were then tested for the hydrogen permeability so as to identify the alloys best suited as a separation membrane.

The thesis comprises eight chapters and starts with a general introduction. The brief description of the production and the purification of hydrogen is given in Chapter 2. The dense metallic membranes are emphasized in Chapter 3 as a main scope of the thesis. The detailed explanation for the adopted combinatorial approach is given in Chapter 4. The production and the characterization of selected ternary alloys Nb-Pd-Ti, Pd-Ag-Ti, and Pd-Ag-Ni are discussed in Chapter 5, Chapter 6, and Chapter 7, respectively. The dissertation is finalized in Chapter 8, where the general conclusions and recommendations are given.

CHAPTER 2

HYDROGEN PRODUCTION AND PURIFICATION

2.1 Hydrogen Production Methods

Currently, fossil fuels have the highest share in the hydrogen production with a value of more than 90%. The major production routes based on fossil fuels are coal gasification and steam reformation of hydrocarbons such as natural gas and methane. More than 90% of the hydrogen in the United States is produced by steam reforming of natural gas, while it is globally between 45-50% [1]. The global share of the oil and the coal in the hydrogen production is 30% and 18%, respectively [2]. Although there are other routes to produce hydrogen, such as electrolysis of water and biomass gasification, they have a very limited share in the total hydrogen production [3]. Thus, hydrocarbons can be considered as a main feedstock for the present and the near future production of hydrogen.

2.1.1 Steam reforming of natural gas

Steam reforming of natural gas is the most widely used and the least expensive process for the industrial production of hydrogen. The technology is well developed and commercially available at a rate ranging from 1 t/h to 100 t/h H_2 [2]. The principal component of natural gas is methane (CH_4). However, the composition varies depending on the region with CH_4 content varies in the range 44% to 92% [4]. In the process of reformation, CH_4 reacts with steam to yield a syngas, i.e. a mixture of CO and H_2. The reaction composed of two steps; reforming of natural gas and water-gas shift reaction. The reaction in the first step can be written as;

$$CH_4\,(g) + H_2O\,(g) \rightarrow CO\,(g) + 3\,H_2\,(g) \qquad \Delta H^{\circ}_{298} = +205.9\ \text{kJ/mol}$$

Equation. 2.1

This reaction takes place in the range of 500-900 °C. Although the stoichiometry in Equation 2.1 shows that 1 mol of H_2O is enough to react with 1 mol of CH_4, generally the ratio of H_2O to carbon is higher than 1, typically between 2.5-3.0. This is for the purpose of preventing carbon deposition on the catalyst surface. The outgas typically consists of 53% H_2, 19% H_2O, 13% CH_4, 9% CO_2, and 6% CO [5].

As seen above, the syngas generated by steam reforming of natural gas yields a mixture which is poor in its hydrogen content. Therefore, a second stage, the so-called water-gas shift reaction, is introduced into the process so as to increase the hydrogen content;

$$CO\,(g) + H_2O\,(g) \rightarrow CO_2\,(g) + H_2\,(g) \qquad \Delta H^{\circ}_{298} = -41.0\ \text{kj/mol}$$

Equation. 2.2

Equilibrium considerations are such that this reaction favors the products at low temperatures. However, the high temperature is generally preferred to provide a practical reaction rate. This problem is addressed through the use of two-stage gas shift reactor. In the first stage, the reaction occurs between 340-450 °C with faster kinetics [6] followed by the second stage with a temperature range between 190-210 °C to increase the equilibrium H_2 concentration [7]. The gas produced as a result has typically 74% H_2 with some CH_4, and CO_2 as well as CO which is typically ~0.1%. Additionally, a low amount of H_2S is generally present in the resulting gas despite the integration of several sulfur removal steps during the processing.

The temperatures used in two-stage gas shift reactions are quite important since it sets the working temperatures for the purification processes. These are 340-450 °C for the first stage water-gas shift reactions and 190-210 °C for the second stage water-gas shift reaction.

2.1.2 Other hydrogen production methods

The coal gasification and biomass gasification are the other common production methods for hydrogen. Coal gasification is a well-established process to convert the coal into its basic chemical components by reacting it with a controlled amount of oxygen and steam at high temperatures and pressures. The syngas generated in the coal gasification generally comprises CO, H_2, CO_2, and CH_4 with some impurities such as H_2S and NH_3. Gasification process requires further purification step to remove the pollutants from the gas mixture. The resulting gas is generally composed of 39-41% H_2, 18-20% CO, 10-12% CH_4, 28-30% CO_2 with some impurities such as 0.5-1% H_2S and 0.5-1% NH_3. [8,9]. Depending on the type of the gasifier, the syngas leaves the reactor at very high temperatures between 1300-1500 °C. The syngas is typically cooled down to ~600 °C by a heat exchanger for the heat recovery. Further, it is cooled down to 350-400 °C by a convective coolant to lower the steam pressure and the further heat recovery [10]. Thus, coal gasification sets two different temperature regime, i.e. 350-400 °C and ~600 °C, for the further purifications processes.

The biomass gasification is a similar process with the coal gasification, except for the resources used. It has become the subject of increasing attention in the last decade since it is a renewable source and is an alternative to fossil fuels. There are several sources as a gasifiable biomass such as municipal solid waste, agriculture waste, livestock waste, industrial residue, and energy crops. The typical temperature range in biomass gasification is 800-1100 °C [11]. The syngas generated in this method significantly varies in composition depending on the feedstock used and the type of reactor. The syngas generated in this process typically contains 30-45% H_2, 20-25% CO, 6-12% CH_4, 20-25% CO_2, 0-1% NH_3 and H_2S [12]. After leaving the reactors, the syngas is subjected to several purification steps via physical separation devices such as scrubbers, cyclone separators, and filters. Each step requires different process temperature which typically varies between 60-350 °C [13].

Fermentation-based biomass conversion is another method to produce hydrogen. Agricultural and food wastes are used as substrates for the conversion of their sugar-rich content to H_2, CO_2 and some organic acids via anaerobic bacteria [14]. H_2 content of the gas mixture produced in this way varies between 35-55% [15]. Depending on the type of the bacteria used the process involves temperature 25-100 °C.

As discussed above each production method yields the gas mixture at a different temperature with a different H_2 content. These temperatures are important for on-site purification of hydrogen.

In addition to these, hydrogen produced can be stored, following the production, as a syngas or as pure H_2 in underground facilities such as caverns and salt domes [16]. Since fuel cells in particular PEM fuel cell require extremely pure hydrogen, gas stored in the caverns may be purified further before they are fed to the cells. Though at the trial stage, hydrogen may be injected into the current natural gas grid to facilitate hydrogen transportation [17,18]. If this is commonly adopted similar low-temperature membrane would be needed to separate hydrogen from the gas-network.

Thus the separation membranes are needed to meet different process temperatures. These vary from ~600 °C in the coal gasification to as low temperature as possible, down to room temperature. Of these, the current volume production of hydrogen centers on the steam reformation of natural gas followed by water-gas shift reactions. Thus, in terms of volume production, there is a need for separation membranes that operate in the temperature interval of 350-450 ° C.

2.2 Hydrogen Purification Methods

There are several commercially available purification methods to separate H_2 out of the gas mixtures produced through a variety of ways. The common purification methods are pressure swing adsorption, cryogenic distillation and the separation based on hydrogen-selective membranes. Each process provides various advantages over each other and involves different problems. A brief description of each method is given in the following section. Hydrogen separation membranes are explained in a greater detail since the separation based on dense metallic membranes is the main interest of this thesis.

2.2.1 Pressure swing adsorption

Pressure swing adsorption (PSA) is the state-of-the-art technology in the chemical and petrochemical industries for the production of high purity hydrogen from a syngas containing 60-90 % H_2 [19]. Globally, more than 85% of the current hydrogen production units use PSA technology for hydrogen purification. The basic concept of a PSA process is relatively simple. This method relies on the adsorption of impurity molecules at high partial pressures and subsequent desorption of these impurities at lower partial pressures. Thus, the gas mixture to be refined is fed through micro and mesoporous adsorbents, typically a zeolite. The impurities in H_2 rich feed gas are selectively adsorbed on the surface of adsorbents at a relatively high pressure [19]. Pure H_2 permeates through, while the undesired gases are adsorbed. During the process, the surface of adsorbents gets saturated by impurity gases with time. That is why the impurities are then desorbed from the absorbent by lowering their partial pressure. In this respect, PSA operates on a cyclic basis to provide hydrogen flow. In the conventional steam reformation process, PSA unit can be integrated into the production line following the high-temperature water-gas shift reactions.

Although the PSA has a widespread use for hydrogen separation and produces a high-purity hydrogen, ~99.9% in an efficient way, there are several limitations in the process. The recovery of hydrogen is relatively low in PSA. That is why outgas has a considerable amount of unreacted CH_4 and unrecovered H_2 as well. It is known that the PSA becomes an economical purification process only when it scales up for large stationary applications (e.g. petroleum refining, petrochemical production or coal gasification) [20].

2.2.2 Cryogenic Distillation

Cryogenic distillation is a low-temperature process and its working principle for the separation relies on the differences in the boiling points of the feed gas ingredients. Cryogenic separation is often used for separating H_2 from hydrocarbons [6]. The boiling point of H_2 is -252.9 °C and it is less than the boiling point of any known gases, except He, -268.9 °C [21]. Thus, the process seems very effective in separating H_2 among the other ingredients in the syngas. However, H_2 purity could be only obtained between 90-98% in this method [22]. The purity and the recovery of H_2 are dependent on feed gas composition, separation pressure, and operating temperature. The typical H_2 recovery is around 95% in the most commercial applications [23]. Similar to PSA, cryogenic separation is quite energy intensive and it is suitable only for a large-scale production [24].

2.2.3 Hydrogen Separation Membranes

Membrane separation process is an economical alternative to pressure swing adsorption and cryogenic distillation. In typical membrane process, a gas mixture is fed through the sealed selective membrane and it is allowed to build up a gas pressure at the inlet. In principle, the membrane selectively allows the permeation of H_2, while the undesired impurities are rejected. H_2 partial pressure across the permeable membrane is the driving force for the hydrogen flow. Thus, hydrogen separation based on membranes are pressure-driven processes and unlike PSA, they provide typically continuous hydrogen throughput [20]. H_2 selective membranes require much less energy and relatively easier to operate. In membrane processes, only parameters that would be considered are partial pressure of H_2 at inlet/outlet and the process temperature [20]. Unlike the others separation methods, membrane processes are suitable for small-scale and portable applications. Membranes also can be operated at a various range of temperature and pressure. One of the key points of the separation membranes is that they can be used in membrane reactors, which allow simultaneous hydrogen production and purification [25]. Also, hydrogen membranes are very convenient to use at intermediate temperatures, 350-450 °C. This range meets the temperature requirement of high-temperature water-gas shift reactions in the steam reformation of natural gas, which is the dominant hydrogen production method.

Table 2.1 Comparison of hydrogen separation membranes [20].

	Membrane Types			
	Porous	**Polymeric**	**Ceramic Ion Conducting**	**Dense Metal**
Typical example	Silica, alumina, zeolites, carbon	Polyimide, Cellulose acetate	Strontium cerate, Barium cerate	Palladium alloys
Diffusion mechanism	Size exclusion	Solution-diffusion	Solution-diffusion	Solution-diffusion
Driving force	Pressure gradient	Pressure gradient	Ionic gradient	Pressure gradient
Operating temperature	≤ 1000 °C	≤ 110 °C	700-1000 °C	150-700 °C
Permeability	Moderate-high	Moderate-high	Moderate	Moderate
Typical selectivity	Low-moderate	Moderate	Very high	Very high
Relative cost	Low	Low	Low	Moderate

In fact, hydrogen separation membranes can yield various level of purity depending on the type of the separation membrane. Membranes are structurally classified in two main groups; porous and dense [26]. Porous membranes may be produced based on polymer including carbon, ceramics and metals. Dense membranes comprise polymeric membranes, ion-conductive ceramics and dense metallic membranes, Table 2.1. A brief description for these separation membranes is given below.

2.2.3.1 Porous separation membranes

Porous separation membranes can be made from a variety of materials such as carbon, polymers, ceramics, and metals. These membranes can be used at very different operating conditions since each material type addresses different process temperature and pressure. There are many commercialized examples of porous membranes such as zeolites, porous alumina, Vycor glass and porous metals [27]. Porous separation membranes make use of the differences in the molecular size and diffusion kinetics of ingredients in the gas mixture.

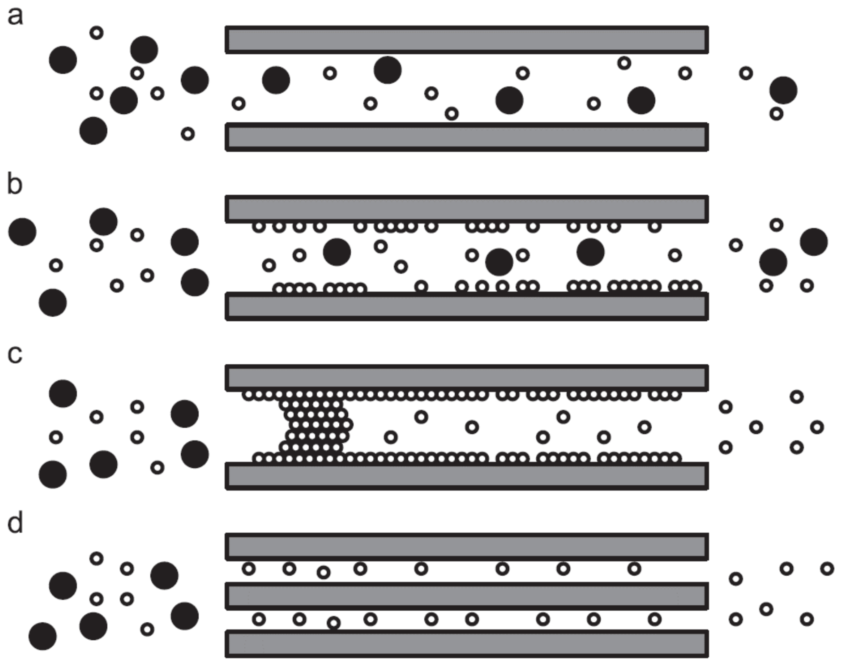

Figure 2.1 Possible transport mechanisms through a porous membrane, (a) Knudsen diffusion, (b) surface diffusion, (c) capillary condensation and (d) molecular sieving [28].

The separation mechanism in porous membranes varies depending on the pore size of the membrane. The pore size of the membrane should be comparable to the mean free path of the gas molecules in order for separation to take place [27]. There are mainly four different separation mechanisms in porous membranes, Figure 2.1. In the case of a pore diameter which is much smaller than the mean free path of the gas molecule, they collide with the pore walls much more than they collide with each other. This type of separation mechanism is called Knudsen diffusion, Figure 2.1 (a). In Knudsen diffusion, the permeability of the gas species is inversely proportional to the square root of their molecular weight and the membrane thickness [29]. Knudsen diffusion generally takes places when the pore diameter of the membranes is in the range of 2-10 nm [30]. Since H_2 has a low molecular weight (~2.015 g/mol [31]), it flows faster through the pores in Knudsen regime than the other gas molecules [21]. However, the selectivity of Knudsen diffusion is quite low, i.e. H_2 to CO_2 selectivity can only reach up to 4.69, which is not sufficient to yield a high purity H_2.

Surface diffusion, Figure 2.1 (b), is another type of separation mechanism and it occurs when one of the gas species in the gas mixture would be absorbed by pore walls and then it is capable of diffusion through this adsorption layer [27,32]. Surface diffusion might simultaneously occur with the Knudsen diffusion and increase the selectivity. However, this decreases the permeability of the gases since the effective pore diameter would be smaller [27]. This type of diffusion generally occurs within a certain pore diameter at a specific temperature due to the type of interaction between gas species and the membrane material.

Another diffusion mechanism is capillary condensation, Figure 2.1 (c), which takes place when one of the gas species condenses within the pores due to capillary forces [33]. The condensed gas occupies the pore and impedes the permeation of other gases. If the pore is completely filled with the condensed gas, only gas molecules that are soluble in this phase can permeate through the pores. Thus, the selectivity in this type of separation is typically higher than the other mechanism. However, it is highly dependent on the gas composition and the pore size uniformity [27].

Molecular sieving is another type of separation mechanism for the porous membranes, Figure 2.1 (d). It takes place when the pore size is smaller than the most of the gas species in the gas mixture. Thus, it only allows the permeation of certain molecules having smaller molecular size. The pore size of the membranes, exhibiting molecular sieving, generally in the range of 0.3-1 nm [27]. The common examples for this type membranes are generally based on carbon [34,35], silica [36,37] and zeolites [38,39]. Although the molecular sieving mechanism provides relatively higher selectivity for small size molecules, the overall flow rate is generally limited due to the formation of high flow resistances caused by fine pores [40].

2.2.3.2 Polymeric separation membranes

Dense polymeric membranes can be used to separate hydrogen from gas mixtures at relatively lower temperature ranges, typically ≤110 °C. The polymeric membranes are divided into two major categories; glassy and rubbery polymeric membranes. The glassy membranes generally yield a relatively higher selectivity with a lower hydrogen flux. Typical hydrogen permeability of common polymeric membranes is given in Table 2.2. The main advantage of polymeric membranes is their low cost [41]. However, the hydrogen permeability and selectivity of the polymeric membranes are much lower compared to dense metallic membranes. They are also vulnerable to contamination in the presence of H_2S, HCl, and CO_2 [26]. Therefore, the polymeric membranes are less attractive compared to other dense membranes.

Table 2.2 Hydrogen permeability and selectivity of various dense polymeric membranes at 25 °C [40].

Polymer type	**Hydrogen permeability ($x10^{-16}$ mol.m^{-1}.s^{-1}.Pa^{-1})**	**Selectivity**		
		H_2/N_2	**H_2/CH_4**	**H_2/CO_2**
Polysulfone	40.5	15.1	30.3	2.0
Polystyrene	79.6	39.7	29.8	2.3
Polymethyl methacrylate	8.0	2.0	4.0	4.0
Polyvinylidene fluoride	8.0	3.4	1.8	2.0

2.2.3.3 Ceramic ion transport membranes

In dense ceramic membranes, hydrogen permeation occurs in the form of ionic (protonic) transport. The transfer mechanism in this type membranes begins with the dissociation of hydrogen to its protons and electrons at the surface of the membrane. The protons and electrons then migrate through the dense membrane and re-associate at the surface of the membrane at the permeate side [42]. Thus, the ceramic membranes must have the capability of proton and electron transfer. This can be achieved with the membrane intrinsic nature or with an external catalytic layer to facilitate H_2 dissociation and re-association reactions. The schematic illustration of hydrogen transport in a typical ceramic ion transport membrane is given in Figure 2.2.

Of the ceramic materials perovskite-type oxides, with a general formula of ABO_3, are quite attractive due to their mixed ionic and electronic conductivity. Doping of perovskite oxides with aliovalent metals is a quite common approach so as to improve their electrical conductivity and increase the number of oxygen vacancies in the structure. Barium cerates ($BaCeO_3$) [43,44] and strontium cerates ($SrCeO_3$) [45,46] are the most attractive perovskite materials with dopants such as Y, Yb, and Gd [6,42,47].

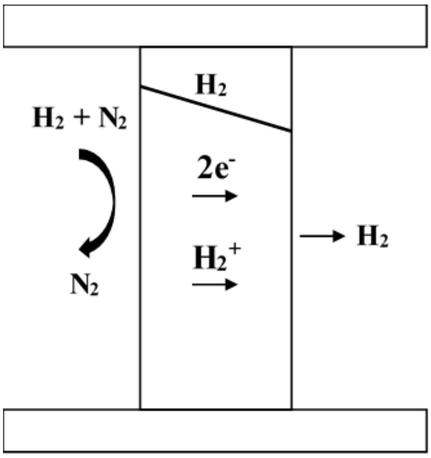

Figure 2.2 A typical hydrogen transport in ion transport membranes [48].

The H_2 selectivity in dense ceramic membranes is quite high and quite comparable to dense metallic membranes [48]. However, they yield a relatively lower hydrogen permeation compared to dense metallic membranes [49]. To improve permeability they require quite high temperatures such as 700-1000 °C [6] since proton conductivity is high at elevated temperatures. This temperature range is higher than those used in hydrogen production processes. Thus, it is necessary to heat up the syngas which brings an additional cost to the process. Therefore, there is a large number of studies [50–52] in order to reduce the operating temperature of ceramic membranes. Another concern of perovskites oxides is that the chemical instability at high temperatures in the presence of major syngas components such as CO_2 and H_2O. They easily form carbonates or secondary oxides, which inhibit the surface reactions [53].

2.2.3.4 Dense metallic membranes and their fabrication

Dense metallic membranes are quite attractive due to their superior hydrogen selectivity and permeability compared to other separation membranes. The comparison of the membrane types is given in Figure 2.3.

The dense metallic membranes can yield hydrogen with up to 6N purity [40,50]. Additionally, they offer very high hydrogen recovery ratio of ≥95% under certain conditions [50]. They often exhibit reasonable H_2 permeation over a wide range of temperature between 300-700 °C. As discussed in Section 2.1, this covers the most of the temperature ranges set by the major production methods such as the steam reformation of natural gas and the coal gasification. Therefore, dense metallic membranes have been the subject of considerable attention. Since the current study centers on dense metallic membranes, this section will be dealt with in more detail and form the subject of the following chapter. For this reason, this section will give a brief overview followed by common methods used in the fabrication of dense metallic membranes.

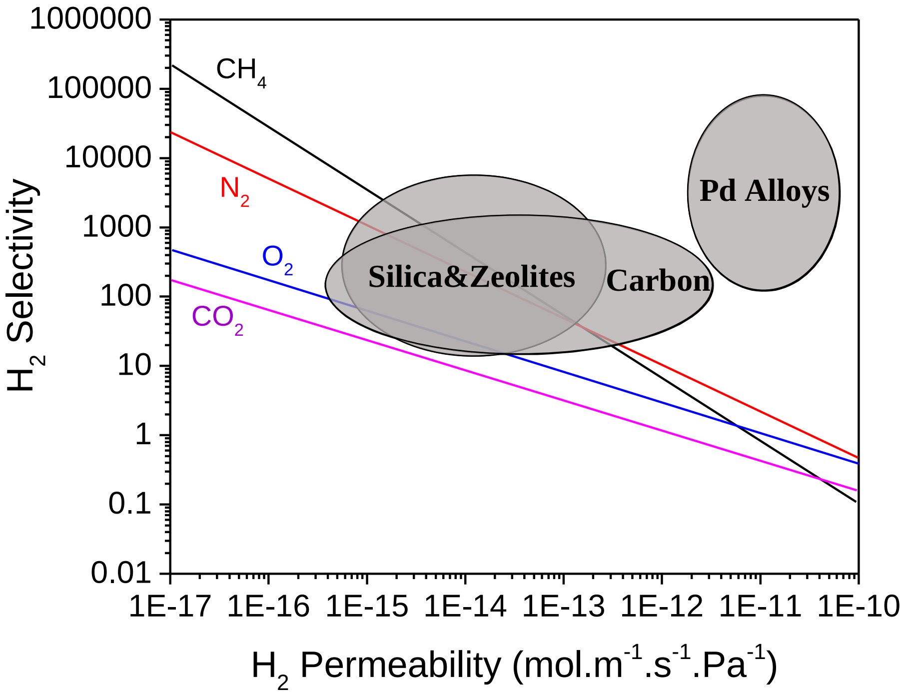

Figure 2.3 Hydrogen selectivity versus permeability of different separation membranes, reproduced from [54]. Lines represent the highest performance of the polymeric membranes for hydrogen separation from certain gas species.

Dense metallic membranes, as reviewed in Chapter 3, could be classified according to their structures into three categories. These are; amorphous, b.c.c. and f.c.c.

membranes. The last category is essentially based on Pd alloyed by a number of different elements. The b.c.c. membranes typically make use of Nb or V, i.e. Group V elements. Amorphous membranes are multi-component compositions based on Group IV and V elements. These membranes are produced via a number of methods, namely melting and casting followed by cold-rolling into foils, melt-spinning, electroplating, electroless plating and more recently via magnetron sputtering.

The earliest production method for metallic membranes is rolling of metal or alloy so as to obtain it in the form of a foil. Typically, the selected metal or alloy is melted and cold-rolled to the desired thickness. It is often around 20 µm or larger in thickness to maintain pin-hole free membrane. Traditionally, separation membranes produced by rolling can be used in the form of free-standing foils [55–57] or welded-tubes [58–60]. Due to the nature of the rolling process, the membrane should have sufficient ductility.

Cold rolling was used as a fabrication method for Pd and Pd alloys as well as b.c.c. separation membranes. Tosti *et al.* [61] produced Pd-Ag membranes via cold-rolling with a thickness of 50-70 µm. Guerreiro *et al.* [55] produced Pd-Cu-Au membranes using mechanical alloying, subsequent sintering and rolling procedures. Typically, 300-350 µm thick membranes were subjected to post heat treatment at 400 °C for 5h. The membranes were tested at ~450 °C and exhibited comparable permeability to pure Pd.

Li *et al.* [62] investigated the hydrogen permeability of as-cast, cold-rolled and annealed Nb40Ti30Co30 alloy membranes. They prepared the ingots with dimensions of 5mmx3mmx1mm by arc melting in an argon atmosphere. They were typically subjected to 50% cold reduction and some also annealed at 1000 °C. All the sample surfaces were coated with 190 nm Pd by magnetron sputtering. The hydrogen permeability tests between 350-450 °C indicated that cold-rolled membranes exhibited much lower permeability compared to as-cast membranes due to the defect formation during the cold-rolling. Following the annealing at 1000 °C for one week, the structure of membranes was recovered and they then exhibited higher permeability with a value of $2.43x10^{-8}$ $mol.m^{-1}.s^{-1}.Pa^{-0.5}$ compared to the as-cast membranes.

Melt-spinning is a very common technique in order to produce amorphous alloys. The desired alloy is melted with induction heating and then injected by an applied gas pressure on a cold rotating copper wheel. The molten alloy is cooled at a rate ranging from 10^4 to 10^6 °C/sec [63]. This rapid cooling results in an amorphous structure. The membranes in this method are typically obtained in the form of a ribbon with a thickness ranging from 20 to 100 µm.

Nb-Zr alloys with substantial addition of Ni are quite common as amorphous membranes. Paglieri *et al.* [64] produced Ni-Nb-Zr and Ni-Nb-Ta-Zr alloys with 50-90 µm thickness by melt-spinning technique. $(Ni_{0.6}Nb_{0.4})70Zr30$ membrane exhibited the highest hydrogen permeability, 1.4×10^{-8} $mol.m^{-1}.s^{-1}.Pa^{-0.5}$, at 450 °C. In a similar study, Shimpo *et al.* [65] produced Ni-Nb-Zr-Co amorphous membranes of ~50 µm in thickness with a width of 20 mm by melt-spinning. $(Ni_{0.6}Nb_{0.4})45Zr50Co5$ membrane exhibited a hydrogen permeability of $\sim 2x10^{-8}$ $mol.m^{-1}.s^{-1}.Pa^{-0.5}$, at 400 °C which is slightly higher than that of the commercial Pd77Ag23 membrane.

Electroplating is another common fabrication method for membranes and has the advantage of reducing the precious metal content. Thin film membranes produced by electroplating require a porous substrate so as to attain mechanical support. In electroplating, deposition takes place in an electrolyte solution containing the desired elements making up the membrane. The process involves reduction of the cations in the electrolyte depositing them onto the conductive substrate.

Examples of membranes produced by electroplating include Pd, Pd-Ad, and Pd- Ni. Chen *et al.* [66] coated Pd membranes on porous stainless steel tubes using an electrolyte composed of $PdCl_2$, $(NH_4)_2SO_4$, and HNO_2. The membranes produced had a thickness of 20 µm tested with a feed gas of 75% H_2-CO_2 mixture yielding a hydrogen gas of 99.98% purity. Uemiya *et al.* [67] fabricated Pd72Ag28 membranes on Ag substrates with an improved electroplating technique. They controlled the composition of the alloy by adjusting pH with H_3BO_3 and $C_2H_5NO_2$ addition into the electrolyte containing $PdCl_2$, $AgNO_3$, HBr, and HNO_2 at 50 °C. They have successfully produce Pd-Ag alloy without any composition gradient. Similarly, Nam *et al.* [68] produced 1 μm thick Pd-Ni membranes on porous stainless steel substrates by a vacuum-assisted electroplating. The electroplating was carried out in an electrolyte containing $PdCl_2$, $NiSO_4.6H_2O$, $(NH_4)_2SO_4$, and NH_3 at 25 °C. The membranes were tested with H_2 and N_2 between 350-550 °C and exhibited an order of magnitude lower hydrogen permeability compared to pure Pd. The selectivity ratio of H_2 over N_2 was 4700 at 550 °C.

Electroless plating is very similar to electroplating which involves the use of reducing agents rather than the electrical current in the deposition process. Therefore, it is possible to extend the choice of substrates with non-conductive materials such as porous Al_2O_3 [69,70]. Chen *et al.* [66] compared Pd membranes produced via both electroplating and electroless deposition. They reported that electroplated membranes were resistant to embrittlement up to 300 °C, while the membrane produced by electroless plating encountered cracking in the same temperature range.

Sputtering is a common physical vapor deposition technique for thin film deposition. The thickness of the films could be in the range from angstroms to several microns. The thickness can be effectively controlled by parameters such as power applied, gas pressure and sputtering time. Sputtering provides a precise control on the film composition and the structure [71].

Typically, two type of power source can be utilized in the sputtering, direct current (DC) and radio frequency (RF) based on alternating current. In DC sputtering, positive ions produced within the plasma typically accumulate on the surface of the target. If the target material is an insulator, charged ions cannot flow and the electric circuit is interrupted. Thus, the potential at the cathode drops and the positive ions could not be accelerated towards the target, which ends the process. Therefore, only conductive materials can be used in DC sputtering. In the case of RF sputtering, it is possible to discharge the positive ions on the surface of targets. An integrated impedance matching network alternates the electrical potential of the current at certain radio frequencies, typically 13.56 MHz, and avoid the charge build-up on non-conductive targets. Thus, dielectric and insulator materials can be used as a target material with RF sputtering.

Examples of dense metallic membranes produced by magnetron stuttering cover Pd-Ag, V-Pd, Zr-Ni, Zr-Cu, and Zr-Cu-Y. In an early study, Xomeritakis *et al.* [72] produced Pd-Ag membranes with thicknesses of 0.1-1.5 µm on alumina substrates using Pd75Ag25 target. They found that increasing DC power yielded higher Pd content in Pd-Ag membranes and yielded larger grain size. They also investigated the effect of deposition temperatures and found that 400 °C was an ideal temperature so as to obtain dense and stress-free thin films. The selectivity ratio measured with H_2/He varied from 20 to 80 depending on the conditions of deposition. Vicinanza *et al.* [73] produced Pd77Ag23 thin films of 2 µm to 11 µm thickness on polished silicon wafers which were then peeled-off and transferred to porous stainless steel substrates. They reported that the solubility of hydrogen increased as the membrane thickness decreased from ~11 µm to 2 µm. In a similar study, Pereira *et al.* [74] deposited Pd-Ag membranes of 0.7-1.4 µm on alumina substrates via co-sputtering of Pd and Ag targets. The membranes had a columnar structure but had apparently pin-holes since the selectivity measured with H_2/N_2 was quite low, typically 10.

A multi-layer thin film membrane was investigated by Fasolin *et al.* [75] where V and Pd were deposited as alternate layers. Films were typically 2-7 µm thick with both surfaces also coated with Pd as a catalytic layer. The study showed that the membranes thicker than ~4 µm exhibited comparable H_2 selectivity and permeability to pure Pd. However, the H_2 flux decreased dramatically after exposure to syngas at 375 °C.

Magnetron sputtering could also be used to deposit amorphous thin films. Thus Nayebossadri *et al.* [76] deposited Zr-Ni, Zr-Cu, and Zr-Cu-Y membranes using very low target currents, < 1.5 A, so as to avoid crystallization. They achieved pin-hole free thin membranes which were thermally more stable compared to similar membranes produced by melt-spinning. In a similar study, Xiong *et al.* [77] produced 6-12 µm thick $Nb_{40}Ti_{30}Ni_{30}$ membranes on Ni substrates at a deposition pressure of 5 mTorr argon. They stated that the lower temperatures yield a large number of defects in the membrane, which was attributed to insufficient diffusion during deposition. Permeability tests indicated that the amorphous structure exhibited higher H_2 permeability with a value of 1.4×10^{-8} mol/m.s.Pa compared to crystalline counterparts at 400 °C.

Tosti *et al.* [61] have carried out a comparative study based on Pd-Ag in which membranes were produced via cold-rolling, electroless plating, and sputtering. The thickness of the membranes was 50-70 µm, 2.5-20 µm, 0.5-5 µm in the respective order. The selectivity tested at 400 °C with H_2/Ar was 50 with electroless plating. In the case of sputtered films, the value was much less, i.e. 4.47, over Ar. Only, foils prepared via cold-rolling successfully exhibited reliable selectivity (N_2 or Ar gas flow could not be detected). The foils also exhibited a quite high permeability and withstood up to 16 bar H_2 pressure at 400 °C.

CHAPTER 3

DENSE METALLIC MEMBRANES

Dense metal membranes can be used for the hydrogen separation at temperatures between 300-700 °C which forms a suitable interval for most hydrogen production processes [42]. The hydrogen separation process which takes place in the dense metal membranes offers very high (theoretically infinite) hydrogen selectivity with a high hydrogen permeability [78].

3.1 Solution-Diffusion Mechanism.

The separation mechanism in dense metallic membranes is based on solution-diffusion mechanism. It involves mainly five steps as illustrated in Figure 3.1.

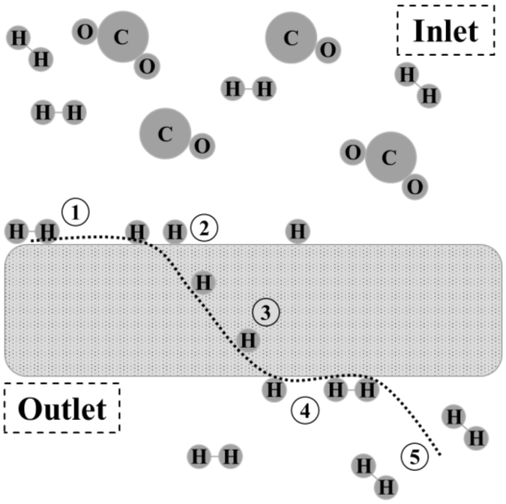

Figure 3.1. Schematic representations of hydrogen permeating through the dense metallic membranes.

H_2 molecules first adsorbed by the metal surface. Molecules then dissociate into the atomic form due to the catalytic activity of the membrane. Thereafter, hydrogen atoms dissolve into the membrane lattice and diffuse through the membrane under the driving force resulting from the concentration gradient. This concentration gradient is created by applying a high hydrogen partial pressure into the feed side while maintaining a relatively lower hydrogen partial pressure at the permeate side [27]. After passing through the dense membrane, the hydrogen atoms re-associate into H_2 molecules at the membrane surface on the permeate side.

The hydrogen flux in the bulk membrane can be described by integration of Fick's First Law;

$$J = -D\frac{dC}{dl} = \frac{D}{l}\left({C^n}_{H_2,feed} - {C^n}_{H_2,permeate}\right)$$

Equation 3.1

Here, J is the hydrogen flux (mol/m^2.s), D is the diffusivity of hydrogen in the membrane (m^2/s) at a given temperature, l is the thickness of the membrane (m), ${C^n}_{H_2}$ and ${C^n}_{H_2}$ are the hydrogen concentrations, (mol/m^3), at the feed and the permeate side, respectively. The hydrogen concentration can be expressed by the equation of $C = Ƙ\eta$, where Ƙ is the constant for hydrogen concentration (mol/m^3) and η is the H/metal atomic ratio. η is linearly dependent on the square root of the partial pressure of hydrogen at dilute concentrations. Therefore; $P_H^{0.5} = K_S.\eta$, where K_S is the Sievert's constant. The integration of these into the previous equation results in;

$$J = \frac{D(\mathrm{K}/K_S)}{l}\left({P^n}_{H_2,feed} - {P^n}_{H_2,permeate}\right)$$

Equation 3.2

K/K_S term normally represented by S with a unit of (mol/m^3.Pa$^{0.5}$) is referred to as hydrogen solubility. The hydrogen permeability then become the product of diffusivity and the solubility of hydrogen;

$$k = D.S$$

Equation 3.3

The integration of equation of permeability into Equation 3.2 results in;

$$J = \frac{k}{l}({P^n}_{H_2,feed} - {P^n}_{H_2,permeate})$$

Equation 3.4

The permeability is an intrinsic property and is independent from the membrane thickness. On the other hand, the hydrogen permeability through the dense metallic membrane is temperature dependent and it follows the Arrhenius relation [79], namely;

$$k = k_0.\exp\ [-\frac{E_a}{RT}]$$

Equation 3.5

Here, E_a is the activation energy for hydrogen permeation (J/mol), R is the universal gas constant (J/mol.K) and T is the temperature (K).

It should be noted that the Equation 3.2 is based on Sievert’s constant that is valid for dilute concentrations of hydrogen. Indeed, the exponent of partial pressure, *n*, varies between 0.5-1.0 depending on the conditions. In the case when the hydrogen diffusion is the rate-limiting step, n takes the value of 0.5. If the rate limiting step is a surface reaction, n then tends to take up values close to 1.0.

In relatively thick membranes, the rate-limiting step is often hydrogen diffusion across the membrane. Hurlbert *et al.* [80] reported when the thickness exceeds 20 µm in Pd membranes, the exponent is n=0.5. Vicinanza *et al.* [73], as well as Athayde *et al.* [81], reported critical thickness values which are much less than 20 microns. The temperature also plays a critical role in the reactions kinetic. Ward *et al.* [81] investigated the effect of temperature in Pd membranes. They reported that the hydrogen diffusion through the Pd membrane is the limiting step above 300 °C, regardless of the membrane thickness.

The surface reactions also become critical when the membrane is poisoned by gas species. This is especially valid in the presence of surface contaminants such as H_2S or CO in the gas mixture. Melendez *et al.* [82] reported that permeation characteristic of Pd-Ag-Au membranes varied in the presence of H_2S and the exponent becomes n=0.6 for alloys having ~3 at.% Au. In another study, Jia *et al.* [83] investigated Pd-Cu-Au membranes and found that the membranes having less than ~8 at.% Au content exhibited surface limited behavior yielding n values up to 0.76 between 300-650 °C.

3.2 Type of the Dense Metallic Membranes

Hydrogen permeability of some pure metals is given in Figure 3.2 [84]. The plot shows that the temperature dependence of permeability differs from metal to metal. For Pd and Ni, the permeability increases with increase in temperature. In the case of Nb, V and Ta, the case is reverse, i.e. permeability decreases with increase in temperature [84]. This reverse relationship is often attributed to a decrease in hydrogen solubility which occurs at elevated temperatures [27].

Dense metallic membranes could be classified according to their structures into three categories. These are; amorphous membranes based on Group IV-V multi-component compositions, b.c.c. membranes based on Group V elements and f.c.c.

membranes based on Pd and Pd alloys. Typical membrane compositions together with their permeability values are summarized in Table 3.1.

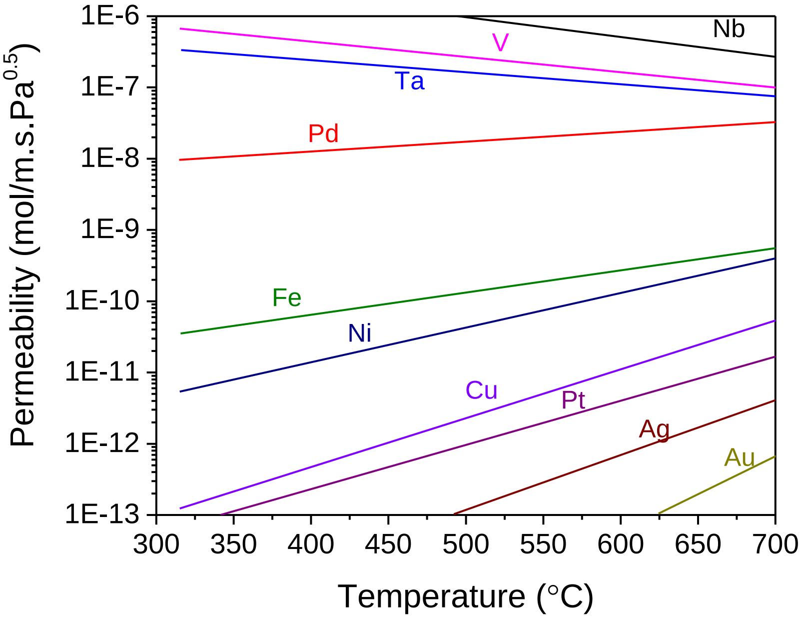

Figure 3.2 Hydrogen permeability of selected pure metals between 300 and 700 °C [84].

Table 3.1. Hydrogen permeability of selected membranes.

	Membranes	**Permeability (mol/m.s.Pa$^{0.5}$)**	**Temperature (°C) [ref.]**
Amorphous	$Ni_{60}Nb_{20}Zr_{20}$	1.9 x 10^{-9}	400 [85]
	$Zr_{36}Ni_{64}$	1.2 x 10^{-9}	350 [86]
	$Nb_{95}Pd_{5}$	1.3 x 10^{-7}	300 [26]
	$Nb_{39}Ti_{31}Ni_{30}$	0.3-2 x 10^{-8}	250-400 [87]
	$V_{90}Al_{10}$	2.7 x 10^{-7}	400 [88]
b.c.c. structure	Nb	1.6 x 10^{-6}	500 [84]
	$Nb_{40}Hf_{30}Co_{30}$	4.9 x 10^{-8}	400 [89]
	V	1.9 x 10^{-7}	500 [84]
	$V_{85}Ni_{15}$	1.5 x 10^{-8}	550 [90]
	Ta	1.3 x 10^{-7}	500 [84]
f.c.c. structure	Pd	1.9 x 10^{-8}	500 [84]
	Pd_{77}-Ag_{23}	3.29 x 10^{-8}	350 [91]
	Pd_{60}-Cu_{40}	2.02 x 10^{-8}	350 [91]
	Pd_{90}-Y_{10}	7.15 x 10^{-8}	350 [91]
	Pd_{95}-Au_{5}	2.02 x 10^{-8}	350 [91]

3.2.1 Amorphous membranes

Amorphous membranes have a more open crystal structure leading a higher hydrogen solubility in the structure [26]. Also, defects in amorphous membranes facilitate the hydrogen permeation with a lower hydrogen embrittlement risk due to different energy binding sites in the lattice [92].

The amorphous alloys commonly consist of multi-components that also combine inexpensive elements. Therefore, they are quite attractive in terms of producing low-cost separation membranes. Amorphous membranes are often produced by melt-spinning or splat quenching. Ni-Nb-Zr and Cu-Zr are the most common alloy systems studied as separation membranes [93,94].

One such composition making use of Ni-Nb-Zr was studied by Lai *et al.* [95] where Zr was also replaced by elements Sn and Ti. The membranes were in the form of a 45 µm thick discs produced by splat quenching with 20 mm diameter. The membranes were then coated with Pd as a catalytic layer by sputtering. They measured hydrogen permeability which was two orders of magnitude lower as compared to Pd77Ag23 at 400 °C. They also observed that the permeability of membranes reduces over time which is attributed to a decrease in free volume due to stable hydride formation. In a similar study, Fe-Ni-Si-B-C multi-component alloys were produced via melt-spinning [96]. The membranes showed no permeability in bare form, i.e. without the use of a catalytic coating layer. Paglieri *et al.* [64] produced $Ni_{60}Nb_{20}Zr_{20}$, $(Ni_{0.6}Nb_{0.4})_{100-x}Zr_x$ and $(Ni_{0.6}Nb_{0.3}Ta_{0.1})_{100-x}Zr_x$ (x=0, 10, 20 or 30) membranes by melt-spinning. The membranes were coated with a 500 nm Pd layer by RF sputtering. Of these, only $(Ni_{0.6}Nb_{0.4})_{70}Zr_{30}$ performed hydrogen permeability (1.4×10^{-8} $mol.m^{-1}.s^{-1}.Pa^{-0.5}$) comparable to the Pd75Ag25 alloy. However, the permeability value reduced down to ~$6.1x10^{-9}$ $mol.m^{-1}.s^{-1}.Pa^{-0.5}$ after 60h operation at 450 °C.

Dolan *et al.* [85] used a planar flow casting technique to produce $Ni_{60}Nb_{40-x}Zr_x$ amorphous 50 μm thick ribbons with a width of 30 mm. The membranes were then coated with 500 nm Pd layer by a magnetron sputtering yielding permeability values that were almost an order of magnitude less than that of Pd membrane at 425 °C. The membranes tended to crystallize above 500 °C.

Nayebossadri *et al.* [76] obtained Zr-Ni, Zr-Cu, Zr-Cu-Y and Zr-Cu-Ti amorphous membranes via magnetron sputtering. For this purpose, they employed very low target currents and made use of 18 runs of sequential depositions. They reported that the structure remained amorphous up to a 400 °C.

From the review given above, it may be stated that the amorphous membranes tend to crystallize at elevated temperatures because of their metastable nature, a concern common to all amorphous membranes. Also, the exothermic nature of hydrogen absorption often results in local changes in the structure and tend to crystallize the membrane [97]. Although efforts still continue, because of their potential to reduce the membrane cost as well as the superior resistance to hydrogen embrittlement, amorphous membranes have lower hydrogen permeability compared to their crystalline counterparts.

3.2.2 b.c.c. based membranes

The b.c.c. membranes based on Group V transition metals, particularly Nb, V, and Ta, have been the subject of considerable interest. This is due to their low cost and the orders of magnitude faster hydrogen permeability compared to Pd, which has been one of the most successful membrane material [98–100]. The high permeability of these metals is attributed to their b.c.c. structure yielding higher hydrogen solubility and diffusivity [101]. The smaller hopping distance in b.c.c. lattice (tetrahedral sites) leads faster hydrogen diffusion, while the less packed crystal structure enables the very high solubility. On the other hand, this excessive hydrogen solubility often leads to the embrittlement in the membranes [87]. Therefore, the efforts in b.c.c. membranes have concentrated on reducing the embrittlement in which attempts [97,98] were made to reduce hydrogen solubility while maintaining reasonably high permeability.

There are mainly two approaches to address the embrittlement in the b.c.c. membranes. The first approach aims to produce a dual phase b.c.c.-cP2 alloys [102–105]. This class of separation membranes generally consist of a Nb/V/Ta-rich b.c.c. phase in a matrix of a eutectic mixture of the same b.c.c. phase and cP2 phase. Here, b.c.c. phase is the responsible for the hydrogen permeability, while the cP2 phase imparts the embrittlement resistance.

Li *et al.* [106] investigated the alloy systems of $Nb_{20}Ti_{40-x}Hf_xNi_{40}$ (x=0-40) and $Nb_{40}Ti_{30-x}Hf_x$Ni30 (x=0-30) where the structure was also two-phase. The membranes were coated with 190 nm Pd with RF sputtering so as to obtain catalytically active surface. They found that the permeability was improved by an increase in Hf content but when Hf amount was close to or higher than that of Ti in the alloy, the ductile eutectic phase, cP2-(Ti, Hf)Ni, starts to transform into brittle orthorhombic-(Hf, Ti)Ni phase. Of the alloys in this study, $Nb_{40}Ti_{20}Hf_{10}Ni_{30}$ exhibited the highest permeability with a value of 2.96×10^{-8} $mol.m^{-1}.s^{-1}.Pa^{-0.5}$ at 400 °C, which also exhibited promising embrittlement resistance.

Luo *et al.* [107] studying of Nb-rich Nb-Ti-Co alloys reported 38 vol.% as critical value to suppress the hydrogen embrittlement. They pointed out that for acceptable resistance to hydrogen embrittlement, the presence of a eutectic phase of at least 38 vol.% was necessary. They found the highest permeability in an alloy with $Nb_{60}Ti_{21}Co_{19}$ composition which had a value of 3.99×10^{-8} $mol.m^{-1}.s^{-1}.Pa^{-0.5}$ at 400 °C. This value is by a factor of 2.6 higher than that of pure Pd.

In a recent study, Li *et al.* [108] investigated V-Cr-Cu dual phase alloys as separation membranes. V-Cr-Cu alloys, composed of V-rich b.c.c. phase and Cu-rich f.c.c. phase were offered as a new type of hydrogen separation membrane in this study. Alloys $(V_{100-x}Cr_x)_{70}Cu_{30}$ (x=0, 5, 10) were produced by arc-melting and then cold rolled to obtain ~100 µm thick membranes. Both sides of the membranes were coated with Pd via RF sputtering. They stated that the addition of Cr in V alloys effectively modify the hydrogen solubility, while the addition of Cu introduces the formation of a Cu-rich f.c.c. phase and improves the ductility. They tested the membranes between 350 and 450 °C in demanding conditions of hydrogen feed pressure of up to 8 bar. They identified $(V_{95}Cr_5)_{70}Cu_{30}$ as the best composition, where the permeability was ~3 times that of Pd, namely $3.98x10^{-8}$ $mol.m^{-1}.s^{-1}.Pa^{-0.5}$, at 400 °C. They concluded that dual-phase structure ensures a favorable ductility with an acceptable hydrogen permeability. However, the long-term stability of the dual phase structure is not known since the permeability tests were carried out for only 4h.

The second approach in order to improve the embrittlement resistance in b.c.c. alloys is to have a single phase solid solution with a controlled hydrogen solubility. In this context, there are a number of studies covering highly permeable metals such as Nb [109–111], V [112–114], or Ta [115]. Here, the aim is to reduce the lattice volume in order to restrict the hydrogen solubility, while maintaining the reasonable hydrogen permeability.

In an extensive study, Paglieri investigated more than 250 compositions based on Nb and V [116]. The most of the membranes especially those based on Nb failed due to the hydrogen embrittlement. V-based alloys exhibited a ductile behavior but had a very low hydrogen permeability. Tsuchimoto *et al.* [117] investigated the effects of W and Mo on the hydrogen solubility in Nb. The membranes based on Nb-W, Nb-Mo, and Nb-W-Mo, all in the form of solid solutions with b.c.c. structure, were surface coated with 200 nm Pd by RF sputtering. They assessed the alloys by measuring hydrogen pressure-composition-isotherms (PCT) so as to determine the equilibrium hydrogen pressure. They found that hydrogen concentration was directly proportional to the amount of W and Mo in the alloys. Furthermore, they found that the hydrogen concentration of 0.2 (H/M) was the critical value for the embrittlement. They identified Nb84W8Mo8 as the most suitable composition which was resistant to embrittlement and also exhibited relatively high hydrogen permeability.

In a similar study, Suzuki *et al.* [118] studied the effect of Ru, W, Mo as an alloying addition on the hydrogen solubility and permeability of Nb. All the alloys were composed of single solid solution phase with a b.c.c. structure. The membranes were coated with 200 nm Pd by RF sputtering and then tested between 400-500 °C. They found that the addition of Ru, W, and Mo into the Nb not only decreases the hydrogen solubility but at the same time enhances the hydrogen diffusivity.

Alimov *et al.* [119] investigating V-Pd alloys found that Pd effectively decreases the hydrogen solubility. The solubility of this alloy system at temperatures between 300 and 550 °C was much lower than the critical level, 0.2 (H/M). They identified V-8-12.3 at.% Pd alloys as the compositions with improved permeability.

The b.c.c. alloys are the most promising class for hydrogen separation membranes of low cost provided that embrittlement could be avoided with a suitable strategy. However, the b.c.c. membranes are often vulnerable to surface oxidation which hinders hydrogen dissociation processes at the surface. Therefore, b.c.c. membranes almost always require an external catalytic layer, e.g. Pd, so as for them to function effectively as separation membranes.

3.2.3 Pd and Pd-based f.c.c. membranes

Pd has unique properties for the purpose of hydrogen separation membrane. It has an electron configuration of $1s^2$ $2s^2p^6$ $3s^2p^6d^{10}$ $4s^2p^6d^{10}$ $5s^0$ and there is an overlapping energy between the 4d and 5s bands. The low energy 5s band could easily fill over the high energy 4d band. Thus, Pd has a high affinity for donor electrons from other atoms. This electronic configuration is responsible for its ability to dissociate molecular H_2 into atomic form [27], which is essential to initiate the hydrogen absorption in the membrane. Moreover, Pd is capable of absorbing hydrogen up to 600 times of its own volume [120] and it is also resistant to surface oxidation at elevated temperatures [121]. Thus, Pd has been the most popular metal for the hydrogen separation membranes. Since the ability of Pd to allow hydrogen permeation was discovered by Sainte-Claire Deville in 1863 [100], the element has been the focus of a significant number of studies [26,27,91].

Pd, as in other metallic membranes, exhibits extremely high hydrogen selectivity and the impurity level may be expressed in the level of parts per billion (ppb) [99]. These properties make Pd particularly attractive for hydrogen separation membranes. However, the high cost of Pd restricts the widespread use in industrial applications. The efforts, therefore, have concentrated on reducing the cost of Pd based membranes. Two approaches may be employed for this purpose; one is reducing the Pd content of the membranes via alloying and the second is reducing the quantity of Pd with the use of thin film membranes.

Pd-H phase diagram, studied in 1936 by Gillespie and Galstaun [122], is given in Figure 3.3. The diagram comprises an interstitial solid solution, α phase, and a Pd hydride, β phase. Below 295 °C, there are three regions in the phase diagram. These are a single phase α region, a miscibility gap, between hydrogen content of 0.02-0.58 wt.%, where α and β phases coexist and a single phase β region. The temperature of 295 °C is critical for the β phase, above which this phase does not occur.

The α and β phases each has f.c.c. structure. The lattice parameter of pure Pd is 3.889Å, while α and β phases have a lattice parameter of 3.895 and 4.025Å, respectively [123]. Thus, cycling of Pd membrane in the miscibility gap region due to the change in temperature or hydrogen pressure leads to approximately 10%

volume change in the lattice [124]. This volume change is the cause of hydrogen embrittlement in Pd based membranes [125]. The change leads to the formation of micro-cracks which severely affects the durability of the membrane.

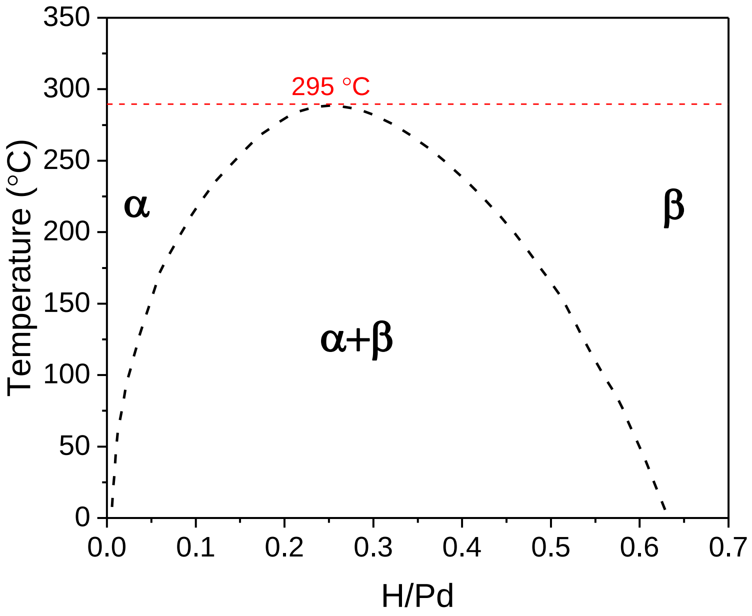

Figure 3.3. Pd-H binary phase diagram, adapted from the study of Huang *et al.* [126].

There are mainly two approaches in order to avoid the embrittlement in Pd based membranes. The first one relies on controlling the process parameters, i.e. temperature, and the hydrogen pressure, during the operation to keep the membrane in the single-phase region. The second approach is to alloy Pd in order to avoid the transformation into the α+β region. This is the common approach by which the onset of the α+β region is depressed to temperatures much lower than those depicted in Figure 3.3.

Of the Pd-based alloys, Pd-Ag system is quite attractive due to its superior properties. The addition of 10-30 at.% Ag brings a significant reduction in the critical temperature for α+β phase transformation [127]. This enables the use of Pd-Ag alloys as durable hydrogen separation membranes. The effect of Ag content on the hydrogen permeability of Pd is given in Figure 3.4. As seen in the figure with 20-30 at.% Ag addition, the permeability is higher than that of pure Pd. In fact, Gryaznov [128] and Holleck [129] reports permeability which is higher by a factor of 1.7 with Ag content of 25-30%. Among these alloys, the Pd77Ag23 composition is particularly attractive in terms of both mechanical durability and high hydrogen permeability that it offers. Therefore, there has been a great interest in Pd77Ag23 which is commercially produced for many membrane applications. Since the Ag is about 60 times less expensive compared to Pd, the cost of these membranes was much less than their pure counterparts.

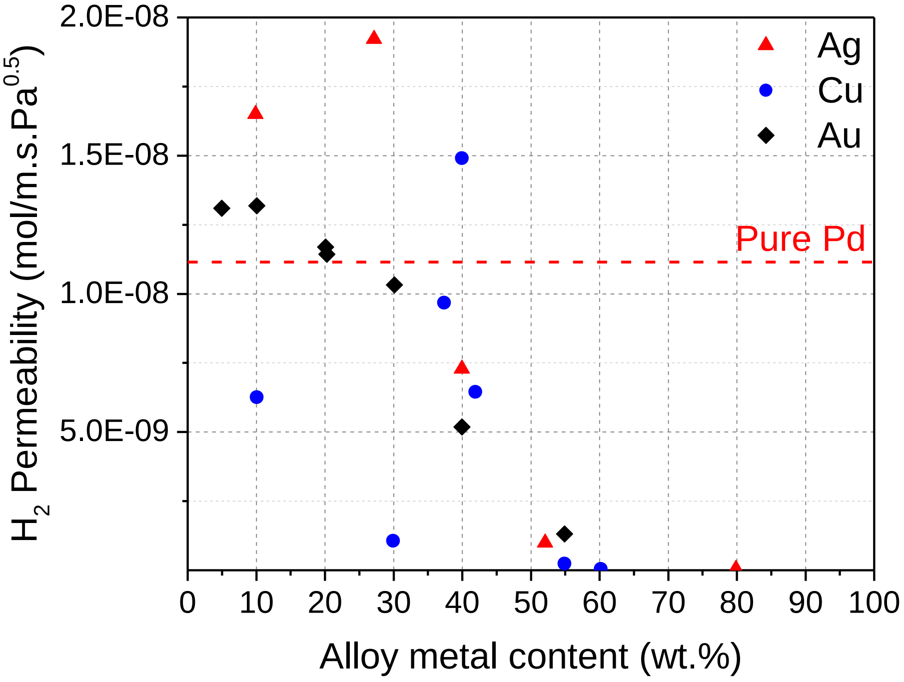

Figure 3.4 The change in hydrogen permeability of Pd binary alloys at 350 °C due to the content of alloying elements of Ag, Cu, and Au, reproduced from [127].

Cu is another common alloying element for Pd membranes. It has been shown that alloying of Pd with Cu initially reduce the permeability and it recovers back and increases with further addition, see Figure 3.4. The permeability reaches its maximum at ~40 wt.% Cu concentration with a value 1.4 times higher than pure Pd.

The crystal structure is normally f.c.c. but it changes to b.c.c. with 40 %Cu. This is considered to be the cause of increased permeability. The alloying with Cu also improves the resistance to sulfur compounds such as H_2S. This is the main advantage of Pd-Cu membranes which is important for applications in coal gasification where H_2S is always present [130,131].

Pd-Au is another binary alloy system that has been extensively studied especially due to its better H_2S resistance. It was shown that addition of Au into Pd up to 15 wt.% or 20 wt.% enhances the H_2S tolerance and also increases the hydrogen permeability, Figure 3.4 [132,133]. According to Gryaznov [128] the permeability of Pd-10 wt.% Au is higher by a factor of 2.2 as compared to pure Pd at 500 °C. It should be noted that alloying with Au does not provide any advantage for cost reduction due to the high cost of Au. Therefore, Pd-Au alloys should be considered for specific applications, especially where H_2S is a risk factor.

Table 3.2. The effect of alloying elements on hydrogen permeability of Pd.

Alloying element	**wt.% of the alloying element**	**Normalized Permeability at 350 °C**
-	-	1.0
Au	5	1.1
Ag	23	1.7
B	0.5	0.9
Ce	7.7	1.6
Cu	40	1.4
Y	10	3.8
Ag, Rh	19, 1	2.6
Ag, Ru	30, 2	2.2
Ru, In	0.5, 0.6	2.8

Other elements that have been considered for alloying include B, Ce, In, Rh, Ru, Y. The maximum permeability and the corresponding alloy compositions as reviewed by Knapton [91] and Gryaznov [128] are tabulated in Table 3.2.

Another approach in reducing the cost of the Pd-based membranes is to reduce the material quantity with the use of thin film membranes. Since the hydrogen flux and the membrane thickness is inversely proportional, thin film membranes allow higher hydrogen permeation as well. Therefore, there has been a great interest in thin film separation membranes in recent years [134–140].

The thin film membranes can be produced with a variety of techniques such as electroplating, electroless plating, and magnetron sputtering as reviewed in section 2.3. They often require a porous substrate so as to attain a mechanical support. For this purpose, many types of materials such as porous stainless steel [134–136], porous Al_2O_3 [137,138], and Vycor glass [139,140] can be employed.

In similar studies, Ryi *et al.* [135] and Zahedi *et al.* [136] investigated thin film Pd membranes on porous stainless steel substrates. They produced membranes with a thickness ranging from 7-12 µm and measured the permeability as high as 2.06×10^{-8} $mol.m^{-1}.s^{-1}.Pa^{-0.5}$ at 450 °C. However, the membranes exhibited H_2 selectivity (over N_2) which had a value of only up to 685. Long-term stability tests at 600 °C also revealed the formation of pinholes in the thin films.

In another work, Li *et al.* [137] produced 5 µm thick Pd membranes on Al_2O_3 substrates via electroless plating. Although, Pd membranes exhibited a permeability very close to its pinhole-free foil form, i.e. thicker than 20 µm, H_2 selectivity over N_2 was achieved around 2100 at temperatures ranging from 350 °C to 450 °C. Uemiya *et al.* [141] differently studied porous glass tubes as substrates and produced relatively thick, i.e.18-20 µm, Pd membranes via electroless deposition. However, the complete selectivity also could not be achieved in this study.

Although thin film deposition techniques are effective in reducing the material quantity to lower the membrane cost, the thickness reduction brings some problems. These are; crack formation under temperature cycles due to thermal expansion mismatch between the film and substrate and the formation of pinholes in the membranes causing lower H_2 selectivity. There is, therefore, a great effort on improving the substrate surface conditions so as to fabricate thin film membranes with a defect-free structure.

CHAPTER 4

COMBINATORIAL DEPOSITION OF THIN FILM MEMBRANES FOR HYDROGEN SEPARATION AND THEIR CHARACTERIZATION

This chapter consists of five sections. The magnetron sputtering system which was developed for the combinatorial study is described in the first section. A brief information on the thin film deposition of membranes via magnetron sputtering is also included in this section. This is followed by a section on material characterization techniques used in the current study. The third section deals with four-probe resistivity measurement used as a screening method to identify candidate compositions for the separation membranes. This is followed by a section which describes the methods used in fabricating selected membranes in the form of foils. The last section comprises a custom-made setup for permeability measurement.

4.1 Combinatorial Thin Film Deposition

A magnetron sputtering system was designed and constructed for the combinatorial thin film deposition. The system had a vacuum chamber of 458 mm diameter and 400 mm height, Figure 4.1. The system comprises three sputter guns in a triangular geometry with the center to center distance of 200 mm. The guns with dedicated shutters are installed in the chamber with high vacuum O-ring based feedthroughs which would allow vertical adjustments. The gun head could also be adjusted by tilting.

The chamber was connected to a turbomolecular pump backed by a rotary pump which can provide a base pressure down to $5x10^{-8}$ Torr. The chamber had quartz thickness sensors, with a sensitivity of ±0.1 Å, mounted next to each gun. All connections types in the chamber are conflate (CF), except the sputter guns and the main door.

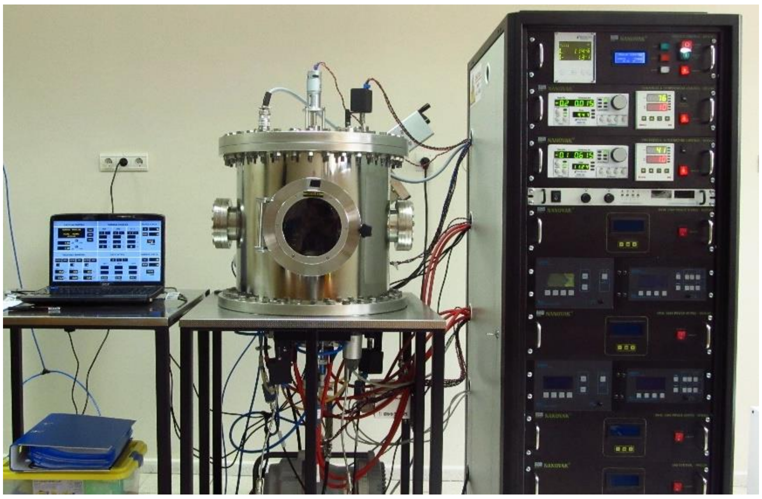

(a)

(b)

Figure 4.1 The view of the magnetron sputtering system and (b) a view from a typical simultaneous deposition.

The chamber had a gas inlet which allows an individual or simultaneous feeding of argon, oxygen, and nitrogen gases for ordinary or reactive sputtering. Each gas is controlled by an individual thermal mass flow controller which allows up to 50 sccm flow rate. The system is connected to a PC which allows the control of the sputtering parameters.

Two of the sputter guns were connected with an RF (300 watts) power supply, while the other one was connected to a DC (600 V, 2A) source. The system as constructed would allow the simultaneous deposition from the three targets, though if needed sequential deposition in the form of multilayers is also possible.

The substrate holder with dedicated shutter was typically 70 mm above the guns and could accommodate substrates up to 6-inch diameter. The system allows the rotation of substrate holder up to 8 rpm. It also has a facility for substrate heating with the use of quartz heating elements which could allow temperatures as high as 400 ºC. In the combinatorial study, the substrate holder was in the form of multiple sample holder accommodating substrates of 18 mm in diameter. A schematic representation of the multiple substrate holder is given Figure 4.2. The holder allows mounting of 21 substrates in a triangular fashion mimicking the geometry of the guns underneath.

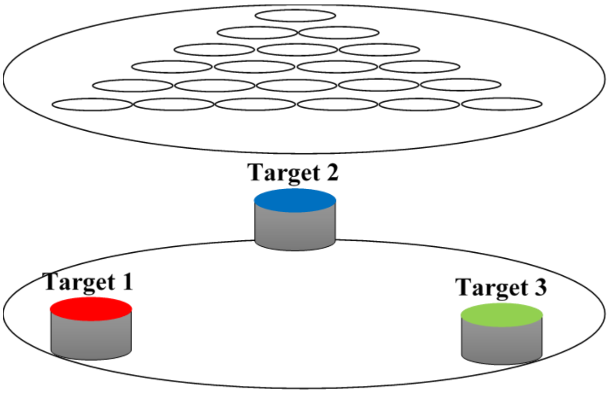

Figure 4.2 Multi-sample holder designed for combinatorial thin film deposition.

4.1.1 Calibration for combinatorial thin film deposition

The combinatorial thin film deposition relies on compositional variation which would be obtained as a result of a substrate having locations that vary with respect to targets underneath. The sputtering system was carefully adjusted so that all thin films would have similar thicknesses while yielding different compositions. Therefore, a deposition rate of 1:3 was aimed, referring to the sample at the center and the sample at the corner of the triangle, see Figure 4.2. In this way, the simultaneous deposition of three targets, each at the same deposition rate, would result in a uniform thickness distribution throughout all 21 samples.

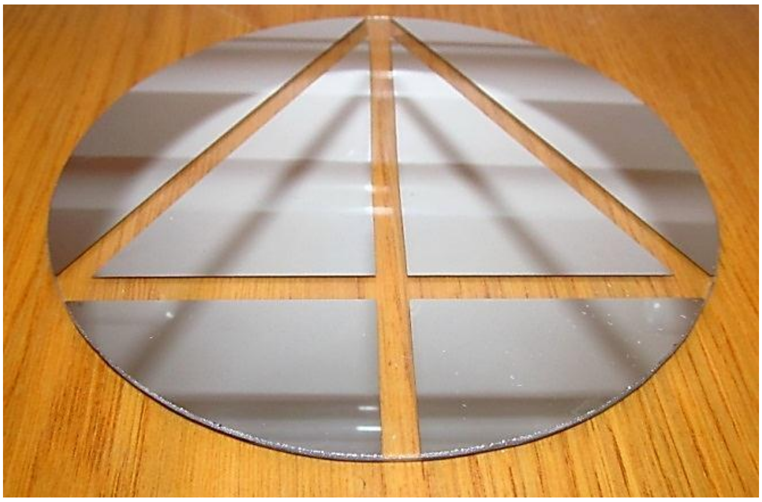

Figure 4.3 The traces of the Kapton tape removed from the glass substrate.

A series of calibration experiments were carried out for each target material used in the study to ensure the 1:3 ratio. The calibration experiments were performed on 6-inch plain glass substrates. Initially, 6 mm Kapton tape was adhered onto the glass substrate in a triangular geometry to imitate the actual holder geometry. The glass substrate was then loaded to the sample holder in the vacuum chamber and each sputtering target was positioned underneath at the corners of the substrate triangle. Typically, a 30 min of deposition was performed using only one target at a rate of 2Å/sec. The tapes on the glass substrate were then removed, Figure 4.3. The thickness of the films was measured along the traces of the Kapton tapes using a profilometer (Veeco, Dektak 6M). The film deposition and thickness measurements were repeated in cycles. Each sputter gun was aligned both vertically and angularly, until the thickness ratio of 1:3 was achieved.

4.1.2 Thin film deposition of ternary alloys

In a typical thin film deposition of a ternary alloy, 150 µm thick glass substrates with 18 mm diameter were placed in the multiple sample holder and then loaded to the vacuum chamber. The chamber was then evacuated down to 5×10^{-8} Torr and then was filled with ultra-high purity argon to 5mTorr.

Pre-sputtering was carried out for 10 minutes for surface cleaning of the target while the shutter was kept closed. Following the pre-sputtering, the gun shutters, as well as the main shutter, were then opened and the simultaneous deposition was carried out at a constant rate of 2 Å/s for each target for 250 min. Typically, each deposition yielded ~3 µm thickness for all samples.

4.2 Structural Characterization

The chemical composition of thin film membranes obtained via magnetron sputtering was determined in SEM (FEI Nova Nano 430) with the use of energy dispersive spectroscopy (EDS). The membranes were characterized morphologically in both secondary and backscattered electron imaging mode. EDS measurements were carried out at 20 kV accelerating voltage with a beam current of 1.5nA. Elemental quantification in analyses with ±2% accuracy was made using atomic absorption fluorescence (ZAF) correction method [142].

Phases present in membranes were determined with X-Ray diffraction in Bragg-Brentano mode using Rigaku DMAX2200 with Cu-Kα radiation. Where necessary the patterns were analyzed with Rietveld refinement using the software Maud [143].

4.3 Four-Probe Resistivity Measurement

Four probe resistivity of thin films were measured in a purpose-built set-up, Figure 4.4 (a). The measurement was carried out in a reaction chamber with a diameter of 47 mm with a height of 175 mm. The chamber had a flange which allowed the chamber to be placed on a cylindrical furnace, 80 mm of which inside the furnace.

The reaction chamber was connected to a line ¼ inch diameter which could be connected to a feeding gas, i.e. argon or hydrogen, or could be taken under vacuum. For this purpose, a vacuum pump station (Pfeiffer HiCube 80 Eco) was used incorporating a turbopump backed by a rotary pump. The reaction chamber had a sample holder connected to the top lid. The holder could accommodate thin film membranes of up to 20 mm diameter placed on a holder located close to the bottom of the chamber, Figure 4.4 (b). Four gold coated tungsten rods of 2 mm diameter were used as electrodes for the four-probe measurements. The rods were attached to the lid with gold plated springs and with quartz guides housed in a stainless steel guiding plate so as to apply gentle pressure to establish good contact with the sample. The distance between each rod was kept equal with a value of 3.5 mm. The lid also incorporated a K-type thermocouple which was extended and was in close proximity to the sample the sample holder.

Measurements were taken by Keithley 2700 digital data acquisition system with an integrated 7700 module providing multi-channel connections. In the measurements, a current, 10 mA ±5%, was applied through the two outer probes and the voltage was measured from the inner probes, Figure 4.5. This configuration allows the measurement of the resistance of the films while eliminating the resistance raised from the wires and the contacts. The resistivity of thin films was calculated with Equation 4.1 and Equation 4.2 [144] which adapted for the equally spaced four-probe geometry.

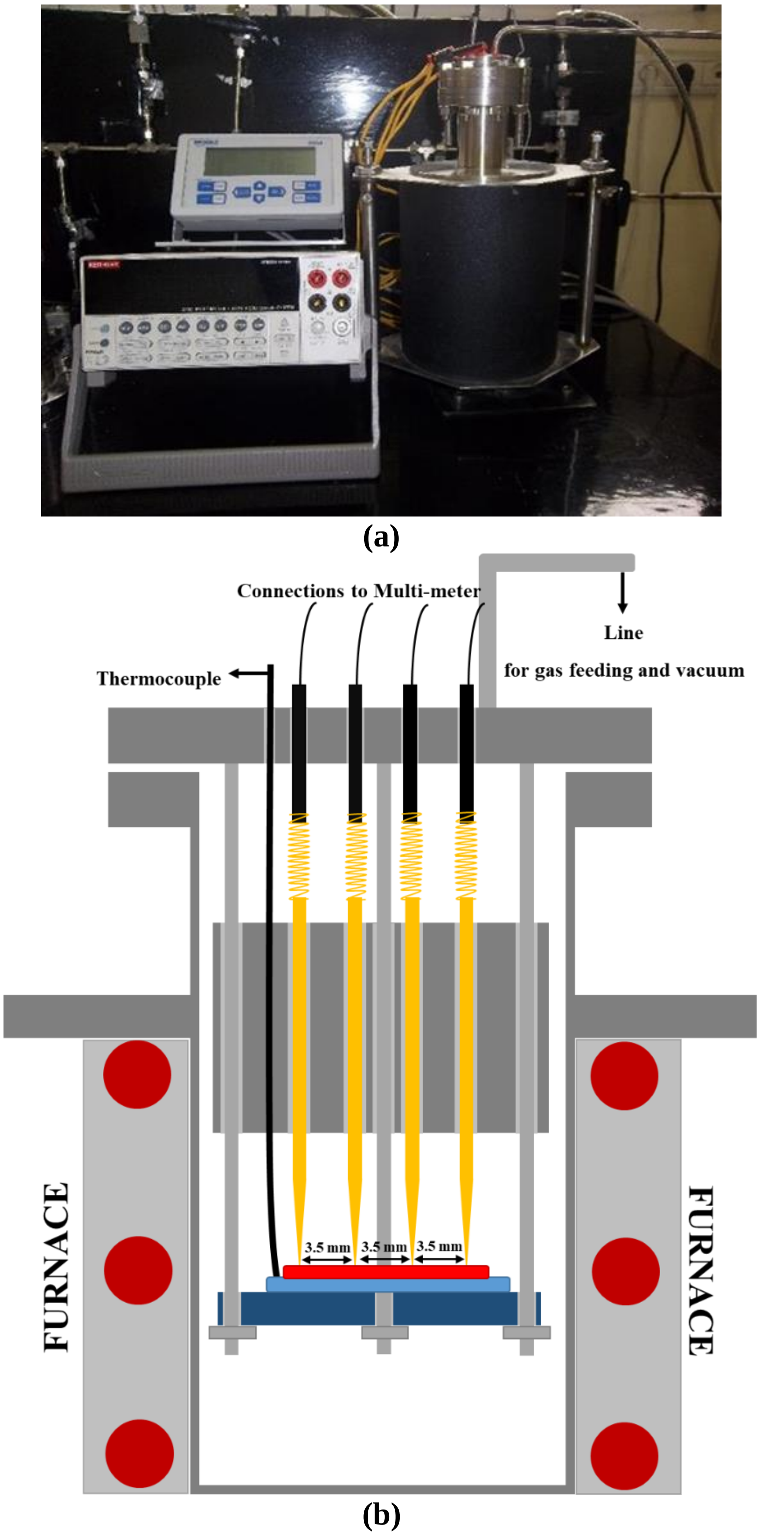

Figure 4.4 (a) Purpose built set-up for four-probe resistivity measurement and (b) drawing of the reaction chamber.

$$R_{\text{sheet}} = \frac{V}{I} \cdot \frac{\pi}{\ln(2)} C\left(\frac{d}{s}\right)$$

Equation 4.1

$$\rho = R_{\text{sheet}} . t$$

Equation 4.2

Here, R_{sheet} is sheet resistance (Ω/sq) and ρ (Ω.cm) is the resistivity of the film, where V is voltage (V), I is current (A), t is the thickness of the sample (cm), and C is a correction factor dependent on d, diameter of sample (cm), and s, distance between the probes (cm).

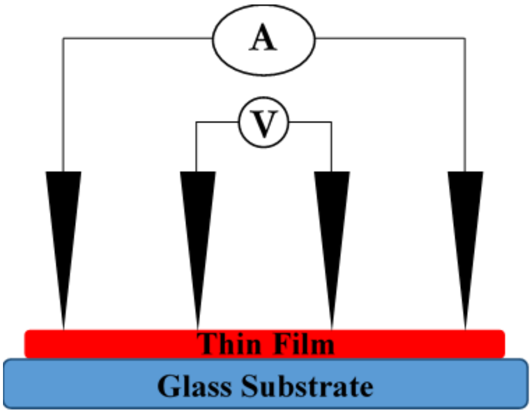

Figure 4.5 Four-probe configuration for resistivity measurement.

For measurements, the lid which had a CF connection to the chamber was opened first and the membrane was placed onto the sample holder which was displaced downwards by unscrewing the holding nuts underneath. The holder was then displaced upwards by screwing the nuts as a result electrodes were allowed to press onto the sample. The lid was then closed and the chamber was taken under vacuum. Thereafter, argon (1 bar, absolute) was fed to the chamber. This process was repeated three times.

Prior to resistivity measurements, membranes were annealed in the reaction chamber under an argon atmosphere at 450 ˚C so as to stabilize their microstructure. During annealing, the resistance in the membrane was monitored as a function of time. The annealing duration, typically 3h, was determined at a point where the resistance change in the membrane became negligible.

4.3.1 Reactivity Index

Resistivity measurements in this thesis were presented on a relative basis with the use of a reactivity index. This involved two measurements one under argon and the other under hydrogen. Initially, the membrane was heated up to 450 °C under an argon atmosphere and then cooled down to the room temperature each with a rate of 5 °C/sec. The resistivity under argon, ρAr, was recorded as a function of temperature during this heating/cooling cycle. The same procedure was repeated under hydrogen, yielding values of ρH_2. The reactivity index as defined as a resistivity ratio, $\rho H_2/\rho Ar$. The reactivity index of $\rho H_2/\rho Ar=1$ implies that the resistivity of the membrane is the same both under argon and under hydrogen. This implies that the membrane does not react with hydrogen, where the membrane reacts with hydrogen the reactivity index becomes higher than 1, $\rho H_2/\rho Ar > 1$.

4.4 Fabrication of foil membrane

Foils of selected compositions were fabricated using an arc melter (Edmund Bühler GmbH, Compact Arc Melter MAM-1). In a typical arc-melting process, the desired amount of elements, typically 2-5 g in total, were loaded onto a copper plate of the arc melter. The chamber was evacuated down to 7.5×10^{-3} Torr and it was then filled with high-purity argon. A top electrode was brought close to the sample and DC current was then applied to initiate an arc through the sample. Thus, the temperature was increased at a point causing the sample to be melted. In order to provide a compositional homogeneity in samples, melting procedure was typically repeated at least three times.

The melt buttons were then fed to a rolling mill. The reduction employed was typically 10-20% for each rolling. In the initial stages, the rolling deformation was followed by an annealing treatment to prevent edge cracking. Having reached a thickness of approximately 1 mm, the rolling as continued without annealing. The final thickness of foils was 50 µm to 100 µm. Finally, foils were annealed at 450 °C for 1h so as to obtain a stable structure.

4.5 Permeability Measurement

Hydrogen permeability is measured based on the Equation 3.4 given in Chapter 3. This equation has the form;

$$J = \frac{k}{l}({P^n}_{H_2,feed} - {P^n}_{H_2,permeate})$$

Here, *J* is the hydrogen flux, *k* is the hydrogen permeability of the membrane, *l* is the membrane thickness and $PH_2, feed$ and $PH_2, permeate$ are the hydrogen partial pressure at the feed and the permeate side, respectively. In order to measure the hydrogen permeability of a membrane with a known thickness, it is necessary to measure the hydrogen flux under defined feed and permeate pressures.

This measurement was carried out in a purpose-built set-up, Figure 4.6. The set-up consisted a test-cell incorporating a heating unit, an inlet line, and the outlet line. Both lines could be connected to either argon or hydrogen or could be taken under vacuum (Pfeiffer HiCube 80 Eco) when needed.

The gas pressure at the feed (inlet) and permeate (outlet) sides was monitored by pressure transmitters (Keller 21Y, 9 bar, and 5 bar, respectively). H_2 flux was monitored with two thermal mass flow meters (Brooks Instruments SLA5850). One of the flow meters was calibrated for a low range H_2 flux between 0-10 sccm, while the other was calibrated for the range of 0-1000 sccm. The pressure transmitters and the flow meters were connected to a four-channel read-out unit (Brooks Instruments, 0254) which could be also connected to a PC.

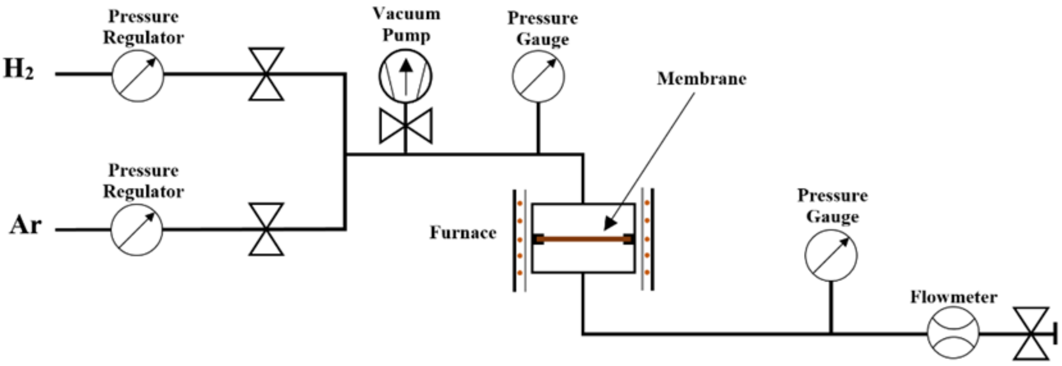

(a)

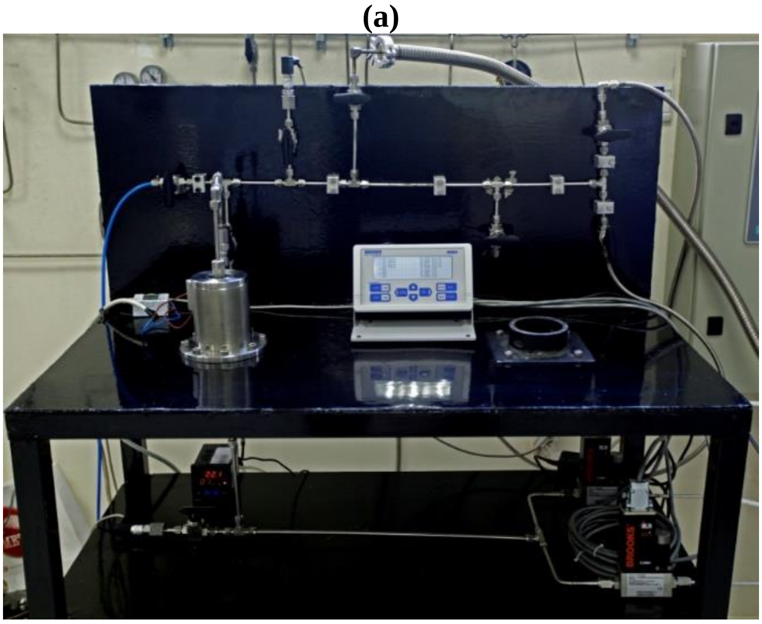

(b)

Figure 4.6 (a) Schematic representation and (b) the view of the set-up used in permeability measurements.

The test cell incorporates an 800-watt heating element which allows the testing at temperatures up to 500 °C, Figure 4.7. The temperature of the sample was monitored via a thermocouple located inside within the test-cell with ±0.1 °C sensitivity. The test-cell allows the testing of samples with a 19 mm diameter.

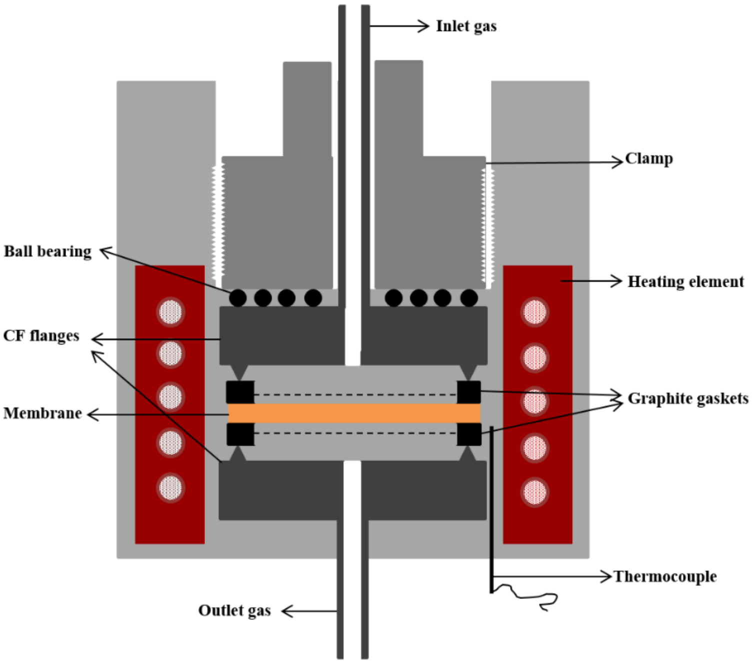

Figure 4.7 Schematic drawing of test cell that was used in permeability tests [145].

In a permeability test, the membrane was placed between two graphite gaskets in a CF configuration in order to attain gas tightness during the test. The flanges were tightened against the gaskets by screwing a hollow nut located above the upper flange. So as to allow free rotation, stainless steel balls of 4.75 mm diameter were used in between the upper flange and the hollow nut. The balls were in a cage so that they could be handled with ease.

The membranes were initially tested with argon to check the gas tightness of the membranes and the connections. The argon pressure at the feed side was increased to as high as 10 bar and the gas flow and the change in pressure at the permeate side was checked. Upon ensuring the gas tightness, the cell was then heated up to test temperatures under argon atmosphere. Argon was then evacuated and the feed side was filled with high-purity hydrogen at the desired pressure.

During measurements, the pressure at the permeate side and the hydrogen flux were monitored as a function of feed pressure. Typically, the initial feed pressure was 1 bar which was increased up to 10 bar with increments of 0.5 bar. At a given feed pressure, the permeate pressure which was initially low increases somewhat and when this was stabilized, both permeate pressure and the flux as monitored by the flowmeter were recorded. This gives delta P versus flux values from which the permeability could be calculated with the use of Equation 3.4 where n was assigned a value of 0.5.

CHAPTER 5

SEPARATION MEMBRANES BASED ON Nb-Pd-Ti

An investigation was carried out into Nb-Pd-Ti ternary system to determine possible body-centered cubic (b.c.c.) membranes that can be used for hydrogen separation. A library of thin films was produced covering the greater portion of Nb-Pd-Ti ternary diagram using combinatorial approach. The library was screened both structurally and in terms of a reactivity index defined as the ratio of the resistivity measured in the films under hydrogen and argon. The study showed that a substantial portion of compositional field stretching from Nb to Ti yield thin films with b.c.c. structure. The evaluation based on the reactivity index showed a narrow region close to Nb corner as possible compositions for separation membranes. The b.c.c. field was also screened with regard to the lattice volume so as to identify regions of acceptable hydrogen solubility. The superposition of two maps; one reactivity index and the other lattice volume yield a field $32<Nb<41$, $27<Pd<44$, $20<Ti<38$ as possible compositions for separation membranes.

5.1 Introduction

Metallic separation membranes are important for purification of hydrogen produced by means of processes such as coal gasification or steam reforming of natural gas [26,146]. Such membranes are quite attractive especially for industrial-scale production since there is an increasing demand for high-purity hydrogen, >99.97% [147], for a variety of applications [147,148].

Metallic separation membranes basically fall into three groups; face-centered cubic (f.c.c.), body-centered cubic (b.c.c.) and amorphous membranes. Among them, Pd and its alloys [56,69,149–153], i.e. f.c.c. based membranes are attractive due to their high hydrogen permeability and selectivity at operating conditions. Indeed, Pd and its alloys are quite convenient as a separation membrane and are commercially available [154]. Even though Pd-based f.c.c. membranes have found practical applications, they suffer from high-cost which restricts their widespread use in industrial applications [155].

Amorphous membranes are generally more attractive than their crystalline equivalents since they exhibit superior hydrogen permeability [26]. However, the metastable nature of these alloys constitutes a risk altering the structure of the alloys under operating conditions [97,156]. This restricts the use of amorphous separation membranes to reduced temperatures, typically less than 300 °C.

For the b.c.c. membranes, Group V transition metals such as Nb, V and Ta have attracted considerable attention due to their superior permeability. Indeed, the permeability of these metals is orders of magnitude faster as compared to that of Pd-based membranes [98]. The high permeability of these membranes is attributed to their more open b.c.c. structure allowing higher hydrogen solubility and faster hydrogen diffusion. However, the solubility of hydrogen in b.c.c. membranes could be excessively high due to this open structure which often leads to the embrittlement [87]. Therefore, the efforts in b.c.c. membranes have concentrated on reducing the level of hydrogen solubility while maintaining reasonably high permeability [87,97,98]. There are mainly two approaches in alleviating the brittleness of b.c.c. membranes. One is to aim for multi-phase alloys where the permeable phase co-exists together with another phase often a eutectic which tolerates and absorbs the ensuing volume changes in the permeable phase [119]. Such multi-phase alloys cover compositions in alloy systems such as Nb-Ti-Ni [106,157–159], Nb-Ti-Co [62,107], V-Ti-Ni [59,160], Ta-Ti-Ni [161]. Another approach is to have a single phase solid solution with controlled hydrogen solubility. There are numerous studies on single solid solutions based on Nb [109,111], V [113,114,119], or Ta [115] so as to improve the embrittlement resistance compared to their pure equivalents.

Studies with regard to alloying whether it is aimed for multiphase alloys, or for a solid solution are quite time-consuming, as there would be many alternatives in the compositions. The combinatorial methodology is particularly suitable for such investigations as this would allow the study of multiple alloy compositions in a single experiment [162–164]. This was previously demonstrated for f.c.c. based membranes in ternary alloy systems Pd-Ag-Ti [165] and Pd-Ag-Ni [166].

The current work focuses on b.c.c. alloys so as to identify the possible compositions as separation membranes. The choice was made for Nb-Pd-Ti ternary system. The basis, for the current work, is Nb which has b.c.c. structure with superior hydrogen permeability. The element Ti, normally with the hexagonal crystal structure, was selected because it could occur in b.c.c. form when sputter deposited [167] and therefore it could extend the b.c.c. field in the ternary alloy system. Here, the Pd was included in the alloy system as it is an essential ingredient due to its catalytic activity in hydrogen separation processes. The emphasis, however, is on Pd lean alloys so as to aim for cost-effective membrane compositions.

5.2 Experimental

Nb-Pd-Ti thin film membranes were produced by simultaneous deposition of Nb, Pd, and Ti via magnetron sputtering. For this purpose, sputter guns each with 50 mm in diameter were arranged in a triangular fashion with a stem-to-stem distance of 200 mm, see Figure 5.1. The chamber was evacuated down to $1x10^{-7}$ Torr base pressure and the deposition was carried out at 5 mTorr argon at room temperature.

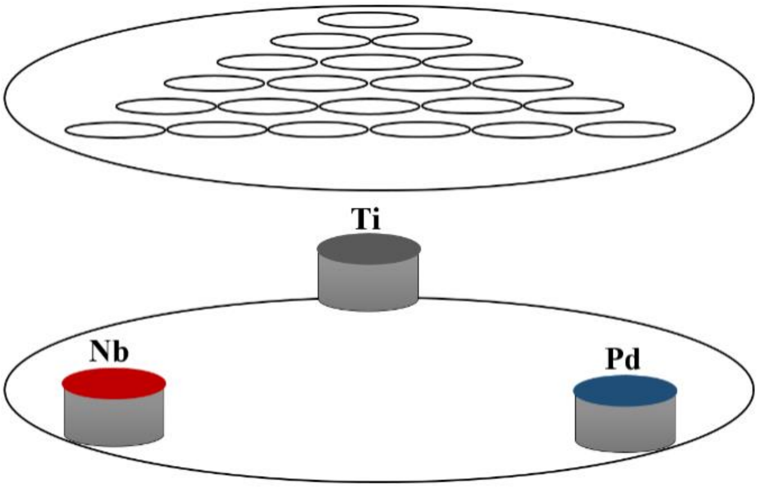

Figure 5.1. Schematic representation of target-substrate holder alignment.

Prior to deposition, target to substrate holder distance as well as the angular position of the targets were carefully aligned in order to yield membranes of the same thickness values. For this purpose, a glass substrate of 6-inch diameter was used and each target was separately aligned to yield a position rate in the middle of the substrate which was one-third of that just above the target. The rate was followed by measuring the film thickness via a profilometer (Veeco, Dektak 6M) removing the Kapton tape adhered onto the glass.

Following the alignment of sputter guns, the substrate was replaced by a multiple sample holder comprising 21 substrate housings in a triangular geometry, positioned above the sputtering targets, Figure 5.1. The glass substrates, each in 18mm diameter with 0.15 mm thickness were loaded to the holder. All three sputter guns operated simultaneously yielding thin films of the same thickness but each with a different composition. The deposition rate measured at the respective corner of the triangle was 2 Å/sec for each target yielding thin film membranes of 3 µm in thickness. Thus, the deposition was carried out for a duration of 250 minutes. In this way, 21 chemically distinct thin film membranes were produced in a single experiment.

All thin films were subjected to an annealing treatment at 450 °C for 3h under argon atmosphere before testing. The purpose of this treatment was to stabilize the film structure. The library of thin films was then screened based on their reactivity to hydrogen. This was evaluated indirectly by measuring the resistivity of the films via a four-probe technique as discussed in section 4.3.

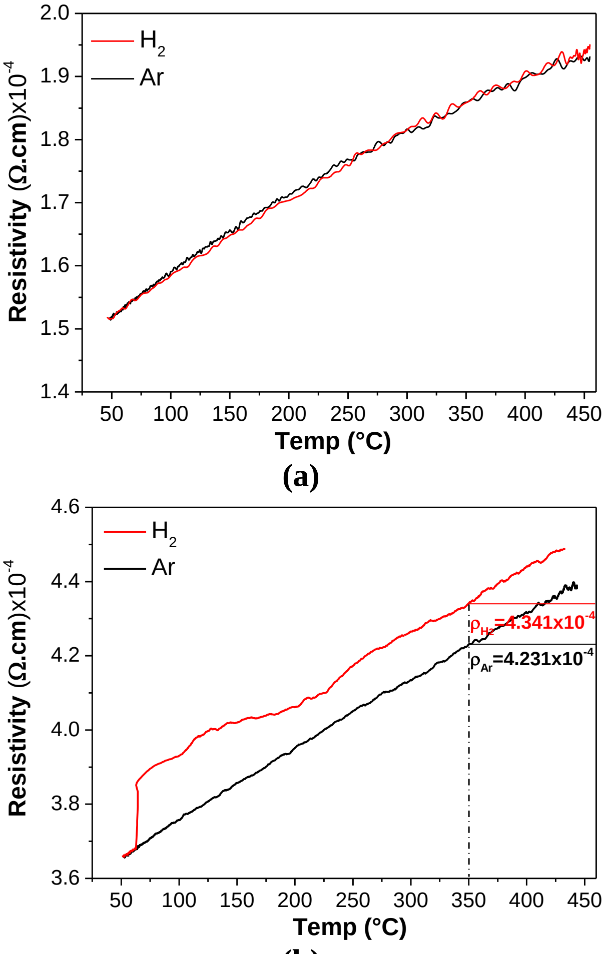

(a)

(b)

Figure 5.2. Resistivity versus temperature profiles recorded under argon and under hydrogen (a) for Nb10Pd13Ti77 exhibiting $\rho H_2/\rho Ar=1$ at all temperatures and (b) for Nb44Pd29Ti27 exhibiting $\rho H_2/\rho Ar=1.026$ at 350 °C.

The resistivity, ρAr, was determined as a function of temperature while the membranes were heated under argon up to 450 °C with 5 °C/min. This procedure was repeated under hydrogen atmosphere (50 mbar, 99.95%) yielding ρH_2. The resistivity ratio, $\rho H_2/\rho Ar$, was calculated at selected temperatures and this was used as the reactivity index for the membranes. Typical examples of resistivity profile recorded under argon and hydrogen are given in Figure 5.2 together with reactivity index determined at 350 °C. Here Figure 5.2 (a) refers to an alloy where the resistivity is the same both under argon and hydrogen giving $\rho H_2/\rho Ar=1$, whereas Figure 5.2 (b) this values $\rho H_2/\rho Ar>1$ implying that the film reacts with hydrogen resulting in the higher values of the resistivity.

The resistivity profile measured both under argon and hydrogen was monitored carefully. The thin film compositions where there was an abrupt change in resistivity with temperature was treated as a sign crack formation and therefore they were discarded. Thus, in all compositions for which the data was reported the change in resistivity was gradual and therefore had a structural origin. This implies that where $\rho H_2/\rho Ar>1$, the thin film reacts with hydrogen which could be due to simply dissolution of hydrogen in the lattice [168] and/or due to hydride formation [169].

Thin film membranes were structurally characterized by X-ray diffraction (XRD). Measurements, $20<2\theta<100$, were taken by a Rikagu DMAX2200 using Cu-Kα radiation. Diffractograms were evaluated with regard to crystal structure and the lattice volume and where necessary the patterns were refined with Rietveld analysis to determine the precise lattice parameters. The morphology of the membranes was investigated by a field emission scanning electron microscope (SEM, FEI Nova Nano 430). The chemical analysis of the membranes was determined in SEM with the use of EDS analysis. This was carried out at an accelerating voltage of 20 kV with a beam spot size of <10 nm yielding an accuracy of ±2 at % for the current elements.

5.3 Results and Discussions

Chemical compositions of the thin film membranes are shown in Figure 5.3. Here the values shown refer to averages obtained from a total of nine measurements distributed over the surface of each thin film. Since the thin films were quite wide, i.e. 18 mm in diameter, the composition varied across the width. The standard deviation of the elements was typically less than 3 at.%.

The distribution of the average thin film compositions given in Figure 5.3 shows that a large proportion of the ternary phase field is covered quite successfully by combinatorial deposition. The compositions that yielded b.c.c. structure are shown with an open circle in Figure 5.3 where they cover an extended range of compositions from Nb corner to Ti corner extending into far right into Pd-Ti binary line. All 21 membranes were evaluated using X-Ray diffraction so as to determine their structure. Figure 5.4 shows typical examples. Figure 5.4 (a) refers to Nb76Pd13Ti11, close to Nb corner, with a b.c.c. crystal structure. SEM micrograph of this film showed an elongated grain structure with widths 100-300 nm and lengths up to 1 µm, Figure 5.4 (b). Another XRD pattern of a b.c.c. thin film away from Nb corner, Nb36Pd28Ti36, is given in Figure 5.4 (c). Here the grain structure is more equiaxed, Figure 5.4 (d). The b.c.c. field in the ternary diagram extends to as far away as Ti corner, Nb10Pd13Ti77. Here, the thin film appears to have a very strong (110) preferred orientation with a refined grain structure, Figure 5.4 (e). The b.c.c. field, in the portion of the ternary diagram covered in this work, see Figure 5.3, was interrupted in Pd corner where there are several thin films with f.c.c. structure as well as very close to Ti-Pd line where there are multiphase membranes. Examples of f.c.c. and multi-phase patterns are given in Figure 5.5. Still, b.c.c. is the most dominant phase in these multiphase thin films.

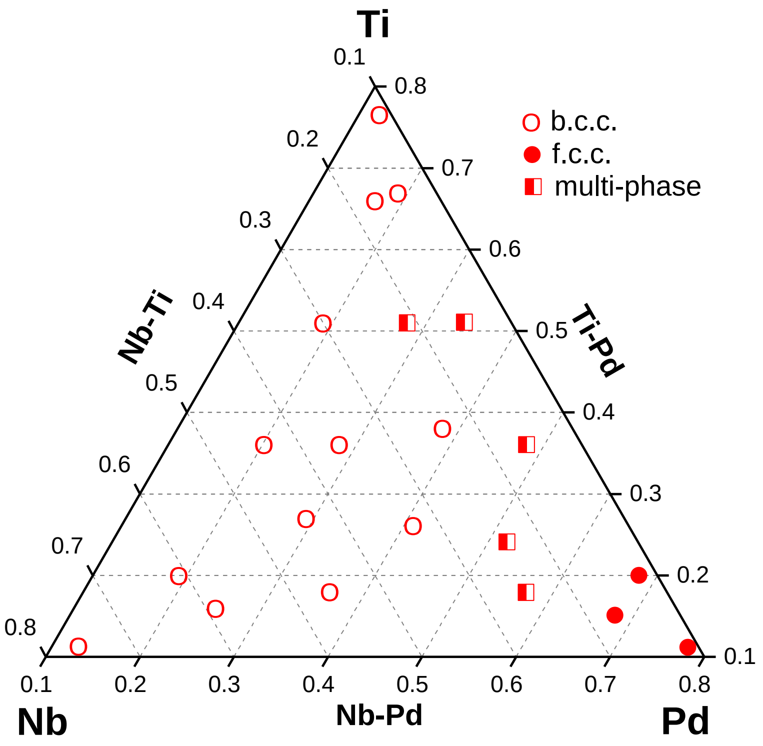

Figure 5.3. The compositional distribution of the membranes on the ternary diagram Nb-Pd-Ti. Open circles refer to thin films with b.c.c. crystal structure, while the filled circles refer to those with f.c.c. structure. Half-filled square symbols refer to multi-phase thin films. Compositions selected for detailed study refer to those shown with open circles, i.e. b.c.c. thin films.

The thin films throughout the ternary field based on b.c.c. phase were tested individually under argon and hydrogen in terms of their reactivity index up to temperatures of 450 °C. However, not all tests were successful. The membranes very near to Nb corner were too brittle and fractured into pieces as soon as they were exposed to hydrogen.

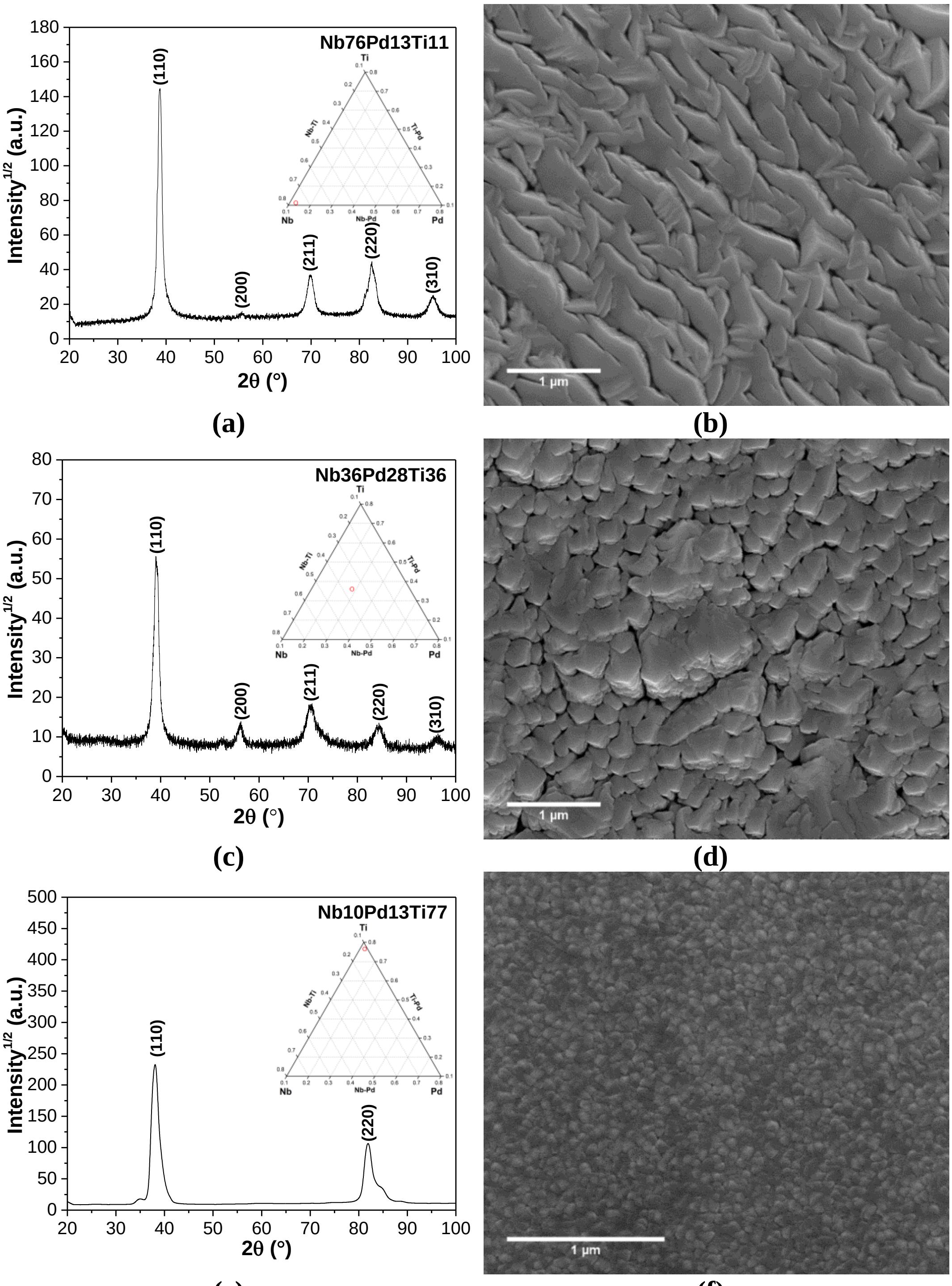

(a) (b)

(c) (d)

(e) (f)

Figure 5.4. XRD patterns of (a) Nb76Pd13Ti11, (c) Nb36Pd28Ti36 and (e) Nb10Pd13Ti77 thin films and their SEM images in the respective order of (b), (d) and (f).

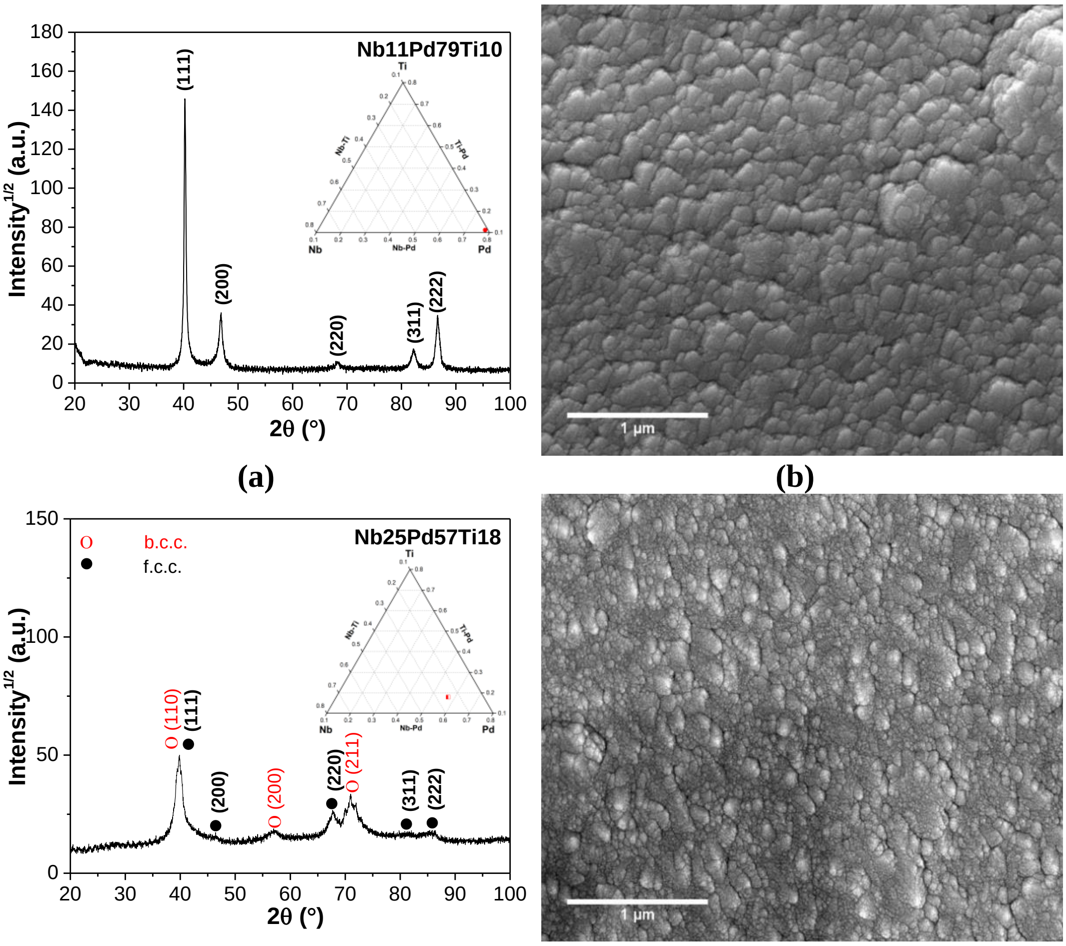

(a) (b)

(c) (d)

Figure 5.5. XRD patterns of (a) f.c.c. Nb11Pd79Ti10 and (c) multi-phase Nb25Pd57Ti18 thin films, and their SEM images in the respective order of (b) and (d).

Plots of the reactivity index, i.e. $\rho H_2/\rho Ar$ where ρH_2 and ρAr are resistivities measured under hydrogen and argon respectively, are mapped in Figure 5.6 at 350 °C as well as at 400 °C. Here, in the greater fraction of the area, $\rho H_2/\rho Ar=1$, i.e. the membranes do not react with hydrogen. Where $\rho H_2/\rho Ar>1$, the membranes that react with hydrogen, compositions are confined to the small region centered on Nb59Pd25Ti16.

There are two possibilities as to why the resistivity increases upon exposure of the thin film to hydrogen. One is that it might form a solid solution, i.e. hydrogen dissolves in the host lattice without forming a separate phase. It is well known that change in resistivity correlates well with the solubility of hydrogen in the lattice. This was clearly shown for b.c.c. membranes by Watanabe *et al.* [168] and for f.c.c. alloys by Pozio *et al.* [170] in which the resistivity change was followed as a function of dissolved hydrogen. The other possibility is that the dissolution might lead to the formation of a new hydride phase. Normally the formation of a hydride phase is associated with a large volume change which, as discussed above, leads to embrittlement problem. So the form of a reaction with hydrogen desirable in the alloys is a solid solution rather than a hydride formation. Thus, for a given alloy system whether in the form of the solid solution or the hydride formation, $\rho H_2/\rho Ar$ could be used as a measure of hydrogen content [166]. Since the permeability is the product of diffusivity and the solubility of hydrogen in the lattice [84], the compositions where $\rho H_2/\rho Ar>1$ could be treated as potential candidates for separation membranes.

It should be mentioned that in b.c.c. membranes, often the problem is excessive solubility of hydrogen in the lattice which makes the membrane quite brittle. In fact, in the present study, membranes very near Nb corner suffered from this brittleness probably due to the excessive hydrogen solubility. Thus, efforts in the literature have concentrated on reducing the level of hydrogen solubility while maintaining reasonably high permeability. One approach is to aim for multi-phase alloys where the permeable phase co-exists together with another phase often a eutectic which tolerates and absorbs the ensuing volume changes, often the cause of brittleness in the membranes [119]. There are multiphase compositions in the current ternary system, see Figure 5.3, which could be considered for this approach. However, none of them reacted with hydrogen, indicating that they are unsuitable as separation membranes.

Another approach is to have a single phase solid solution with controlled hydrogen solubility. Here, the choice of operating conditions for the membrane is quite relevant as the solubility could be controlled by a careful choice of operating conditions [111]. With regard to current compositions, the measured values of $\rho H_2/\rho Ar$ within the triangular region are lower at 400 °C than those at 350 °C. Thus the choice of higher operating temperature might be beneficial in improving the resistance to brittleness.

Perhaps, the more fruitful approach in this respect is the structural modification of the alloys which would have inherently lower hydrogen solubility. An easy way of controlling the hydrogen solubility in b.c.c. membranes is via alteration of the lattice volume. This has been well illustrated by studies carried on Nb-W-Mo [109] and Nb-W-Ru [111]. It is well known that the solubility in Nb-based b.c.c. membranes decreases with decreasing lattice volume [171]. In fact, the choice of the current elements is suitable for this approach as the atomic radii of Ti and Pd are smaller than that of Nb allowing volume contraction with alloying. Yukawa *et al.* [111] showed that the limiting value for hydrogen solubility could be taken as H/M=0.20 so as to avoid brittleness in Nb-based membranes. Data collected from the literature [109,111] imply that this limiting H/M value corresponds to a lattice volume that ranges from 35.43 to 35.50. Taking the upper limit of this volume, i.e. 35.5 $Å^3$ as an indicator for acceptable lattice volume, a contour mapping of lattice volumes is prepared as shown in Figure 5.7. It is seen that thin films with $25<Nb<45$, $22<Pd<54$ and $18<Ti<45$, have lattice volumes less than 35.5 $Å^3$.

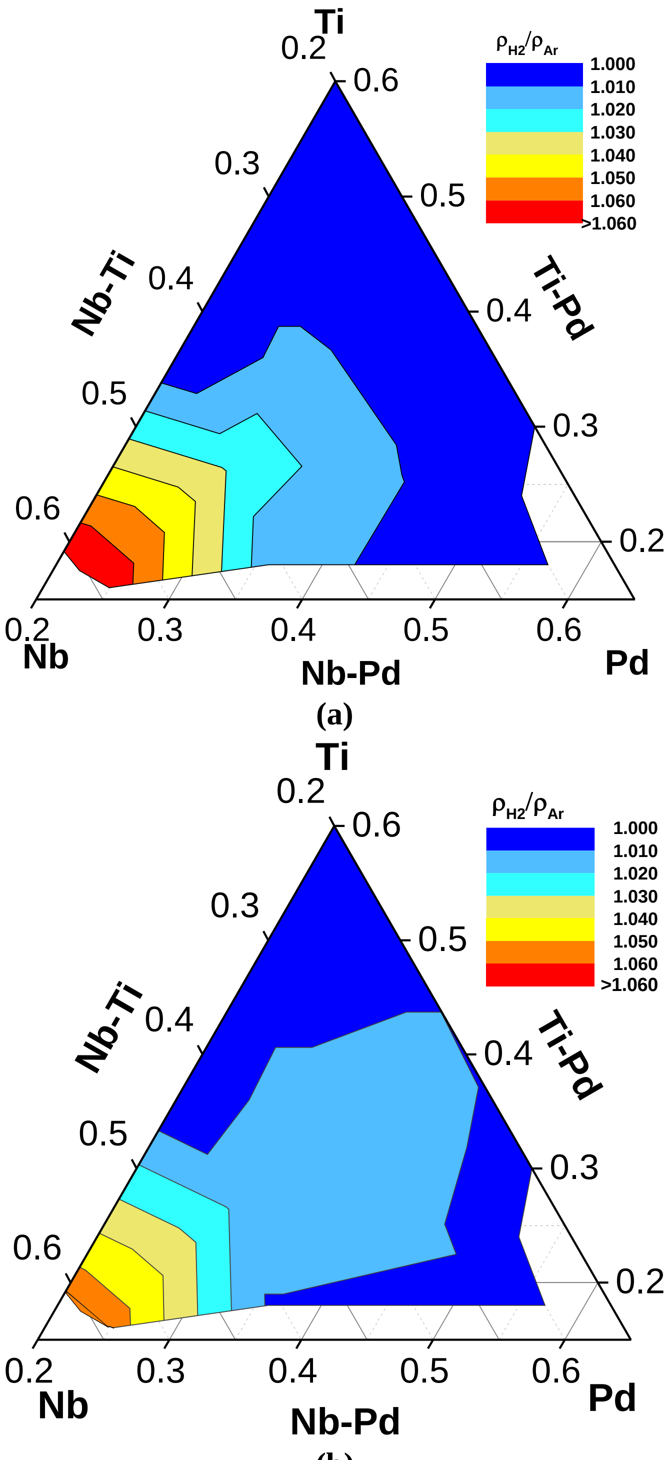

(a)

(b)

Figure 5.6. Contour mapping of reactivity index $\rho H_2/\rho Ar$ for Nb-Pd-Ti ternary system. (a) 350 °C and (b) 400 °C. Regions mapped refer to thin films with b.c.c. crystal structure.

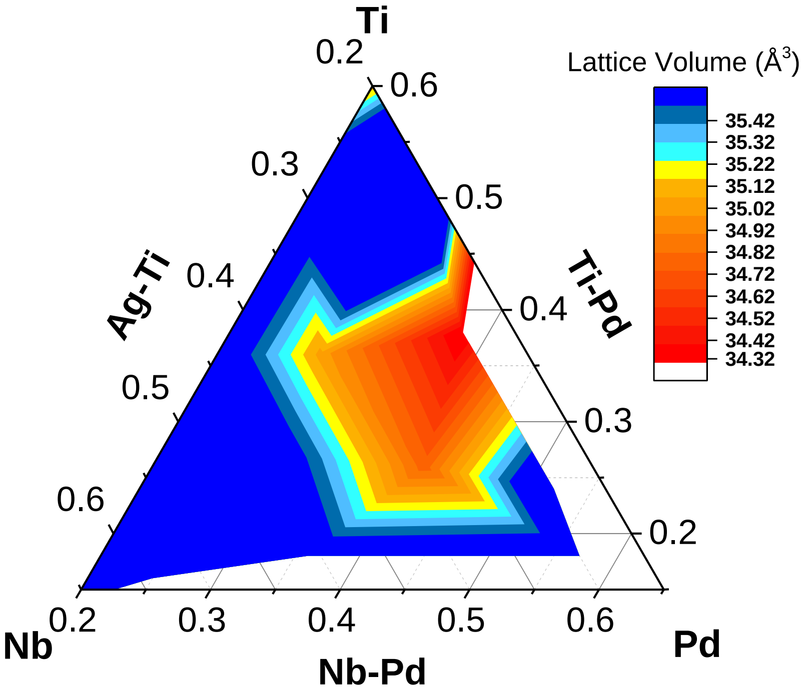

Figure 5.7. Contour mapping of lattice volume of b.c.c. phase in Nb-Pd-Ti Ternary system. Note that the lattice volume decreases in mid-compositions.

The two measures used in the current work, one reactivity index $\rho H_2/\rho Ar$, and the other lattice volume could be used in identifying the potential candidates for separation membranes. The reactivity index eliminates many of the compositions in Nb-Pd-Ti ternary system since the most membranes do not react with hydrogen. The compositions that are reactive with b.c.c. structure are confined to a small triangular region in the Nb-rich corner. Since Nb corner is extremely brittle, it is necessary to further screen these compositions so as to aim for potential membranes with acceptable durability. The requirement of the lattice volume less than 35.5 Å^3 yield quite a wide area in the ternary diagram, but the intersecting compositional field is quite narrow. The intersecting compositional field between the two maps is reproduced in Figure 5.8. It is therefore concluded that compositions within this intersecting field, covering alloys in $32<Nb<41$, $27<Pd<44$ $20<Ti<38$ could be considered as potential compositions for hydrogen separation membranes.

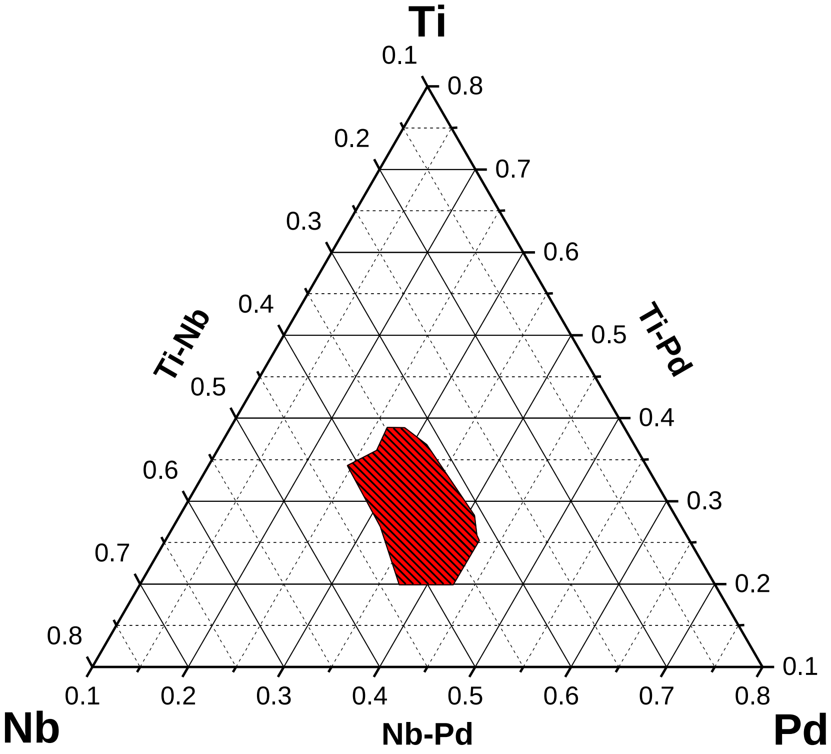

Figure 5.8. Intersecting compositional field between the maps of reactivity index where $\rho H_2/\rho Ar>1$ and the b.c.c. lattice volume <35.5 Å^3.

5.4 Conclusions

In the present work, a combinatorial study was carried out so as to identify b.c.c. membranes in Nb-Pd-Ti ternary system for hydrogen separation. A library of thin films was sputter deposited in a single experiment covering the greater portion of the ternary diagram. The thin films were screened structurally showing that;

i. the choice of Nb-Pd-Ti alloy system is quite suitable for b.c.c. membranes as the substantial portion of the compositional field is a single phase with b.c.c. crystal structure.

The library of thin films was screened in terms of a reactivity index, defined as the ratio of the membrane resistivity under hydrogen and argon. The map of reactivity index was plotted in the ternary diagram indicating that;

ii. Most b.c.c. alloys in Nb-Pd-Ti do not react with hydrogen and therefore are unsuitable as separation membranes. The thin films that do react with hydrogen are restricted to a narrow compositional region close to Nb corner.

The reactivity index in this narrow region has quite high values implying excessive hydrogen solubility in the lattice. Since the excessive hydrogen solubility is a sign of potential brittleness in the membrane, an additional criterion was introduced based on the lattice volume. Taking, based on the literature data, 35.5 $Å^3$ as the tolerable value, the lattice volumes of the thin films were mapped in the ternary diagram;

iii. The superposition of two maps; one reactivity index and the other lattice volume yield a field $32<Nb<41$, $27<Pd<44$ $20<Ti<38$ as possible compositions for separation membranes.

It may be pointed out that the area identified above cover a range of resistivity and the lattice volume values both satisfying the selected criteria. It is difficult to single out specific b.c.c. compositions in this area, but keeping the lattice volume close to the tolerable limit and selecting the composition with as high reactivity index as possible yield two compositions, namely Nb33Pd41Ti26 and Nb36Pd28Ti36. Finally, it may be emphasized that, if the permeability of these membranes is sufficiently high and comparable to that of commercial Pd77Ag23 f.c.c. membrane, the identified compositions would allow a significant reduction in Pd content. The compositions represent one-third to one-half reduction in Pd content on the weight basis.

CHAPTER 6

SEPARATION MEMBRANES BASED ON Pd-Ag-Ti (*)

An investigation was carried out into Pd-Ag separation membranes to check whether a reduction in their Pd content was possible through the incorporation of a third element, namely Ti. For this purpose, a combinatorial thin film deposition system was developed incorporating three sputter targets arranged in triangular form. The system had a substrate in the form of a magazine, 6-inch in diameter, accommodating 21 discs arranged again in a triangular form aligned with the targets underneath. With this geometry, a library of thin film membranes was obtained in a single experiment covering a wide compositional field, Pd content up to of approx. 75%. The thin film library was then screened with respect their tendency to react with hydrogen. This was accomplished by the resistivity measurements carried out on the membranes, while they are subjected to heating-cooling cycle under hydrogen, the values being compared with identical cycle carried out under argon. Since permeability is a product of hydrogen solubility and diffusivity, membranes that react with hydrogen, i.e. either forming a solid solution or a hydride, delineate compositions which are candidates for separation membranes. In the present work, this procedure was applied to a portion of Ag-Ti-Pd ternary system aiming for separation membranes with f.c.c. crystal structure. Mapping based on the resistivity measurement indicated, Ag35Ti22Pd43, Ag13Ti25Pd62 and their near compositions as possible candidates for separation membranes.

(*) This chapter was published with a title “Ti modified Pd-Ag membranes for hydrogen” in the International Journal of Hydrogen Energy, 40, (2015), 7553-7558.

6.1 Introduction

Hydrogen separation membranes allow filtration of hydrogen from mixed gases. Such mixtures may be produced via steam reforming of natural gas/coal/lignite [172] or through gasification of municipal wastes [173].

Hydrogen separated in this way may be used in fuel cells to generate electricity or may be fed directly to the natural gas grid. It is likely that the current network of natural gas will soon be transformed into a "gas" grid where hydrogen would be an essential ingredient [174]. All these require the use of efficient separation membranes, which when made possible would lead to an easy availability of hydrogen as is currently the case for natural gas.

Among the all metallic membranes, Pd is the essential element due not only its high permeability but also its catalytic effect and oxidation resistance even at elevated temperature [121]. However, membranes based on Pd are extremely expensive and therefore efforts have concentrated either on alloying to reduce Pd content [175,176] or to switch to non-Pd membranes making use of Pd only as a catalytic layer [112]. A reduction in membrane thickness through the use of thin films also reduces Pd content and thus has attracted considerable attention in recent years [177,178]. It is worth emphasizing that even pure palladium has its problems as a separation membrane. As could be verified from Pd-H phase diagram [122] when the Pd-H is cooled from an elevated temperature, initially a single phase f.c.c. the alloy is converted into a two-phase structure which results in a considerable volume expansion [179]. This phenomenon leads to the formation of microcracks which severely affects the durability of the Pd membrane.

There are two approaches in handling this embrittlement problem. One method is to control the temperature and pressure during operation so that the membrane is always in one phase region. The other is to alloy Pd so that transformation to the two-phase structure is avoided. This is most commonly achieved by alloying Pd with Ag. An addition of 20-30 at. % Ag is quite common which not only reduces the critical temperature for two-phase transition but also yields the permeability values which are up to 1.7-2.0 times of that of the pure Pd [128]. A similar result could also be obtained via alloying with Cu [130]. It was shown that that 40 wt. % addition of Cu can reduce the critical transformation temperature below the room temperature [180]. This addition also results in a %10 increase in hydrogen permeability [181] which arises mainly from an increase in hydrogen diffusivity [182]. In addition to Ag and Cu, elements such as Y, Fe, and Ni could also be used as alloying elements in Pd [128]. Of these, according to Fort *et al.* [183], Pd-Y is quite comparable to Pd-25%Ag alloy with a higher hydrogen permeability and better durability. Pd-Fe alloy membranes are interesting as they show no phase transformation [184].

All membranes reported above were developed via the traditional approach of synthesizing one membrane composition at a time and testing it for permeability. This is quite time-consuming and not always successful. The current work aims for f.c.c. membranes, similar to those reviewed above, but adopts the so-called combinatorial approach that would allow the synthesis of multiple material compositions in a single experiment. A library of thin film membranes produced is then evaluated by a rapid screening to identify the material composition as candidates for separation membrane. This approach was applied to a ternary alloy system Ag-Ti-Pd, i.e. Ag-Pd modified with Ti.

6.2 Experimental

In this work, a thin film deposition system was used, especially designed for the purpose of combinatorial studies. The system had a vacuum chamber 65 lt. in volume with all connections CF type, except for sputter gun stems and the main door. The chamber is connected to a turbomolecular-rotary pump system which can provide a base pressure in the range of $1x10^{-7}$-$5x10^{-8}$ Torr. The system had three sputter guns two of which were powered by RF (300 watts) and the third with DC (600 V, 2A) source. Each sputter target has individual quartz thickness monitor to measure the deposition rate with a sensitivity of ±0.1 Å.

Sputter guns each with 50 mm in diameter were arranged in a triangular fashion with a stem-to-stem distance of 200 mm. The targets loaded were Ag, Pd, and Ti. Target to substrate holder distance, as well as angular positions of the targets, were carefully aligned so that deposited film has the same thickness in the triangular area just above the targets, Figure 6.1 (a). This has been achieved by carefully aligning each target separately using a 6-inch diameter glass substrate. To obtain a uniform thickness, a given sputter target has to yield a deposition rate which is in the ratio of 1:3, the rates referring to the middle and the corner of the triangular region close to the target.

Having made the necessary alignment, the system was used with a substrate holder in the form of a magazine, 6-inch in diameter, accommodating 21 discs arranged in a triangular form aligned with the targets underneath, Figure 6.1 (b). Substrates loaded onto the magazine were ~0.15 mm thick soda-lime glass, 18 mm in diameter.

The reaction of the thin films with hydrogen was followed in a purpose-built reaction chamber with in-situ four-probe resistance measurement as discussed in section 4.3. Before measurements, thin film membranes were annealed at 450 ˚C for 3 hours in order to stabilize their microstructure.

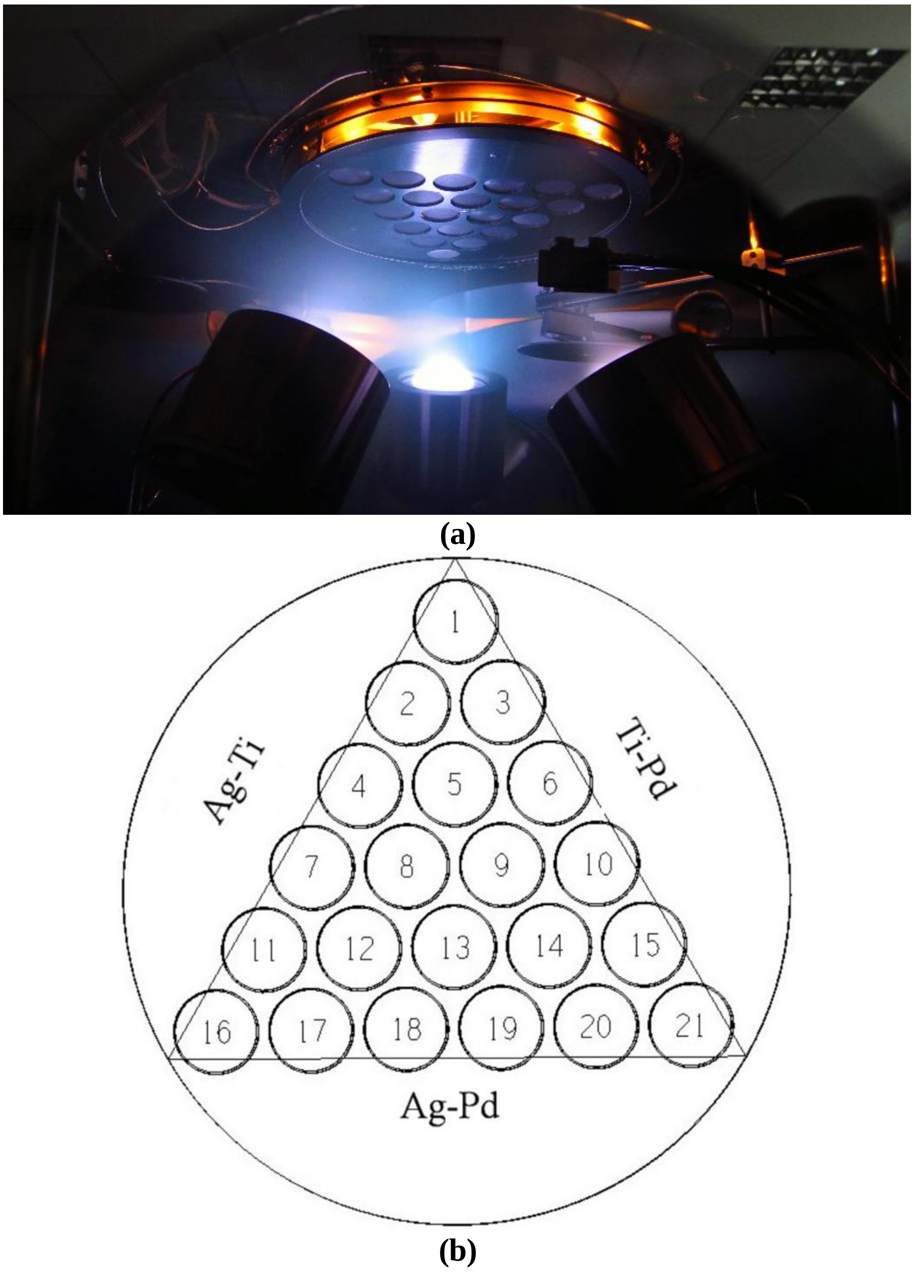

Figure 6.1. Sputter deposition of thin film membranes. (a) a viewgraph showing the targets and substrate magazine incorporating 21 glass substrates, (b) Triangular distribution of substrates in the substrate magazine.

6.3 Results and Discussions

Since the interest in present work was to investigate Pd lean composition, the deposition was carried out in such a manner as to cover compositions away from Pd rich corner. Having deposited the films, the resulting chemical composition of each membrane was determined with EDS analysis. Figure 6.2 shows the distribution of membrane compositions in the ternary diagram.

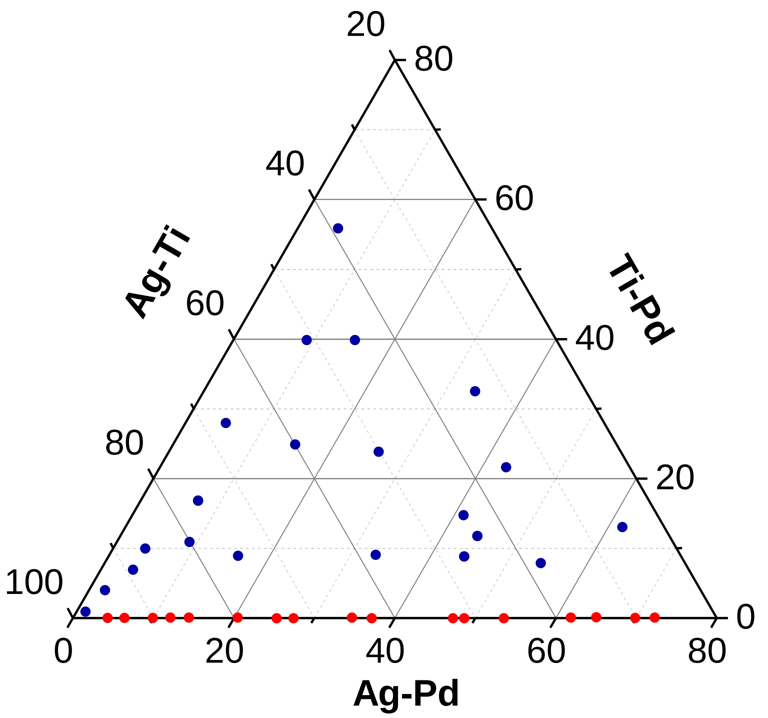

Figure 6.2. The chemical composition of thin film membranes in the ternary diagram. The diagram combines the samples that are generated in two experiments. Compositions of Ag-Pd binary thin films that were deposited separately are also indicated in the diagram.

Deposited films were 3 µm thick. Since the ultimate aim of this study was to produce membranes through classical metallurgical processing, i.e. membranes in the form of foils, this thickness was considered to be adequate and representative of bulk materials. Since the separation membranes are used at elevated temperature, the structure as it occurs in deposited films are not necessarily stable and may be subject to a change during its use. To take care of these changes and to ensure the use of more representative structure, preliminary experiments were carried out to determine the conditions for structural stabilization. For this purpose, a representative membrane was annealed at 450 °C for an extended period of time while the resistivity is monitored. As seen in Figure 6.3, a change in the resistivity is initially quite large but is reduced with time and becomes negligible after 3 hours. Following this observation, all membranes were subjected to stabilizing heat treatments which involved annealing under argon atmosphere for 3 hours at 450 ˚C.

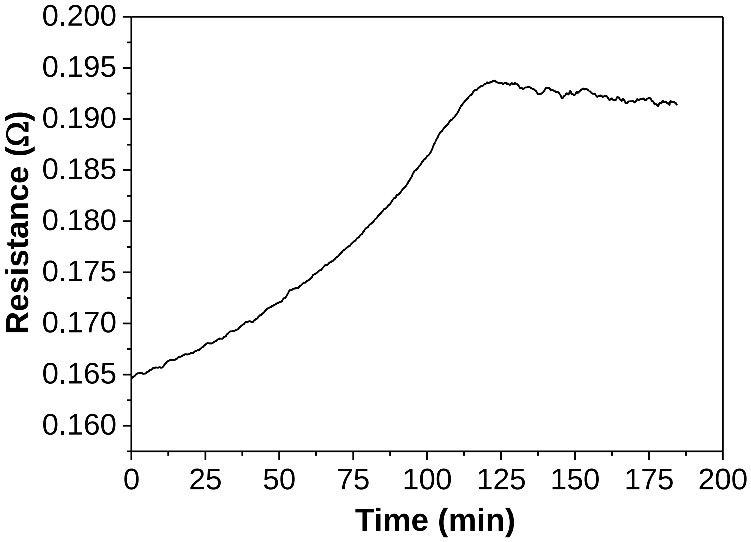

Figure 6.3. Resistivity versus time in a typical membrane annealed at 450 ˚C.

Membranes after having been annealed 3 hours at 450 ˚C were structurally characterized by X-ray diffraction. Since the aim of the current work is separation membranes with f.c.c. structure, structural characterization concentrated on to delineate the area in the ternary diagram which has this particular structure. Figure 6.4 gives XRD pattern of representative samples where the main phase was f.c.c. It should be noted that membrane close to Ag corner has a strong (111) preferred orientation, Figure 6.4 (a), which might be useful in improving the catalytic activity of the membrane [185]. This also true for membrane close to Pd corner, Figure 6.4 (d), though the degree of preferred orientation there was not as pronounced. In regions away from these corners XRD pattern comprises all diffraction lines indicating that the membranes do not have a strong preferred orientation.

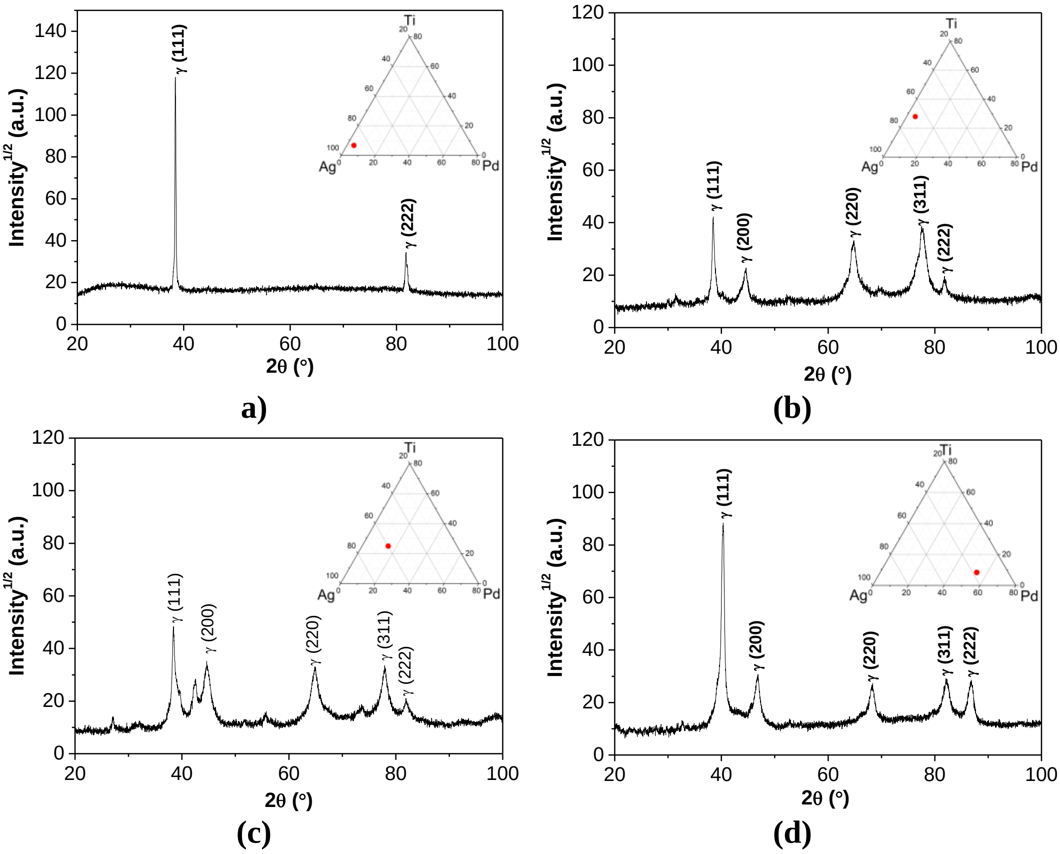

Figure 6.4. XRD pattern of membranes delineating the area in the ternary field where the structure is predominantly f.c.c. The membrane compositions are indicated in the inset.

Most deposited thin films displayed the resistivity versus temperature curve which was identical under argon and hydrogen indicating that the films did not react with hydrogen. Here the resistivity ratio has a value of $\rho H_2/\rho Ar = 1$. An example of the membrane that did react with hydrogen is given in Figure 6.5 (a). Here the curves are quite different. The resistivity ratio $\rho H_2/\rho Ar$ was calculated at various temperatures. The values are shown mapped in Figure 6.6 which shows that Ag38Ti8Pd54 and its near compositions do react with hydrogen. This implies that the corner of the mapped area covering, Ag35Ti22Pd43 and Ag13Ti25Pd62 could be considered as a candidate for separation membrane.

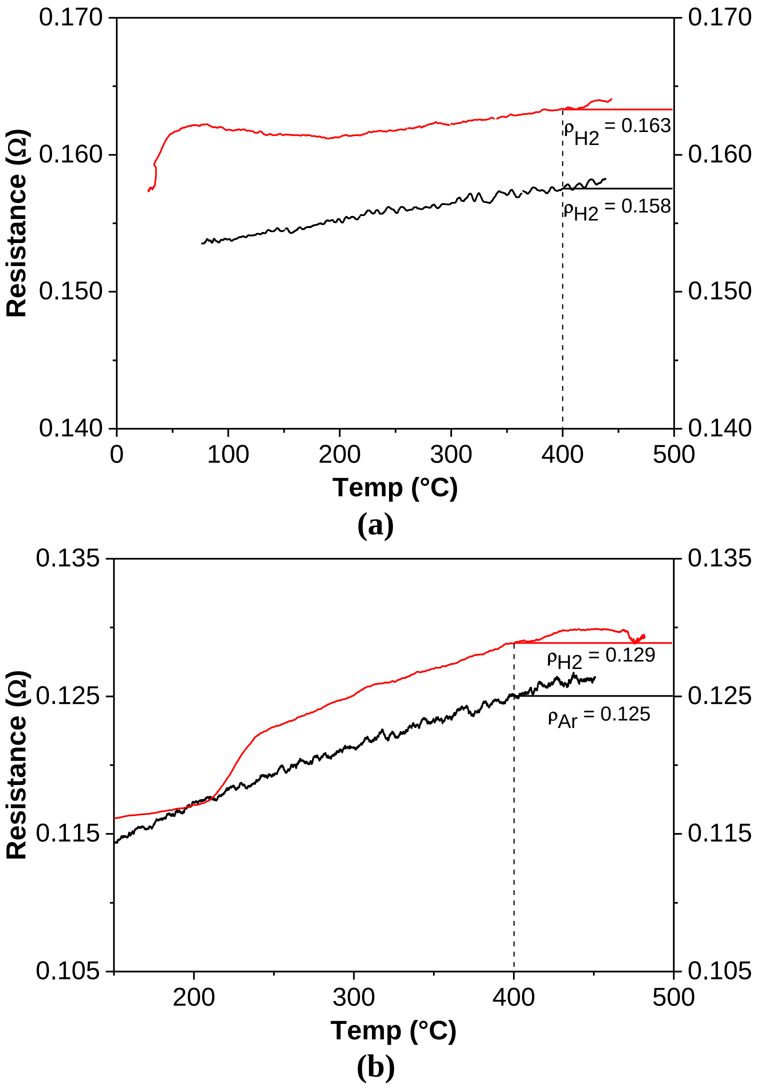

Figure 6.5. Resistance values measured in thin film membranes as a function of temperature for (a) a membrane Ag35Ti22Pd43 and (b) a membrane Pd72Ag28 , both heating up to 450 ˚C. Reactivity index defined as ρ_{H2}/ρ_{Ar} has a value of 1.032 at 400 ˚C for both membranes.

There are two aspects which may be worth emphasizing with regard to the relevance of resistivity mapping to permeability. The fact that there is a resistance change in the thin film is an indication that the membrane does react with hydrogen. This might be in the form of forming a solid solution, i.e. hydrogen dissolving in the host lattice without forming a separate phase. Since the permeability is the product of solubility and diffusivity of hydrogen in the membrane, the higher solubility would be desirable for improved permeability. This would tend to promote compositions in the mapping where the resistivity change is high. On the other hand, the reaction might be in the form of a formation of a new hydride phase. In this case, the resistance change is also expected to be high. Normally the formation of a hydride phase is associated with a large volume change which, as discussed above, leads to embrittlement problem. So what is desirable is normally the reaction with hydrogen to form a solid solution.

So as to provide a basis for the interpretation of reactivity mapping, a separate experiment was carried out in which Pd-Ag binary thin films were deposited using two sputter guns covering the commercial alloy Ag23Pd77. The positions of these samples were included in the ternary diagram given in Figure 6.2. A thin film sample with Pd72Ag28 composition is quite close to the commercial Pd77Ag23 alloy. Reactivity index of this membrane is shown in Figure 6.5 (b). Here the index has a value of 1.032 at 400 ˚C (the value at 350 ˚C was 1.033). This value is quite comparable those measured for the ternary compositions. Mapping in Figure 6.6 shows that compositions with high reactivity index center along a line that starts at Ag35Ti22Pd43 and terminates at the composition Ag28Pd72 which is quite near the commercial alloy Ag23Pd77. Thus there is a strong indication that the area centering along this line cover the compositions which are likely to have a high permeability and therefore they are candidates for separation membranes. Taking the composition Ag13Ti25Pd62, here Pd content is 62% instead of the usual 77%. This represents a reduction of 15 at% in Pd, which is quite substantial.

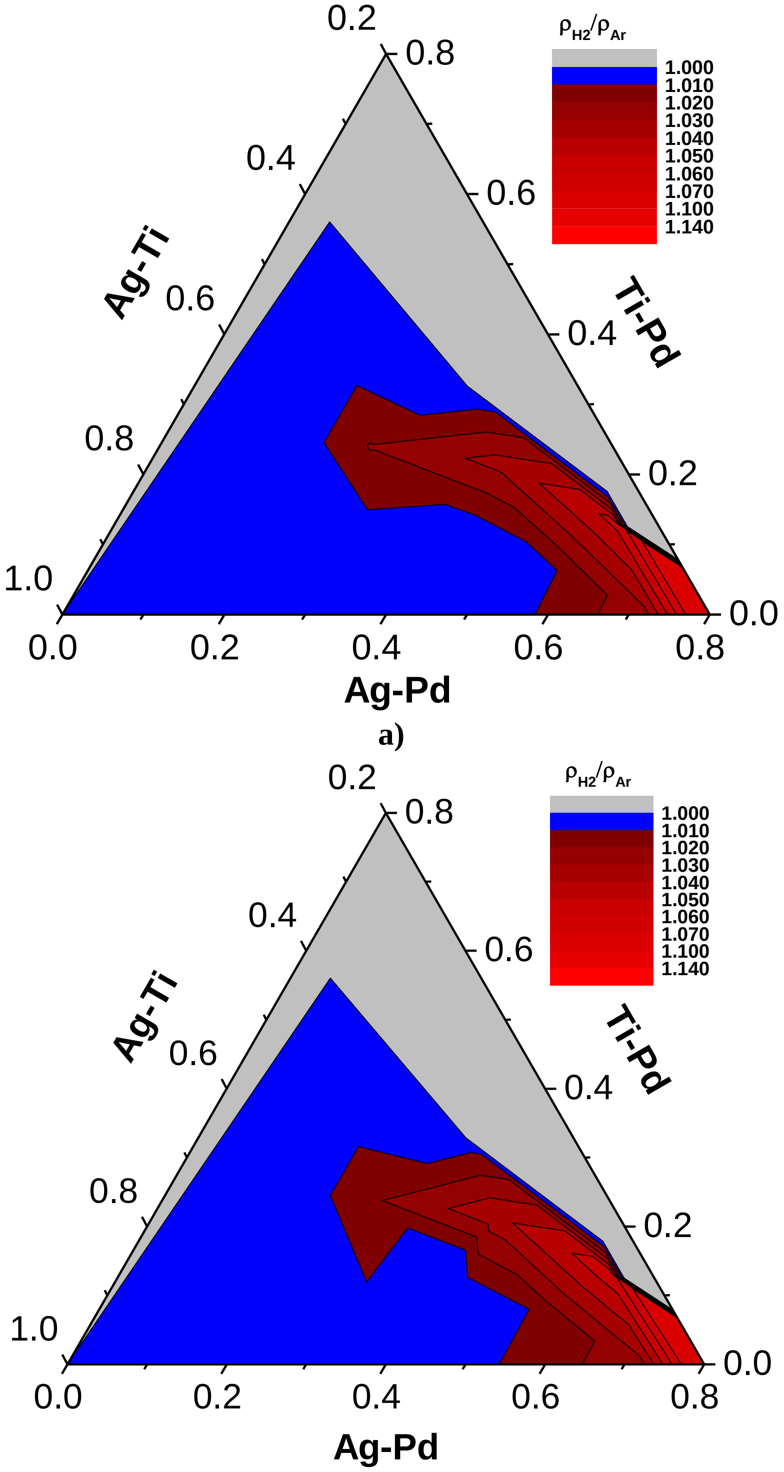

a)

(b)

Figure 6.6. Contour mapping of reactivity index in Ag-Ti-Pd system (a) at 350 ˚C and (b) at 400 ˚C.

Whether the predicted compositions could be developed as separation membranes require further study. It would be necessary to measure the permeability to see if they are indeed as high as those of the commercial compositions, as suggested by their reactivity indices. It is also necessary to carry out a structural investigation in the membranes to ensure that they are not embrittled due to cycling under hydrogen. From this point of view, the methodology given in this study is useful in narrowing down the compositions which are worth further study. In this way, it saves considerable time by eliminating many compositions that do not react with hydrogen, which obviously has no potential as a separation membrane.

6.4 Conclusions

In this study, a vacuum deposition unit was constructed which would allow deposition of multiple thin film membranes in a single experiment covering a wide compositional field. The library of thin film membranes was then screened with regard to their tendency to react with hydrogen using a reactor with in-situ resistivity measurement. The approach was applied to a portion of Ag-Ti-Pd ternary system aiming for separation membranes with f.c.c. crystal structure. Mapping based on the resistivity measurement indicated an area centered on a line connecting Ag35Ti22Pd43 to Pd72Ag28 as candidates for separation membranes.

CHAPTER 7

SEPARATION MEMBRANES BASED ON Pd-Ag-Ni (*)

As an effort to reduce Pd content, a combinatorial study was carried out on Pd-Ag system with the addition of Ni as a third element. A magnetron sputtering system was used to create a thin film material library using three sputter targets arranged in a triangular fashion. A total of 21 glass discs were used as a substrate onto which membranes typically 3 µm thick were deposited, each with a different composition covering a wide compositional field in Pd-Ag-Ni ternary phase diagram. Membranes produced were screened by a four probe resistivity measurement in terms of a reactivity index, defined as the ratio of resistivity under hydrogen to that under argon in the same conditions. Mapping based on the resistivity measurements indicated three alloys, namely Pd33Ag59Ni8, Pd55Ag28Ni17 and Pd76Ag18Ni6 where the reactivity index was relatively high, implying that they could be possible membrane compositions. Foils were prepared with matching compositions by melting and casting followed by rolling to ≈100 µm in thickness. This has shown that a permeability value of 6.50×10^{-10} mol/m.s.Pa$^{1/2}$ could be obtained at 400 °C in Pd55Ag28Ni17 where Pd content is nearly two-thirds of the commercial alloy Pd77Ag23.

(*) This chapter was published with a title “Combinatorial screening of Pd-Ag-Ni membranes for hydrogen separation” in the Journal of Membrane Science, 524, (2017), 631-636.

7.1 Introduction

Hydrogen separation membranes offer a potential pathway for economical hydrogen purification. Among the separation membranes, dense metallic membranes are attractive due to their high hydrogen selectivity, ease of implementation and working temperature suitable for the water gas shift reactions in steam reforming of methane/natural gas [186]. Dense metallic membranes fall into several groups; Pd and Pd alloys [187], Group IV-V alloys with b.c.c. crystal structure [121] and multi-component amorphous alloys [125]. Commercial metallic membranes are normally based on Pd and Pd alloys which have f.c.c. crystal structure [187]. The interest in Pd is due not only its high permeability but also due to its catalytic activity and its resistance to oxidation at elevated temperature [121]. However, the practical application of pure Pd membranes is rare as a result of its high cost and due to embrittlement caused by α-β phase transformation [124,125]. Therefore, efforts have concentrated on alloying Pd for the purpose of reducing the cost as well as suppressing the α-β transition.

Hydrogen permeation in Pd based f.c.c. alloys as in other metallic dense membranes follow the solution-diffusion mechanism. Hydrogen flux across the membrane is then follows;

$$J = \frac{k}{l}\left({P^n}_{H_2\,In} - {P^n}_{H_2\,Out}\right)$$

Equation 7.1

where J is the hydrogen flux (mol/m^2.s), k is the hydrogen permeability in the membrane (mol/m.s.Pa^n), l is the membrane thickness (m), $P^n_{H2\,In}$ and $P^n_{H2\,Out}$ are the hydrogen pressure at inlet and outlet. Except for very thin membranes [188] and extreme conditions [189], generally, the rate-limiting step for permeability is the diffusion of hydrogen through the membrane which results in a value of $n=0.5$. It should be pointed out that the permeability, k, is the product of diffusivity, D, (m^2/s) and the solubility of hydrogen, S, ($mol/m^3.Pa^{0.5}$) in the membrane, i.e. k=D.S.

In order to maximize the permeability, it is necessary to improve the diffusivity as well as the solubility of hydrogen. Alloying Pd with other elements normally results in a decrease in the hydrogen diffusivity [190]. This is true in Pd-Ag system as well as in most other Pd based binary systems. The solubility in f.c.c. membranes decreases with increasing temperature. This results in a well-known negative slope in a permeability-temperature relationship. This is despite the fact that diffusivity increases with increasing temperature, implying that the solubility has a more dominant effect on permeability.

Many of the studies [184,191–194] in the literature agrees that solubility is the relatively more important in affecting the permeability. Studies indicate that there is an optimum alloying addition where the solubility and therefore the permeability is maximized. Wilcox [191] determining the pressure-composition isotherms, investigated the solubility of hydrogen in Pd-Ag system and found that the maximum occurs at around 30 at.% Ag addition. This is close to Pd-23 at.% Ag, a well-known commercial composition used as separation membranes. Similar studies [191,192] for Pd-Y and Pd-Au yielded the respective compositions of 8 and 20 at.% for maximum solubility. Other f.c.c. membranes that have been considered in the literature include Pd-Ce [190], Pd-La [193], Pd-Fe [184] and Pd-Ni [194].

The current study was undertaken for the purpose of developing f.c.c. membranes that would be lean in its Pd content. Ni, with its catalytic properties, is considered as a third alloying element in Pd-Ag system as it could partially replace Pd whereby reducing the cost. An added advantage of Ni is that it has f.c.c. structure, therefore, it could yield separation membranes of f.c.c. structure over a wide compositional range in Pd-Ag-Ni. The current work makes use of combinatorial approach whereby, a multitude of thin film membranes were fabricated with sputter deposition. A large number of samples having different compositions produced in this way were screened by a resistivity measurement carried out both under hydrogen and argon. Possible candidates identified based on resistivity measurements were selected for permeability measurement.

7.2 Experimental

A library of thin film membranes was produced via combinatorial approach. Details of sputter deposition system used for this purpose were described previously [165] and therefore only a brief description will be given here. Prior to deposition, all the sputtering targets, Pd, Ag, and Ni, arranged in triangular fashion were carefully aligned with respect to their angular positions as well as the distance with respect to the substrates magazine placed above. A total of 21 substrates were used, arranged in a triangular fashion similar to the targets underneath, Figure 7.1. Subsequent to the loading of substrates to the magazine, the system was evacuated down to $1x10^{-7}$ Torr. Then, the chamber was filled with ultra-high purity argon, stabilized at a 5 mTorr. The main shutter between the target and the magazine kept closed, the pre-sputtering was carried out for 10 minutes so as to clean the targets. The main shutter was then opened and deposition was initiated over all 21 glass substrates. Typically, deposition was continued for 4 hours which yielded thin film membranes of approx. 3 microns in thickness.

The library of thin film membranes produced was screened by a four probe resistivity measurement [165]. The resistivity shows a good correlation with pressure-composition isotherms [170,195] and could be used as a measure of the solubility of hydrogen in the alloy system. So as to stabilize the structure, prior to resistivity measurements, based on the preliminary tests, the thin films were annealed at 450 °C for 3 hours. The resistivity measurements were carried out by heating up to 450 °C and cooling down to room temperature (both 5 K/min). The experiment was repeated under argon as well as under hydrogen atmosphere. The results were expressed in terms of a reactivity index, defined as $\rho H_2/\rho Ar$, where ρH_2 and ρAr are resistivity values under hydrogen and argon respectively both measured at the same temperature. For many of the membranes, $\rho H_2/\rho Ar = 1$, i.e. the resistivity was the same in both argon and hydrogen meaning that the membrane did not react with hydrogen and therefore they were unsuitable as a separation membrane.

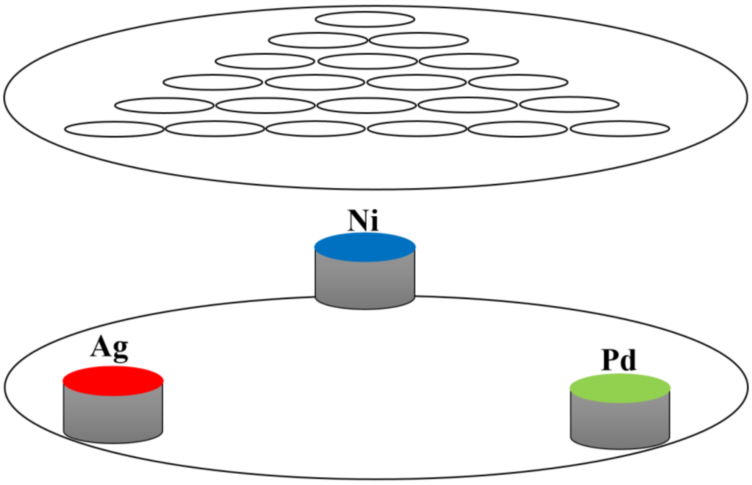

Figure 7.1. Schematic representation of thin film membranes produced via sputter deposition. Note triangular arrangements of sputter guns as well as the substrates above them. A total of 21 membranes are produced in a single experiment each with a different composition.

Compositions, selected based on the mapping of reactivity index, were fabricated by melting and casting under a protective atmosphere. Buttons which were typically 5 grams were cold rolled to a foil of ≈100 µm in thickness.

Foils were then tested for their hydrogen permeability by a custom-made testing unit. This unit, shown in Figure 7.2 consists of a gas feeding system, a test-cell, two pressure transmitters and flow meters. The unit may be connected to either argon or hydrogen gas or may be taken under vacuum via a turbomolecular vacuum pump. The test cell consists of a compartment housing the membrane 19 mm in diameter. The membrane is in-between two CF flanges made gas-tight using graphite gaskets. The test cell is inside a small tubular furnace where the temperature could be controlled with a sensitivity of ±0.1 °C at the test temperature via a thermocouple located inside the test cell. Gas pressure on the inlet side of the membrane was monitored via a pressure transmitter (1 MPa). On the outlet side, H_2 flux permeating the membrane was monitored by a mass flow meter (with the full range capacity of either 10 sccm or 100 sccm), the pressure was also measured on this side with a pressure transmitter (0.6 MPa). Both the pressure transmitters and the mass flow meters are connected to a four-channel read-out unit.

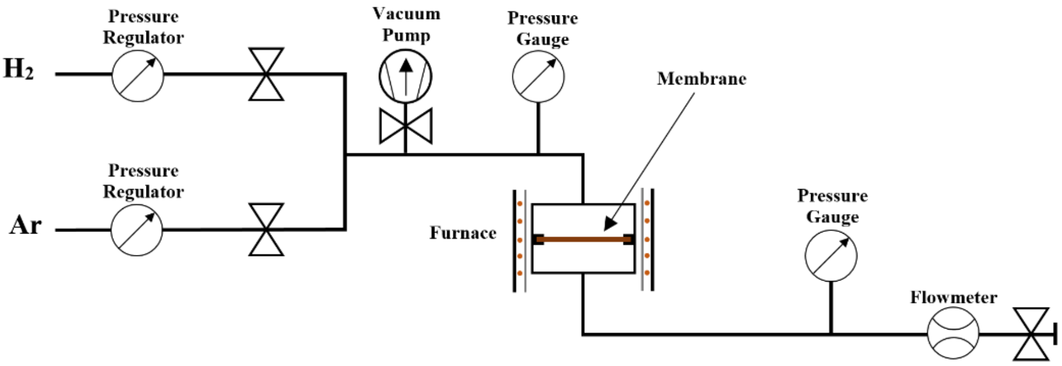

Figure 7.2. The schematic representation of a test set-up used for permeability measurements.

The effective area of the membrane exposed to a permeating gas was ≈1.8 cm^2. All membranes were first tested with argon up to 1 MPa at room temperature for gas tightness. The unit, membrane loaded, is heated up under an argon atmosphere to the desired temperature. Following the temperature stabilization, argon was evacuated and the test was initiated by loading hydrogen. The pressure and the hydrogen flux was recorded in the outlet side as a function of inlet pressure up to 1MPa with the increment of 0.02 MPa. The membranes were rechecked with argon for gas tightness after the test.

7.3 Results and Discussion

Two experiments were carried out to produce thin film membranes. In one, 21 samples were deposited simultaneously, each with a different composition in Pd-Ag-Ni. In the other, samples were produced in the binary Pd-Ag system. Parameters of depositions were adjusted in both experiments such that membranes with Pd content greater than 77 at.%, i.e. commercial alloy, was avoided. Distribution of sample compositions obtained from both experiments is shown plotted in Figure 7.3. Here it is seen that samples cover quite a wide range where Pd content varies from 4 to 76 at.%.

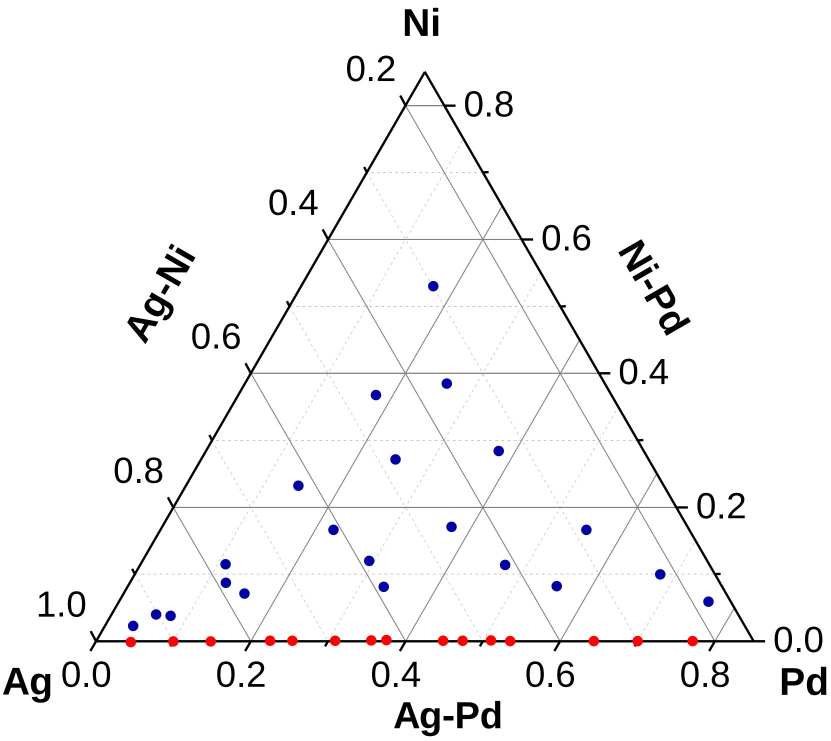

Figure 7.3. The distribution of the membrane compositions in the Pd-Ag-Ni ternary diagram.

Typical XRD pattern of thin film membranes deposited and annealed at 450 °C for 3h is given in Figure 7.4. Here patterns refer to Pd33Ag59Ni8, Pd55Ag28Ni17, and Pd77Ag23. The last pattern is a single phase f.c.c. alloy (commercial composition) with a= 3.934 Å. The other two are more typical of Pd-Ag-Ni ternary system which are two-phase alloys, both with f.c.c. crystal structure. The relative proportion of these phases; one Ag rich and the other Ni-rich as well as their lattice parameters vary depending on the position in the ternary diagram (see below).

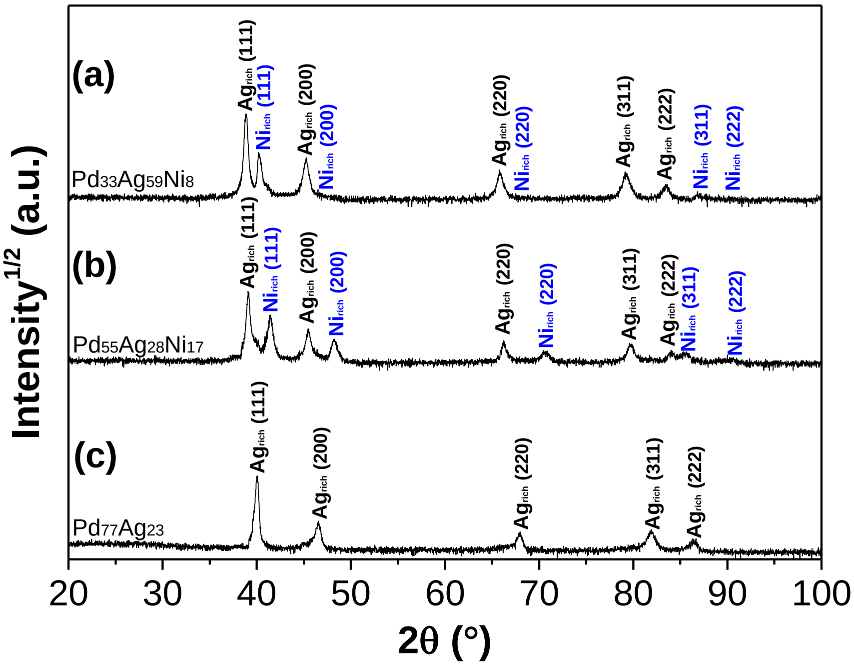

Figure 7.4. XRD patterns of thin film membranes (a) Pd33Ag59Ni8, (b) Pd55Ag28Ni17 and (c) Pd77Ag23.

A greater portion of Pd-Ag-Ni phase diagram is bi-phasic and comprise a two-phase f.c.c. structure. There is a small region in the Pd corner which is a single phase. This single phase extends to Ag as well as Ni corner but it is extremely narrow. Membrane Pd76Ag18Ni6, marked in Figure 7.5, based on its XRD pattern is just at the edge of the two-phase region implying that the boundary separating two-phase region from the single phase is probably located near this composition. A typical micrograph in a thin film membrane which refers to Pd76Ag18Ni6 is shown in Figure 7.6.

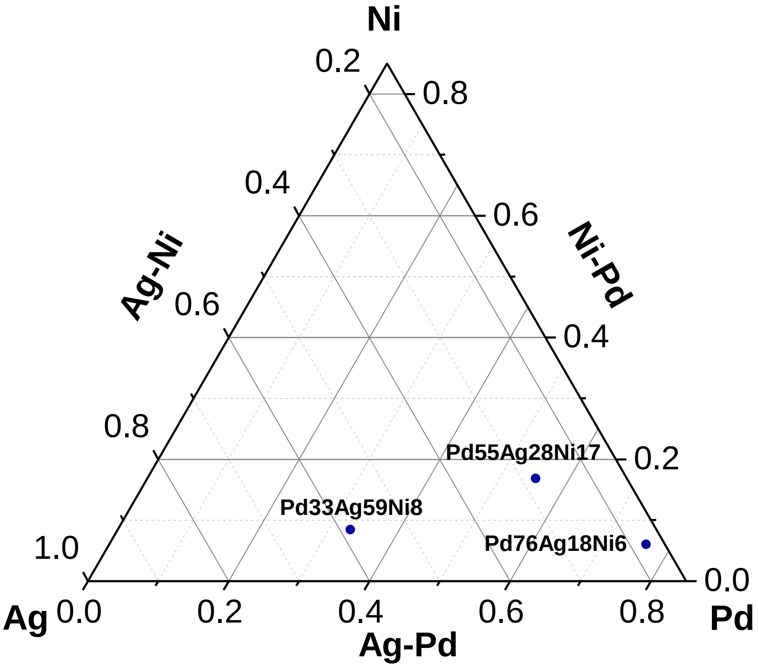

Figure 7.5. The position of the selected compositions on the Pd-Ag-Ni system.

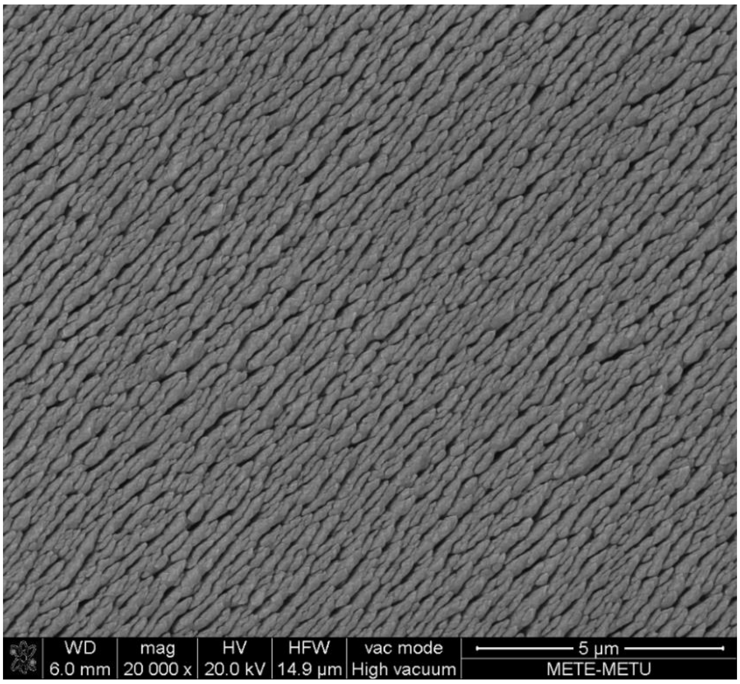

Figure 7.6. The morphology of Pd76Ag18Ni6 membrane.

Thin film membranes were screened with resistivity measurements while they were heated up to 450 °C and cooled down to room temperature. Reactivity indices determined for all samples were mapped in the ternary phase diagram at two temperatures; 350 °C and 400 °C, Figure 7.7. Here contour mapping was obtained by triangulation and linear interpolation procedures [196]. Binary compositions in Pd-Ag system were also included in this mappings. The mapping shows that for many of the compositions, $\rho H_2/\rho Ar= 1$. This reactivity index increases in compositions close to Pd corner and reach a value as high as $\rho H_2/\rho Ar = 1.065$ at 400 °C. The maximum reached in 350 °C is even higher and has a value of 1.070.

Since the resistivity correlates well with the solubility of hydrogen, the mappings given in Figure 7.7 could be considered as an approximate mapping of hydrogen solubility in the respective alloys. This correlation is quite useful since the permeability in f.c.c. membranes is dominated by the hydrogen solubility. Thus resistivity mappings could yield compositions that are potential candidates as a separation membrane.

It may be noted that Pd77Ag23, commercial composition, has a reactivity index of $\rho H_2/\rho Ar = 1.038$ at 350 °C. This index is less at 400 °C and has a value of 1.035, indirectly verifying that the solubility decreases with increase in temperature. It is interesting to note that mappings contain values of reactivity index which are higher than that of the commercial compositions.

The mappings given in Figure 7.7 show three regions of high reactivity index. These regions center on compositions Pd33Ag59Ni8, Pd55Ag28Ni17, and Pd76Ag18Ni6, Figure 7.5. The values of reactivity index for these compositions are given in Table 7.1 both for 350 °C and 400 °C. As shown in the table, the highest reactivity index is obtained in Pd76Ag18Ni6. This is followed by Pd55Ag28Ni17 and then by Pd33Ag59Ni8.

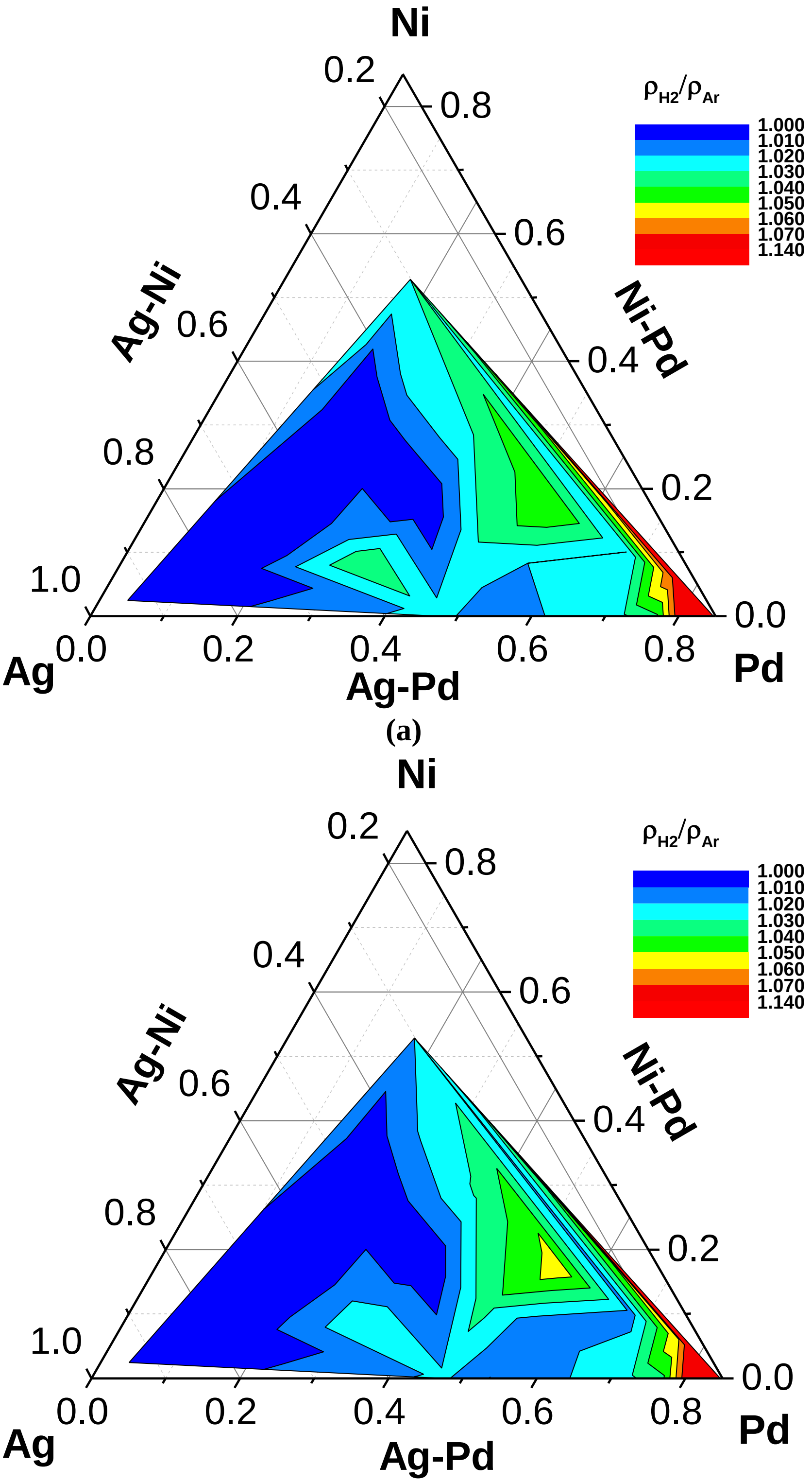

(a)

(b)

Figure 7.7. Contour mapping of reactivity index in Pd-Ag-Ni system (a) at 350 ˚C and (b) at 400 ˚C.

Table 7.1. Reactivity indices of selected thin film membranes.

	Reactivity Index			
Temperature	**Pd77Ag23**	**Pd33Ag59Ni8**	**Pd55Ag28Ni17**	**Pd76Ag18Ni6**
350 °C	1.038	1.032	1.056	1.070
400 °C	1.035	1.029	1.055	1.065

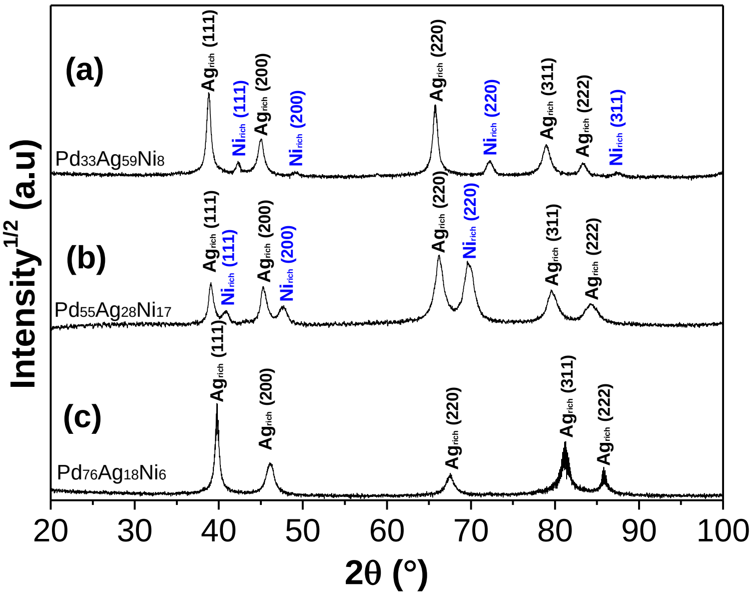

Figure 7.8. XRD patterns of fabricated alloys (a) Pd33Ag59Ni8, b) Pd55Ag28Ni17 and (c) Pd76Ag18Ni6.

Based on the values of reactivity index, three compositions referred to above were selected for further study. Compositions Pd33Ag59Ni8, Pd55Ag28Ni17 and Pd76Ag18Ni6 were fabricated by melting and casting. Typically, buttons of 5 grams were produced which were then rolled down to approx. 100 μm in thickness. XRD patterns of rolled foils were compatible with those measured on the corresponding thin film membranes, Figure 7.8.

Foils produced were annealed at 450 °C for 3h before they were taken for the permeability testing. Hydrogen fluxes measured in the membranes, at 400 °C, as a function of square root of pressure differential are given in Figure 7.9. It should be noted that the variation is linear implying that the exponent n has a value of 0.5, see

Equation 7.1. Values of hydrogen permeability for these compositions are reported in Table 7.2. It should be noted that there is a correlation between reactivity index and the permeability values in that where the index is high, the composition has a higher permeability.

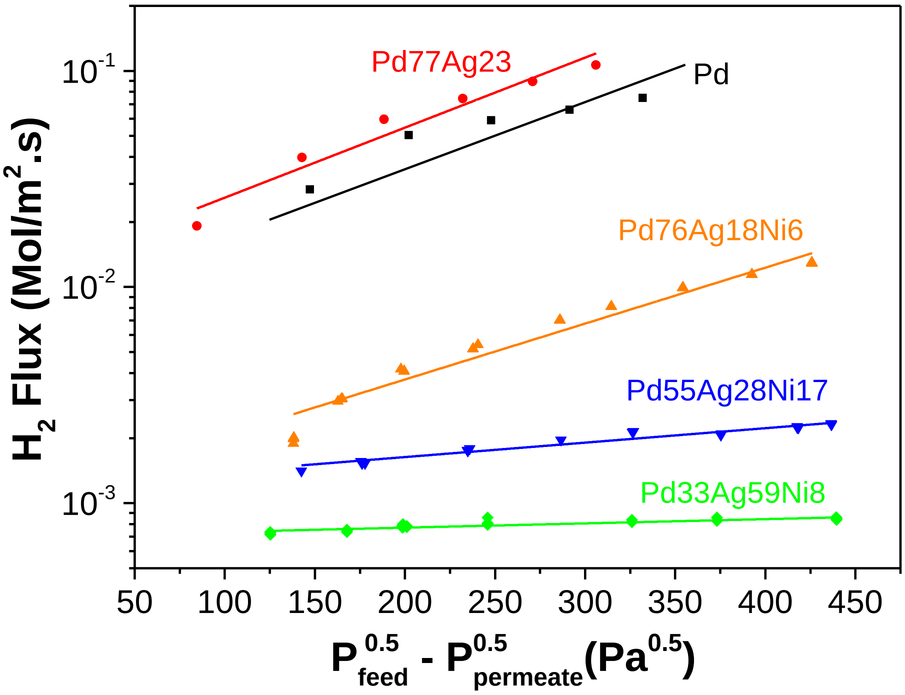

Figure 7.9. The hydrogen flux vs. the square root of pressure differential applied to Pd33Ag59Ni8, Pd55Ag28Ni17, Pd76Ag18Ni6 and Pd77Ag23 membranes.

The lattice parameters of f.c.c. based membranes of highest permeability reported in the literature are listed in Table 7.3. It is seen that though the quantity of alloying additions varies from one alloy system to the other, the lattice parameters are quite similar. Thus in Pd-23 at.% Ag which has the highest permeability in Pd-Ag has a lattice parameter of a= 3,942 Å. The corresponding values in Pd-20 at.% Au and Pd-8 at.% Y are 3.930 Å and 3.939 Å, respectively. Thus overall the lattice parameter ranges from a= 3.930 Å to 3.942 Å. These values should be compared to the lattice parameters of the current membranes, see Table 7.2. It should be noted that Pd76Ag18Ni6 with a value of a= 3.929 is quite close to the range reported above. This is, in fact, the membrane which has permeability value higher than the other two.

Table 7.2. Lattice parameter and the hydrogen permeability of selected Pg-Ag-Ni membranes.

	Pd77Ag23	**Pd33Ag59Ni8**	**Pd55Ag28Ni17**	**Pd76Ag18Ni6**
Lattice Parameter Ag_{rich} (Å)	3.940	4.018	3.985	3.929
Lattice Parameter Ni_{rich} (Å)	-	3.688	3.807	-
Permeability (mol/m.s.$Pa^{1/2}$)	$2.93x10^{-8}$	$2.78x10^{-10}$	$6.50x10^{-10}$	$2.67x10^{-9}$

The lattice parameters of f.c.c. based membranes of highest permeability reported in the literature are listed in Table 7.3. It is seen that though the quantity of alloying additions varies from one alloy system to the other, the lattice parameters are quite similar. Thus in Pd-23 at.% Ag which has the highest permeability in Pd-Ag has a lattice parameter of a= 3,942 Å. The corresponding values in Pd-20 at.% Au and Pd-8 at.% Y are 3.930 Å and 3.939 Å, respectively. Thus overall the lattice parameter ranges from a= 3.930 Å to 3.942 Å. These values should be compared to the lattice parameters of the current membranes, see Table 7.2. It should be noted that Pd76Ag18Ni6 with a value of a= 3.929 is quite close to the range reported above. This is, in fact, the membrane which has permeability value higher than the other two.

Table 7.3. Lattice parameters of binary alloys of highest permeability reported in the literature.

Alloy	Lattice Parameter (Å)	Reference
Pd-23 at.% Ag	3.942	[197]
Pd-8 at.% Y	3.939	[184]
Pd-20 at.% Au	3.930	[198]

The purpose of this study was to identify compositions which are lean in their Pd content but has highest possible permeability. From this point of view, the composition Pd76Ag18Ni6 is quite close to the Pd77Ag23 commercial alloy in terms of its Pd content and would not offer any significant advantage. Perhaps the composition which should be highlighted is Pd55Ag28Ni17. Even though the permeability of this alloy (k= 6.50×10^{-10} mol/m.s.$Pa^{1/2}$) is less than that of Pd76Ag18Ni6, its Pd content is one third less, i.e. instead of 76 at.%, the Pd content in the current alloy is 55 at.%. Fine tuning of this alloy composition is, of course, possible which might bring the permeability closer to that of Pd76Ag18Ni6 alloy. This tuning may be more efficiently implemented using the same methodology, i.e. the combinatorial search employed for the Pd-Ag-Ni triangle may now be confined to the Pd33Ag59Ni8-Pd55Ag28Ni17-Pd76Ag18Ni6 triangle, Figure 7.5, with a better compositional resolution.

7.4 Conclusions

In this study, a combinatorial study was carried out as an effort to develop a low-cost separation membrane based on Pd-Ag system with Ni addition. A magnetron sputtering system was used to create a thin film material library comprising a total of 21 membranes covering a wide compositional field in Pd-Ag-Ni ternary system. Membranes produced were screened by a four probe resistivity measurement in terms of a reactivity index, defined as the ratio of resistivity under hydrogen to that under argon in the same conditions. Mapping based on the resistivity measurements indicated three alloys, namely Pd33Ag59Ni8, Pd55Ag28Ni17 and Pd76Ag18Ni6 as candidates for separation membrane. Foils were prepared with matching compositions by melting and casting followed by rolling to ≈100 μm in thickness. This has shown that a permeability value of 6.50×10^{-10} mol/m.s.$Pa^{1/2}$ could be obtained at 400 °C in Pd55Ag28Ni17 where Pd content is nearly two-thirds of the commercial alloy Pd77Ag23.

CHAPTER 8

GENERAL CONCLUSIONS

The current work is an outcome of an effort to develop low-cost hydrogen separation membranes on the basis of combinatorial materials science. For this purpose, a total of three ternary systems, i.e. Nb-Pd-Ti, Pd-Ag-Ti, and Pd-Ag-Ni, were investigated. 21 thin films each with a different composition were produced in a single experiment via magnetron sputtering so as to cover a wide compositional field in each ternary system. The thin film libraries were then structurally characterized and screened by a four-probe resistivity measurement in terms of a reactivity index.

The methodology adopted in this study was used to narrow down the compositions in the ternary systems which were worth for further study. The purpose, here, was to save time by eliminating compositions that did not react with hydrogen, which obviously had no potential as a separation membrane. The present work as summarized below demonstrated that the approach is a very fruitful and as implemented in the current work allow thin films depositions that cover a wide compositional field in the ternary phase diagram. Moreover, it has shown that four-probe resistivity measurement is an effective method that rapidly screens the thin films indicating the compositional range with a potential as separation membranes.

Nb-Pd-Ti alloy system was studied with a focus on b.c.c. membranes. The structural characterization revealed that the choice of Nb-Pd-Ti alloy system was quite suitable since a significant portion of the ternary field had a single phase b.c.c. structure.

The map of reactivity index was plotted in Nb-Pd-Ti ternary diagram indicated that many of the b.c.c. compositions did not react with hydrogen and therefore were unsuitable as separation membranes. The b.c.c. membranes that did react with hydrogen was restricted to a narrow region close to Nb corner which had a potential as a separation membrane. The reactivity index in this narrow region had quite high values implying an excessive hydrogen solubility in the lattice. Since the excessive hydrogen solubility is a sign of potential brittleness in the membrane, an additional criterion was introduced based on the lattice volume. Considering the relationship between the lattice volume and hydrogen solubility in Nb-based b.c.c. alloys, a lattice volume of 35.5 $Å^3$ was taken as the tolerable maximum. Accordingly, the lattice volumes of the thin films were mapped in the ternary diagram. The intersection of the two maps; one reactivity index and the other lattice volume yielded an area, $32<Nb<41$, $27<Pd<44$, and $20<Ti<38$, as possible compositions for separation membranes. Of the selected region two alloys were singled out Nb33Pd41Ti26 and Nb36Pd28Ti36 where the reactivity index had a high value while the lattice volume was less than the tolerable limit.

Pd-Ag-Ti alloy system was selected to produce f.c.c. membranes and the structural characterization of the ternary systems indicated that the most of the thin films yielded a single phase f.c.c. structure. Similar to the previous system, the thin films were screened with respect to their reactivity index. Since the hydrogen embrittlement in f.c.c. membranes is not as severe as in b.c.c. membranes, the criteria based on the lattice volume was not applied to this ternary alloy system.

Mapping based on reactivity index in Pd-Ag-Ti system indicated that the compositions with high reactivity indices center along a line that starts at Pd43Ag35Ti22 and terminates at the composition Pd72Ag28 which is quite near the commercial alloy Pd77Ag23. This reactive region covers the Pd54Ag38Ti8 and Pd62Ag13Ti25 compositions which are considered as candidates for separation membranes.

Pd-Ag-Ni alloy system was also investigated so as to extend the f.c.c. membranes that are lean in Pd content. The structural characterizations revealed that the thin films produced in this system exhibited only the f.c.c. structure single phase or multiphase. Mapping based on reactivity index indicated that Pd33Ag59Ni8, Pd55Ag28Ni17, and Pd76Ag18Ni6 alloys exhibited relatively high reactivity indices, where the highest reactivity index was obtained in Pd76Ag18Ni6 followed by Pd55Ag28Ni17 and then by Pd33Ag59Ni8.

The three compositions identified in Pd-Ag-Ni ternary system, namely, Pd33Ag59Ni8, Pd55Ag28Ni17, and Pd76Ag18Ni6 was selected for further evaluation as a separation membrane. The compositions were fabricated in the form of foils with ~100 µm in thickness via arc melting and cold rolling. The permeability measurements showed that Pd76Ag18Ni6 alloy exhibited the highest hydrogen permeability with a value of 2.67×10^{-9} mol/m.s.Pa$^{1/2}$ at 400 °C, while Pd55Ag28Ni17 and Pd33Ag59Ni8 exhibited $6.50\text{x}10^{-10}$ and $2.78\text{x}10^{-10}$ mol/m.s.Pa$^{1/2}$, respectively. Of these, though the permeability is not as high, the composition Pd55Ag28Ni17 may be selected, since it represents one-third reduction in its Pd content as compared to the commercial Pd77Ag23 alloy. It should be mentioned that by focusing the combinatorial search to the Pd33Ag59Ni8-Pd55Ag28Ni17-Pd76Ag18Ni6 triangle a fine tuning of the compositions would be possible with a potential for further reduction in Pd and/or with a higher permeability.

Although in the present work, the magnetron sputtering was employed as a tool to produce compositional spread for the respective ternary systems, it is also an effective method to produce thin film membranes. Thus, the compositions which are identified as candidates for separation membranes may be produced as thin film membranes deposited onto a suitable substrate. It should be emphasized that with this approach the choice of substrate is as critical as the membrane itself. The substrate has to be porous with a porosity size not more than one-third of the membrane thickness. Thus if the choice is made for films that are several microns in thickness, the substrate has to have porosity at the nanoscale.

It should be emphasized that the thin film membrane approach would be particularly suitable for compositions selected in Nb-Pd-Ti ternary system where the combinatorial search has singled out two compositions Nb33Pd41Ti26 and Nb36Pd28Ti36. If such approach was adopted, Pd saving in the membrane composition would be improved further top one half of the original composition.

REFERENCES

[1] Y.H. Ma, Hydrogen Separation Membranes, in: Adv. Membr. Technol. Appl., John Wiley & Sons, Inc., Hoboken, NJ, USA, 2008: pp. 671–684. doi:10.1002/9780470276280.ch25.

[2] R.B. Gupta, Hydrogen fuel: Production, Transport, and Storage, 2009.

[3] I. Dincer, A.S. Joshi, Hydrogen Production Methods, in: Springer US, New York, NY, 2013: pp. 7–20. doi:10.1007/978-1-4614-7431-9_2.

[4] K. Liu, C. Song, V. Subramani, eds., Hydrogen and Syngas Production and Purification Technologies, John Wiley & Sons, Inc., Hoboken, NJ, USA, 2009. doi:10.1002/9780470561256.

[5] M.I. Sosa, J.L. Silveira, A. Fushimi, Natural gas steam reforming for hydrogen production. An energetic approach, in: 17th Int. Congr. Mech. Eng., Sao Paulo, 2003.

[6] A. Damle, Hydrogen Separation and Purification, in: R.B. Gupta (Ed.), Hydrog. Fuel Prod. Transp. Storage, 2009: pp. 283–324.

[7] S. P. L., D. D. C., Preliminary Screening - Technical and Economic Assessment of Synthesis Gas to Fuels and Chemicals With Emphasis on the Potential for Biomass-Derived Syngas, Goldon, Colorado, 2003.

[8] K. Liu, Z. Cui, T.H. Fletcher, Coal Gasification, in: K. Liu, C. Song, V. Subramani (Eds.), Hydrog. Syngas Prod. Purif. Technol., A John Wiley & Sons, Inc., 2009: pp. 156–218.

[9] J.C. Molburg, R.D. Doctor, Hydrogen from Steam-Methane Reforming with CO2 Capture, in: Pittsburgh, 2003: pp. 1–20. http://www.uxc.com/smr/Library%5CAlternative Uses/2003 - Hydrogen from Steam-Methane Reforming with CO2 Capture.pdf.

[10] E. Shoko, B. McLellan, A.L. Dicks, J.C.D. da Costa, Hydrogen from coal: Production and utilisation technologies, Int. J. Coal Geol. 65 (2006) 213–222. doi:10.1016/j.coal.2005.05.004.

[11] A. Molino, S. Chianese, D. Musmarra, Biomass gasification technology: The state of the art overview, J. Energy Chem. 25 (2016) 10–25. doi:10.1016/j.jechem.2015.11.005.

[12] R. Rauch, J. Hrbek, H. Hofbauer, Biomass gasification for synthesis gas production and applications of the syngas, Wiley Interdiscip. Rev. Energy Environ. 3 (2014) 343–362. doi:10.1002/wene.97.

[13] S. De, A.K. Agarwal, V.S. Moholkar, B. Thallada, eds., Coal and Biomass Gasification, Springer Singapore, Singapore, 2018. doi:10.1007/978-981-10-7335-9.

[14] P.C. Hallenbeck, Fermentative hydrogen production: Principles, progress, and prognosis, Int. J. Hydrogen Energy. 34 (2009) 7379–7389. doi:10.1016/j.ijhydene.2008.12.080.

[15] N. Azbar, F.T.Ç. Dokgöz, Z. Peker, Optimization of Basal Medium for Fermentative Hydrogen Production from Cheese Whey Wastewater, Int. J. Green Energy. 6 (2009) 371–380. doi:10.1080/15435070903107049.

[16] N. Ferrari, L. Mancuso, P. Cotone, J. Davison, Operating flexibility of power plants with CCS, Cheltenham, 2012.

[17] H. Iskov, Field test of hydrogen in the natural gas grid, Hørsholm, 2010.

[18] M.W. Melaina, O. Antonia, M. Penev, Blending Hydrogen into Natural Gas Pipeline Networks: A Review of Key Issues, Goldon, Colorado, 2013.

[19] S. Sircar, T.C. Golden, Pressure Swing Adsorption Technology for Hydrogen Production, in: K. Liu, C. Song, V. Subramani (Eds.), Hydrog. Syngas Prod. Purif. Technol., A John Wiley & Sons, Inc., 2009: pp. 414–450.

[20] D. Edlund, Hydrogen Membrane Technologies and Application in Fuel Processing, in: K. Liu, C. Song, V. Subramani (Eds.), Hydrog. Syngas Prod. Purif. Technol., A John Wiley & Sons, Inc., New Jersey, 2010: pp. 357–384.

[21] J. Emsley, Nature’s Building Blocks: An A-Z Guide to the Elements, 2011. doi:978-0-19-960563-7.

[22] P. Bernardo, E. Drioli, G. Golemme, Membrane Gas Separation: A Review/State of the Art, Ind. Eng. Chem. Res. 48 (2009) 4638–4663. doi:10.1021/ie8019032.

[23] I. Uehara, Separation and Purification of Hydrogen, in: T. Ohta, T.N. Veziroglu (Eds.), Energy Carriers Convers. Syst. with Emphas. Hydrog., 2008: pp. 268–282.

[24] A.B. Hinchliffe, K.E. Porter, A Comparison of Membrane Separation and Distillation, Chem. Eng. Res. Des. 78 (2000) 255–268. doi:10.1205/026387600527121.

[25] Y. Shirasaki, T. Tsuneki, Y. Ota, I. Yasuda, S. Tachibana, H. Nakajima, K. Kobayashi, Development of membrane reformer system for highly efficient hydrogen production from natural gas, Int. J. Hydrogen Energy. 34 (2009) 4482–4487. doi:10.1016/j.ijhydene.2008.08.056.

[26] N.W. Ockwig, T.M. Nenoff, Membranes for Hydrogen Separation, Chem. Rev. 107 (2007) 4078–4110. doi:10.1021/cr0501792.

[27] N.A. Al-Mufachi, N.V. Rees, R. Steinberger-Wilkens, Hydrogen selective membranes: A review of palladium-based dense metal membranes, Renew. Sustain. Energy Rev. 47 (2015) 540–551. doi:10.1016/j.rser.2015.03.026.

[28] R. Rautenbach, Membrane Separations Technology - Principles and Applications, Chemie Ing. Tech. 68 (1996) 168–169. doi:10.1002/cite.330680128.

[29] A. Kapoor, R.T. Yang, C. Wong, Surface Diffusion, Catal. Rev. 31 (1989) 129–214. doi:10.1080/01614948909351350.

[30] H. Li, K. Haas-Santo, U. Schygulla, R. Dittmeyer, Inorganic microporous membranes for H2 and CO2 separation—Review of experimental and modeling progress, Chem. Eng. Sci. 127 (2015) 401–417. doi:10.1016/j.ces.2015.01.022.

[31] J. Meija, T.B. Coplen, M. Berglund, W.A. Brand, P. De Bièvre, M. Gröning, N.E. Holden, J. Irrgeher, R.D. Loss, T. Walczyk, T. Prohaska, Atomic weights of the elements 2013 (IUPAC Technical Report), Pure Appl. Chem. 88 (2016). doi:10.1515/pac-2015-0305.

[32] A. Kapoor, R.T. Yang, C. Wong, Surface Diffusion, Catal. Rev. 31 (1989) 129–214. doi:10.1080/01614948909351350.

[33] K.-H. Lee, S.-T. Hwang, The transport of condensible vapors through a microporous vycor glass membrane, J. Colloid Interface Sci. 110 (1986) 544–555. doi:10.1016/0021-9797(86)90407-8.

[34] W. Jiao, Y. Ban, Z. Shi, X. Jiang, Y. Li, W. Yang, Gas separation performance of supported carbon molecular sieve membranes based on soluble polybenzimidazole, J. Memb. Sci. 533 (2017) 1–10. doi:10.1016/j.memsci.2017.03.022.

[35] K. Briceño, A. Iulianelli, D. Montané, R. Garcia-Valls, A. Basile, Carbon molecular sieve membranes supported on non-modified ceramic tubes for hydrogen separation in membrane reactors, Int. J. Hydrogen Energy. 37 (2012) 13536–13544. doi:10.1016/j.ijhydene.2012.06.069.

[36] H.H. El-Feky, K. Briceño, E.D.O. Jardim, J. Silvestre-Albero, T. Gumí, Novel silica membrane material for molecular sieve applications, Microporous Mesoporous Mater. 179 (2013) 22–29. doi:10.1016/j.micromeso.2013.04.029.

[37] K. Ghasemzadeh, S.M. Sadati Tilebon, A. Basile, Silica Membranes Application for Hydrogen Separation, in: Curr. Trends Futur. Dev. Membr., Elsevier, 2017: pp. 243–264. doi:10.1016/B978-0-444-63866-3.00010-8.

[38] K. Xu, C. Yuan, J. Caro, A. Huang, Silver-exchanged zeolite LTA molecular sieving membranes with enhanced hydrogen selectivity, J. Memb. Sci. 511 (2016) 1–8. doi:10.1016/j.memsci.2016.03.036.

[39] M. Peydayesh, T. Mohammadi, O. Bakhtiari, Effective hydrogen purification from methane via polyimide Matrimid ® 5218- Deca-dodecasil 3R type zeolite mixed matrix membrane, Energy. 141 (2017) 2100–2107. doi:10.1016/j.energy.2017.11.101.

[40] S. Adhikari, S. Fernando, Hydrogen Membrane Separation Techniques, Ind. Eng. Chem. Res. 45 (2006) 875–881. doi:10.1021/ie050644l.

[41] T.M. Nenoff, R.J. Spontak, C.M. Aberg, Membranes for Hydrogen Purification: An Important Step toward a Hydrogen-Based Economy, MRS Bull. 31 (2006) 735–744. doi:10.1557/mrs2006.186.

[42] J.W. Phair, S.P.S. Badwal, Materials for separation membranes in hydrogen and oxygen production and future power generation, Sci. Technol. Adv. Mater. 7 (2006) 792–805. doi:10.1016/j.stam.2006.11.005.

[43] J.-H. Xu, J. Xiang, H. Ding, T.-Q. Yu, J.-L. Li, Z.-G. Li, Y.-W. Yang, X.-L. Shao, Synthesis and electrical properties of BaCeO3-based proton conductors by calcinations of metal-polyvinyl alcohol gel, J. Alloys Compd. 551 (2013) 333–337. doi:10.1016/j.jallcom.2012.10.107.

[44] K. Xie, R. Yan, X. Liu, A novel anode supported BaCe0.4Zr0.3Sn0.1Y0.2O3−δ electrolyte membrane for proton conducting solid oxide fuel cells, Electrochem. Commun. 11 (2009) 1618–1622. doi:10.1016/j.elecom.2009.06.011.

[45] S.-J. Song, T.H. Lee, E.D. Wachsman, L. Chen, S.E. Dorris, U. Balachandran, Defect Structure and Transport Properties of Ni–SrCeO[sub 3−δ] Cermet for Hydrogen Separation Membrane, J. Electrochem. Soc. 152 (2005) J125. doi:10.1149/1.2060690.

[46] W. Xing, P. Inge Dahl, L. Valland Roaas, M.-L. Fontaine, Y. Larring, P.P. Henriksen, R. Bredesen, Hydrogen permeability of SrCe0.7Zr0.25Ln0.05O3−δ membranes (Ln=Tm and Yb), J. Memb. Sci. 473 (2015) 327–332. doi:10.1016/j.memsci.2014.09.027.

[47] G.C. Mather, D. Poulidi, A. Thursfield, M.J. Pascual, J.R. Jurado, I.S. Metcalfe, Hydrogen-permeation characteristics of a SrCeO3-based ceramic separation membrane: Thermal, ageing and surface-modification effects, Solid State Ionics. 181 (2010) 230–235. doi:10.1016/j.ssi.2009.03.014.

[48] T. Norby, R. Haugsrud, Dense Ceramic Membranes for Hydrogen Separation, in: Nonporous Inorg. Membr., Wiley-VCH Verlag GmbH & Co. KGaA, Weinheim, FRG, 2006: pp. 1–48. doi:10.1002/3527608796.ch1.

[49] J.W. Phair, S.P.S. Badwal, Review of proton conductors for hydrogen separation, Ionics (Kiel). 12 (2006) 103–115. doi:10.1007/s11581-006-0016-4.

[50] S. Emerson, N. Magdefrau, Y. She, C. Thibaud-Erkey, Advanced Palladium Membrane Scale-up for Hydrogen Separation, Pittsburgh, PA, and Morgantown, WV (United States), 2012. doi:10.2172/1063878.

[51] M.E. Ivanova, S. Escolástico, M. Balaguer, J. Palisaitis, Y.J. Sohn, W.A. Meulenberg, O. Guillon, J. Mayer, J.M. Serra, Hydrogen separation through tailored dual phase membranes with nominal composition BaCe0.8Eu0.2O3-δ:Ce0.8Y0.2O2-δ at intermediate temperatures, Sci. Rep. 6 (2016) 34773. doi:10.1038/srep34773.

[52] T. Wei, L.A. Zhang, Y. Chen, P. Yang, M. Liu, Promising Proton Conductor for Intermediate-Temperature Fuel Cells: Li13.9Sr0.1Zn(GeO4)4, Chem. Mater. 29 (2017) 1490–1495. doi:10.1021/acs.chemmater.6b03471.

[53] Y. Wei, J. Xue, H. Wang, J. Caro, Hydrogen permeability and stability of BaCe0.85Tb0.05Zr0.1O3−δ asymmetric membranes, J. Memb. Sci. 488 (2015) 173–181. doi:10.1016/j.memsci.2015.04.035.

[54] L.S. Mcleod, Hydrogen Permeation Through Microfabricated Palladium-Silver Alloy Membranes, 2008.

[55] B.H. Guerreiro, M.H. Martin, L. Roué, D. Guay, Hydrogen permeability of PdCuAu membranes prepared from mechanically-alloyed powders, J. Memb. Sci. 509 (2016) 68–82. doi:10.1016/j.memsci.2016.02.040.

[56] S. Nayebossadri, J. Speight, D. Book, Effects of low Ag additions on the hydrogen permeability of Pd–Cu–Ag hydrogen separation membranes, J. Memb. Sci. 451 (2014) 216–225. doi:10.1016/j.memsci.2013.10.002.

[57] A.L. Mejdell, T.A. Peters, M. Stange, H.J. Venvik, R. Bredesen, Performance and application of thin Pd-alloy hydrogen separation membranes in different configurations, J. Taiwan Inst. Chem. Eng. 40 (2009) 253–259. doi:10.1016/j.jtice.2008.12.013.

[58] S. Tosti, F. Borgognoni, A. Santucci, Multi-tube Pd–Ag membrane reactor for pure hydrogen production, Int. J. Hydrogen Energy. 35 (2010) 11470–11477. doi:10.1016/j.ijhydene.2010.06.102.

[59] P. Jiang, D. Liang, M. Kellam, G. Song, T. Yuan, W. Wu, X. Li, Effect of rolling and annealing on microstructures and mechanical properties of V-Ti-Ni alloy for hydrogen separation, J. Alloys Compd. 728 (2017) 63–70. doi:10.1016/j.jallcom.2017.08.288.

[60] S. Tosti, Characterization of thin wall Pd–Ag rolled membranes, Int. J. Hydrogen Energy. 28 (2003) 105–112. doi:10.1016/S0360-3199(02)00034-4.

[61] S. Tosti, Sputtered, electroless, and rolled palladium–ceramic membranes, J. Memb. Sci. 196 (2002) 241–249. doi:10.1016/S0376-7388(01)00597-X.

[62] X. Li, D. Liu, X. Liang, R. Chen, M. Rettenmayr, Y. Su, J. Guo, H. Fu, Hydrogen transport behavior of as-cast, cold rolled and annealed Nb 40 Ti 30 Co 30 alloy membranes, J. Memb. Sci. 514 (2016) 294–304. doi:10.1016/j.memsci.2016.04.055.

[63] R.W. Cahn, P. Haasen, Physical Metallurgy, 1996. doi:http://dx.doi.org/10.1016/B978-0-444-89875-3.50041-7.

[64] S.N. Paglieri, N.K. Pal, M.D. Dolan, S.-M. Kim, W.-M. Chien, J. Lamb, D. Chandra, K.M. Hubbard, D.P. Moore, Hydrogen permeability, thermal stability and hydrogen embrittlement of Ni–Nb–Zr and Ni–Nb–Ta–Zr amorphous alloy membranes, J. Memb. Sci. 378 (2011) 42–50. doi:10.1016/j.memsci.2011.04.049.

[65] Y. Shimpo, S.-I. Yamaura, M. Nishida, H. Kimura, A. Inoue, Development of melt-spun Ni–Nb–Zr–Co amorphous alloy for high-performance hydrogen separating membrane, J. Memb. Sci. 286 (2006) 170–173. doi:10.1016/j.memsci.2006.09.031.

[66] S.C. Chen, G.C. Tu, C.C.Y. Hung, C.A. Huang, M.H. Rei, Preparation of palladium membrane by electroplating on AISI 316L porous stainless steel supports and its use for methanol steam reformer, J. Memb. Sci. 314 (2008) 5–14. doi:10.1016/j.memsci.2007.12.066.

[67] S. Uemiya, T. Endo, R. Yoshiie, W. Katoh, T. Kojima, Fabrication of Thin Palladium-Silver Alloy Film by Using Electroplating Technique, Mater. Trans. 48 (2007) 1119–1123. doi:10.2320/matertrans.48.1119.

[68] S.-E. Nam, S.-H. Lee, K.-H. Lee, Preparation of a palladium alloy composite membrane supported in a porous stainless steel by vacuum electrodeposition, J. Memb. Sci. 153 (1999) 163–173. doi:10.1016/S0376-7388(98)00262-2.

[69] D. Alique, M. Imperatore, R. Sanz, J.A. Calles, M. Giacinti Baschetti, Hydrogen permeation in composite Pd-membranes prepared by conventional electroless plating and electroless pore-plating alternatives over ceramic and metallic supports, Int. J. Hydrogen Energy. 41 (2016) 19430–19438. doi:10.1016/j.ijhydene.2016.06.128.

[70] J. Melendez, E. Fernandez, F. Gallucci, M. van Sint Annaland, P.L. Arias, D.A. Pacheco Tanaka, Preparation and characterization of ceramic supported ultra-thin (~1 µm) Pd-Ag membranes, J. Memb. Sci. 528 (2017) 12–23. doi:10.1016/j.memsci.2017.01.011.

[71] P.. J. Kelly, R.. D. Arnell, Magnetron sputtering: a review of recent developments and applications, Vacuum. 56 (2000) 159–172. doi:10.1016/S0042-207X(99)00189-X.

[72] G. Xomeritakis, Y.S. Lin, Fabrication of thin metallic membranes by MOCVD and sputtering, J. Memb. Sci. 133 (1997) 217–230. doi:10.1016/S0376-7388(97)00084-7.

[73] N. Vicinanza, I.-H. Svenum, L.N. Næss, T.A. Peters, R. Bredesen, A. Borg, H.J. Venvik, Thickness dependent effects of solubility and surface phenomena on the hydrogen transport properties of sputtered Pd77%Ag23% thin film membranes, J. Memb. Sci. 476 (2015) 602–608. doi:10.1016/j.memsci.2014.11.031.

[74] A.I. Pereira, P. Pérez, S.C. Rodrigues, A. Mendes, L.M. Madeira, C.J. Tavares, Deposition of Pd–Ag thin film membranes on ceramic supports for hydrogen purification/separation, Mater. Res. Bull. 61 (2015) 528–533. doi:10.1016/j.materresbull.2014.10.055.

[75] S. Fasolin, S. Barison, S. Boldrini, A. Ferrario, M. Romano, F. Montagner, E. Miorin, M. Fabrizio, L. Armelao, Hydrogen separation by thin vanadium-based multi-layered membranes, Int. J. Hydrogen Energy. 43 (2018) 3235–3243. doi:10.1016/j.ijhydene.2017.12.148.

[76] S. Nayebossadri, D. Smith, J. Speight, D. Book, Amorphous Zr-based thin films fabricated by magnetron sputtering for potential application in hydrogen purification, J. Alloys Compd. 645 (2015) S56–S60. doi:10.1016/j.jallcom.2015.01.230.

[77] L. Xiong, S. Liu, L. Rong, Fabrication and characterization of Pd/Nb40Ti30Ni30/Pd/porous nickel support composite membrane for hydrogen separation and purification, Int. J. Hydrogen Energy. 35 (2010) 1643–1649. doi:10.1016/j.ijhydene.2009.12.081.

[78] J.-Y. Han, C.-H. Kim, S.-H. Kim, D.-W. Kim, Development of Pd Alloy Hydrogen Separation Membranes with Dense/Porous Hybrid Structure for High Hydrogen Perm-Selectivity, Adv. Mater. Sci. Eng. 2014 (2014) 1–10. doi:10.1155/2014/438216.

[79] P.P. Mardilovich, Y. She, Y.H. Ma, M.-H. Rei, Defect-free palladium membranes on porous stainless-steel support, AIChE J. 44 (1998) 310–322. doi:10.1002/aic.690440209.

[80] R.C. Hurlbert, J.O. Konecny, Diffusion of Hydrogen through Palladium, J. Chem. Phys. 34 (1961) 655–658. doi:10.1063/1.1701003.

[81] T.L. Ward, T. Dao, Model of hydrogen permeation behavior in palladium membranes, J. Memb. Sci. 153 (1999) 211–231. doi:10.1016/S0376-7388(98)00256-7.

[82] J. Melendez, N. de Nooijer, K. Coenen, E. Fernandez, J.L. Viviente, M. van Sint Annaland, P.L. Arias, D.A.P. Tanaka, F. Gallucci, Effect of Au addition on hydrogen permeation and the resistance to H 2 S on Pd-Ag alloy membranes, J. Memb. Sci. 542 (2017) 329–341. doi:10.1016/j.memsci.2017.08.029.

[83] H. Jia, P. Wu, G. Zeng, E. Salas-Colera, A. Serrano, G.R. Castro, H. Xu, C. Sun, A. Goldbach, High-temperature stability of Pd alloy membranes containing Cu and Au, J. Memb. Sci. 544 (2017) 151–160. doi:10.1016/j.memsci.2017.09.012.

[84] S.A. Steward, Review of Hydrogen Isotope Permeability Through Materials, Livermore, CA (United States), 1983. doi:10.2172/5277693.

[85] M. Dolan, N. Dave, L. Morpeth, R. Donelson, D. Liang, M. Kellam, S. Song, Ni-based amorphous alloy membranes for hydrogen separation at 400°C, J. Memb. Sci. 326 (2009) 549–555. doi:10.1016/j.memsci.2008.10.030.

[86] S. Hara, K. Sakaki, N. Itoh, H.-M. Kimura, K. Asami, A. Inoue, An amorphous alloy membrane without noble metals for gaseous hydrogen separation, J. Memb. Sci. 164 (2000) 289–294. doi:10.1016/S0376-7388(99)00192-1.

[87] K. Hashi, K. Ishikawa, T. Matsuda, K. Aoki, Microstructures and Hydrogen Permeability of Nb-Ti-Ni Alloys with High Resistance to Hydrogen Embrittlement, Mater. Trans. 46 (2005) 1026–1031. doi:10.2320/matertrans.46.1026.

[88] S.E. Roark, R. Mackay, M. V. Mundschau, Dense, layered membranes for hydrogen separation, US7001446 B2, 2006.

[89] E. Yan, X. Li, D. Liu, M. Rettenmayr, Y. Su, J. Guo, Nb–HfCo alloys with pronounced high hydrogen permeability: A new family of metallic hydrogen permeation membranes, Int. J. Hydrogen Energy. 39 (2014) 8385–8389. doi:10.1016/j.ijhydene.2014.03.173.

[90] I. Sipatov, N. Sidorov, S. Pryanichnikov, E. Pastukhov, Structure and properties study of V-based membrane alloys for ultra-high purity hydrogen production, in: J. Chem. Phys., 2016: p. 020031. doi:10.1063/1.4962615.

[91] A.G. Knapton, Palladium alloys for hydrogen diffusion membranes: A Review of High Permeability Materials, Platin. Met. Rev. 21 (1977) 44–50.

[92] A. V. Gapontsev, V. V. Kondrat'ev, Hydrogen diffusion in disordered metals and alloys, Uspekhi Fiz. Nauk. 173 (2003) 1107. doi:10.3367/UFNr.0173.200310c.1107.

[93] S. Sarker, D. Chandra, M. Hirscher, M. Dolan, D. Isheim, J. Wermer, D. Viano, M. Baricco, T.J. Udovic, D. Grant, O. Palumbo, A. Paolone, R. Cantelli, Developments in the Ni–Nb–Zr amorphous alloy membranes, Appl. Phys. A. 122 (2016) 168. doi:10.1007/s00339-016-9650-5.

[94] L. Ge, X. Hui, E.R. Wang, G.L. Chen, R. Arroyave, Z.K. Liu, Prediction of the glass forming ability in Cu–Zr binary and Cu–Zr–Ti ternary alloys, Intermetallics. 16 (2008) 27–33. doi:10.1016/j.intermet.2007.07.008.

[95] T. Lai, S.S. Singh, A.S.S. Singaravelu, K.S. Vadari, A. Khosravi, N. Chawla, M.L. Lind, Hydrogen permeability and mechanical properties of NiNb-M (M = Sn, Ti and Zr) amorphous metallic membranes, J. Alloys Compd. 684 (2016) 359–365. doi:10.1016/j.jallcom.2016.05.100.

[96] E. Evard, Permeation of hydrogen through amorphous ferrum membrane, Int. J. Hydrogen Energy. 26 (2001) 457–460. doi:10.1016/S0360-3199(00)00078-1.

[97] D. Zander, H. Leptien, U. Köster, N. Eliaz, D. Eliezer, Hydrogenation of Zr-based metallic glasses and quasicrystals, J. Non. Cryst. Solids. 250–252 (1999) 893–897. doi:10.1016/S0022-3093(99)00200-8.

[98] M.D. Dolan, Non-Pd BCC alloy membranes for industrial hydrogen separation, J. Memb. Sci. 362 (2010) 12–28. doi:10.1016/j.memsci.2010.06.068.

[99] S.N. Paglieri, J.D. Way, Innovations in Palladium Membrane Research, Sep. Purif. Methods. 31 (2002) 1–169. doi:10.1081/SPM-120006115.

[100] S.N. Paglieri, Palladium Membranes, in: Nonporous Inorg. Membr., Wiley-VCH Verlag GmbH & Co. KGaA, Weinheim, FRG, 2006: pp. 77–105. doi:10.1002/3527608796.ch3.

[101] H. Wipf, Solubility and Diffusion of Hydrogen in Pure Metals and Alloys, Phys. Scr. T94 (2001) 43. doi:10.1238/Physica.Topical.094a00043.

[102] K. Hashi, K. Ishikawa, T. Matsuda, K. Aoki, Hydrogen permeation characteristics of multi-phase Ni-Ti-Nb alloys, J. Alloys Compd. 368 (2004) 215–220. doi:10.1016/j.jallcom.2003.08.064.

[103] K. Hashi, K. Ishikawa, T. Matsuda, K. Aoki, Hydrogen permeation characteristics of (V, Ta)–Ti–Ni alloys, J. Alloys Compd. 404–406 (2005) 273–278. doi:10.1016/j.jallcom.2005.02.085.

[104] K. Hashi, K. Ishikawa, T. Matsuda, K. Aoki, Microstructure and hydrogen permeability in Nb–Ti–Co multiphase alloys, J. Alloys Compd. 425 (2006) 284–290. doi:10.1016/j.jallcom.2006.01.028.

[105] K. Ishikawa, T. Takano, T. Matsuda, K. Aoki, High hydrogen permeability in the Nb–Zr–Ni eutectic alloy containing the primary body-centered-cubic (Nb, Zr) phase, Appl. Phys. Lett. 87 (2005) 081906. doi:10.1063/1.2006985.

[106] X. Li, D. Liu, R. Chen, E. Yan, X. Liang, M. Rettenmayr, Y. Su, J. Guo, H. Fu, Changes in microstructure, ductility and hydrogen permeability of Nb–(Ti, Hf)Ni alloy membranes by the substitution of Ti by Hf, J. Memb. Sci. 484 (2015) 47–56. doi:10.1016/j.memsci.2015.03.002.

[107] W. Luo, K. Ishikawa, K. Aoki, Highly hydrogen permeable Nb–Ti–Co hypereutectic alloys containing much primary bcc-(Nb, Ti) phase, Int. J. Hydrogen Energy. 37 (2012) 12793–12797. doi:10.1016/j.ijhydene.2012.06.005.

[108] X. Li, F. Huang, D. Liu, X. Liang, R. Chen, M. Rettenmayr, Y. Su, J. Guo, H. Fu, V-Cr-Cu dual-phase alloy membranes for hydrogen separation: An excellent combination of ductility, hydrogen permeability and embrittlement resistance, J. Memb. Sci. 524 (2017) 354–361. doi:10.1016/j.memsci.2016.11.020.

[109] Y. Awakura, T. Nambu, Y. Matsumoto, H. Yukawa, Hydrogen solubility and permeability of Nb–W–Mo alloy membrane, J. Alloys Compd. 509 (2011) S877–S880. doi:10.1016/j.jallcom.2010.10.133.

[110] D.A. Cooney, J.D. Way, C.A. Wolden, A comparison of the performance and stability of Pd/BCC metal composite membranes for hydrogen purification, Int. J. Hydrogen Energy. 39 (2014) 19009–19017. doi:10.1016/j.ijhydene.2014.09.094.

[111] H. Yukawa, T. Nambu, Y. Matsumoto, N. Watanabe, G. Zhang, M. Morinaga, Alloy Design of Nb-Based Hydrogen Permeable Membrane with Strong Resistance to Hydrogen Embrittlement, Mater. Trans. 49 (2008) 2202–2207. doi:10.2320/matertrans.MA200805.

[112] H. Yukawa, C. Tsukada, T. Nambu, Y. Matsumoto, Hydrogen solubility and permeability of V-W-Mo alloy membrane for hydrogen separation and purification, J. Alloys Compd. 580 (2013). doi:10.1016/j.jallcom.2013.03.144.

[113] M.D. Dolan, K.G. McLennan, G. Song, D. Liang, M.E. Kellam, The effect of Ti on hydrogen absorption and diffusivity in V–Ti–Al alloy membranes, J. Memb. Sci. 446 (2013) 405–409. doi:10.1016/j.memsci.2013.07.003.

[114] K.H. Kim, H.C. Park, J. Lee, E. Cho, S.M. Lee, Vanadium alloy membranes for high hydrogen permeability and suppressed hydrogen embrittlement, Scr. Mater. 68 (2013) 905–908. doi:10.1016/j.scriptamat.2013.02.028.

[115] K.S. Rothenberger, B.H. Howard, R.P. Killmeyer, A. V. Cugini, R.M. Enick, F. Bustamante, M. V. Ciocco, B.D. Morreale, R.E. Buxbaum, Evaluation of tantalum-based materials for hydrogen separation at elevated temperatures and pressures☆, J. Memb. Sci. 218 (2003) 19–37. doi:10.1016/S0376-7388(03)00134-0.

[116] S.N. Paglieri, Development of Group V Based Metal Membranes for Hydrogen Separation, in: AlChE Annu. Meet., Philadelphia, 2008.

[117] K. Tsuchimoto, H. Yukawa, T. Nambu, Y. Matsumoto, Y. Murata, Design of Nb-W-Mo alloy membrane for hydrogen separation and purification, J. Alloys Compd. 580 (2013). doi:10.1016/j.jallcom.2013.03.143.

[118] A. Suzuki, H. Yukawa, T. Nambu, Y. Matsumoto, Y. Murata, Analysis of hydrogen mobility in Nb-based alloy membranes in view of new description of hydrogen permeability based on hydrogen chemical potential, J. Alloys Compd. 645 (2015) S107–S111. doi:10.1016/j.jallcom.2014.12.265.

[119] V.N. Alimov, A.O. Busnyuk, M.. Notkin, E.Y. Peredistov, A.I. Livshits, Hydrogen transport through V–Pd alloy membranes: Hydrogen solution, permeation and diffusion, J. Memb. Sci. 481 (2015) 54–62. doi:10.1016/j.memsci.2015.01.058.

[120] T. Graham, On the Absorption and Dialytic Separation of Gases by Colloid Septa, Philos. Trans. R. Soc. London. 156 (1866) 399–439. http://www.jstor.org/stable/108953.

[121] K. Zhang, H. Gao, Z. Rui, P. Liu, Y. Li, Y.S. Lin, High-temperature stability of palladium membranes on porous metal supports with different intermediate layers, Ind. Eng. Chem. Res. 48 (2009) 1880–1886. doi:10.1021/ie801417w.

[122] L.J. Gillespie, F.P. Hall, The Palladium-Hydrogen Equilibrium and Palladium Hydride, J. Am. Chem. Soc. 48 (1926) 1207–1219. doi:10.1021/ja01416a015.

[123] M.L.H. Wise, J.P.G. Farr, I.R. Harris, X-ray studies of the α/β miscibility gaps of some palladium solid solution-hydrogen systems, J. Less Common Met. 41 (1975) 115–127. doi:10.1016/0022-5088(75)90099-5.

[124] L.W. McKeehan, The Crystal Structures of the System Palladium-Hydrogen, Phys. Rev. 21 (1923) 334–342. doi:10.1103/PhysRev.21.334.

[125] F.A. Lewis, The Palladium Hydrogen System, Platin. Met. Rev. 26 (1982) 20–27.

[126] W. Huang, S.M. Opalka, D. Wang, T.B. Flanagan, Thermodynamic modelling of the Cu–Pd–H system, Calphad. 31 (2007) 315–329. doi:10.1016/j.calphad.2007.02.002.

[127] Ø. Hatlevik, S.K. Gade, M.K. Keeling, P.M. Thoen, A.P. Davidson, J.D. Way, Palladium and palladium alloy membranes for hydrogen separation and production: History, fabrication strategies, and current performance, Sep. Purif. Technol. 73 (2010) 59–64. doi:10.1016/j.seppur.2009.10.020.

[128] V. Gryaznov, Metal Containing Membranes for the Production of Ultrapure Hydrogen and the Recovery of Hydrogen Isotopes, Sep. Purif. Methods. 29 (2000) 171–187. doi:10.1081/SPM-100100008.

[129] G.L. Holleck, Diffusion and solubility of hydrogen in palladium and palladium--silver alloys, J. Phys. Chem. 74 (1970) 503–511. doi:10.1021/j100698a005.

[130] H. Gao, Y.S. Lin, Y. Li, B. Zhang, Chemical Stability and Its Improvement of Palladium-Based Metallic Membranes, Ind. Eng. Chem. Res. 43 (2004) 6920–6930. doi:10.1021/ie049722f.

[131] B.D. Morreale, M.V. Ciocco, B.H. Howard, R.P. Killmeyer, A.V. Cugini, R.M. Enick, Effect of hydrogen-sulfide on the hydrogen permeance of palladium?copper alloys at elevated temperatures, J. Memb. Sci. 241 (2004) 219–224. doi:10.1016/j.memsci.2004.04.033.

[132] A. Iulianelli, M. Alavi, G. Bagnato, S. Liguori, J. Wilcox, M. Rahimpour, R. Eslamlouyan, B. Anzelmo, A. Basile, Supported Pd-Au Membrane Reactor for Hydrogen Production: Membrane Preparation, Characterization and Testing, Molecules. 21 (2016) 581. doi:10.3390/molecules21050581.

[133] J. Way, M. Lusk, P. Thoen, Sulfur-Resistant composite Metal Membranes, US20080038567 A1, 2008.

[134] S. Nayebossadri, S. Fletcher, J.D. Speight, D. Book, Hydrogen permeation through porous stainless steel for palladium-based composite porous membranes, J. Memb. Sci. 515 (2016) 22–28. doi:10.1016/j.memsci.2016.05.036.

[135] S.-K. Ryi, S.-W. Lee, D.-K. Oh, B.-S. Seo, J.-W. Park, J.-S. Park, D.-W. Lee, S.S. Kim, Electroless plating of Pd after shielding the bottom of planar porous stainless steel for a highly stable hydrogen selective membrane, J. Memb. Sci. 467 (2014) 93–99. doi:10.1016/j.memsci.2014.04.058.

[136] M. Zahedi, B. Afra, M. Dehghani-Mobarake, M. Bahmani, Preparation of a Pd membrane on a WO3 modified Porous Stainless Steel for hydrogen separation, J. Memb. Sci. 333 (2009) 45–49. doi:10.1016/j.memsci.2009.01.053.

[137] Y. Li, W. Ding, X. Jin, J. Yu, X. Hu, Y. Huang, Toward extensive application of Pd/ceramic membranes for hydrogen separation: A case study on membrane recycling and reuse in the fabrication of new membranes, Int. J. Hydrogen Energy. 40 (2015) 3528–3537. doi:10.1016/j.ijhydene.2014.09.017.

[138] E. David, J. Kopac, Devlopment of palladium/ceramic membranes for hydrogen separation, Int. J. Hydrogen Energy. 36 (2011) 4498–4506. doi:10.1016/j.ijhydene.2010.12.032.

[139] E. Gobina, R. Hughes, D. Monaghan, D. Arnell, High-Temperature Selective Membranes for Hydrogen Separation, Dev. Chem. Eng. Miner. Process. 2 (2008) 105–114. doi:10.1002/apj.5500020203.

[140] A. Santucci, S. Tosti, A. Basile, Alternatives to palladium in membranes for hydrogen separation: nickel, niobium and vanadium alloys, ceramic supports for metal alloys and porous glass membranes, in: Handb. Membr. React., Elsevier, 2013: pp. 183–217. doi:10.1533/9780857097330.1.183.

[141] S. Uemiya, N. Sato, H. Ando, Y. Kude, T. Matsuda, E. Kikuchi, Separation of hydrogen through palladium thin film supported on a porous glass tube, J. Memb. Sci. 56 (1991) 303–313. doi:10.1016/S0376-7388(00)83040-9.

[142] B. Hafner, Energy Dispersive Spectroscopy on the SEM: A Primer, Charact. Facil. Univ. Minnesota. (2006) 7–10. http://scholar.google.com/scholar?hl=en&btnG=Search&q=intitle:Energy+Dispersive+Spectroscopy+on+the+SEM+:#8.

[143] L. Lutterotti, D. Chateigner, S. Ferrari, J. Ricote, Texture, residual stress and structural analysis of thin films using a combined X-ray analysis, Thin Solid Films. 450 (2004) 34–41. doi:10.1016/j.tsf.2003.10.150.

[144] F.M. Smits, Measurement of Sheet Resistivities with the Four-Point Probe, Bell Syst. Tech. J. 37 (1958) 711–718. doi:10.1002/j.1538-7305.1958.tb03883.x.

[145] F. Pişkin, Deposition and Testing of Thin Film Hydrogen Separation Membranes, Middle East Technical University, 2013.

[146] H. Wang, X. Dong, Y.S. Lin, Membrane reactors for hydrogen production from coal, in: Membr. React. Energy Appl. Basic Chem. Prod., Elsevier, 2015: pp. 145–186. doi:10.1016/B978-1-78242-223-5.00005-4.

[147] A. Murugan, A.S. Brown, Review of purity analysis methods for performing quality assurance of fuel cell hydrogen, Int. J. Hydrogen Energy. 40 (2015) 4219–4233. doi:10.1016/j.ijhydene.2015.01.041.

[148] M.H. Xie, J.Y. Chen, K.W. Sun, Improvement in the light conversion efficiency of silicon solar cells by pure hydrogen annealing, Mater. Sci. Semicond. Process. 39 (2015) 200–204. doi:10.1016/j.mssp.2015.05.009.

[149] B. Anzelmo, J. Wilcox, S. Liguori, Natural gas steam reforming reaction at low temperature and pressure conditions for hydrogen production via Pd/PSS membrane reactor, J. Memb. Sci. 522 (2017) 343–350. doi:10.1016/j.memsci.2016.09.029.

[150] V.N. Alimov, A.O. Busnyuk, M.E. Notkin, E.Y. Peredistov, A.I. Livshits, Substitutional V–Pd alloys for the membranes permeable to hydrogen: Hydrogen solubility at 150–400 °C, Int. J. Hydrogen Energy. 39 (2014) 19682–19690. doi:10.1016/j.ijhydene.2014.09.122.

[151] S. Nayebossadri, J.D. Speight, D. Book, Pd–Cu–M (M = Y, Ti, Zr, V, Nb, and Ni) Alloys for the Hydrogen Separation Membrane, ACS Appl. Mater. Interfaces. 9 (2017) 2650–2661. doi:10.1021/acsami.6b12752.

[152] W.-H. Chen, M.-H. Hsia, Y.-H. Chi, Y.-L. Lin, C.-C. Yang, Polarization phenomena of hydrogen-rich gas in high-permeance Pd and Pd–Cu membrane tubes, Appl. Energy. 113 (2014) 41–50. doi:10.1016/j.apenergy.2013.07.014.

[153] A.M. Tarditi, F. Braun, L.M. Cornaglia, Novel PdAgCu ternary alloy: Hydrogen permeation and surface properties, Appl. Surf. Sci. 257 (2011) 6626–6635. doi:10.1016/j.apsusc.2011.02.089.

[154] A. Basile, A. Iulianelli, T. Longo, S. Liguori, M. De Falco, Membrane Reactors for Hydrogen Production Processes, Springer London, London, 2011. doi:10.1007/978-0-85729-151-6.

[155] B.D. Adams, A. Chen, The role of palladium in a hydrogen economy, Mater. Today. 14 (2011) 282–289. doi:10.1016/S1369-7021(11)70143-2.

[156] B. LIU, W. ZHANG, W. DAI, J. DENG, Thermal stability, hydrogen adsorption and separation performance of Ni-based amorphous alloy membranes, J. Memb. Sci. 244 (2004) 243–249. doi:10.1016/j.memsci.2004.07.012.

[157] E. Yan, X. Li, M. Rettenmayr, D. Liu, Y. Su, J. Guo, D. Xu, H. Fu, Design of hydrogen permeable Nb–Ni–Ti alloys by correlating the microstructures, solidification paths and hydrogen permeability, Int. J. Hydrogen Energy. 39 (2014) 3505–3516. doi:10.1016/j.ijhydene.2013.12.060.

[158] E. Magnone, S. Il Jeon, J.H. Park, E. Fleury, Relationship between microstructure and hydrogen permeation properties in the multiphase Ni21Ti23Nb56 alloy membranes, J. Memb. Sci. 384 (2011) 136–141. doi:10.1016/j.memsci.2011.09.014.

[159] Y. Saeki, Y. Yamada, K. Ishikawa, Relationship between hydrogen permeation and microstructure in Nb–TiCo two-phase alloys, J. Alloys Compd. 645 (2015) S32–S35. doi:10.1016/j.jallcom.2015.01.248.

[160] M.D. Dolan, G. Song, K.G. McLennan, M.E. Kellam, D. Liang, The effect of Ti on the microstructure, hydrogen absorption and diffusivity of V–Ni alloy membranes, J. Memb. Sci. 415–416 (2012) 320–327. doi:10.1016/j.memsci.2012.05.012.

[161] W. Luo, K. Ishikawa, K. Aoki, Hydrogen permeable Ta–Ti–Ni duplex phase alloys with high resistance to hydrogen embrittlement, J. Alloys Compd. 460 (2008) 353–356. doi:10.1016/j.jallcom.2007.06.061.

[162] P. Decker, D. Naujoks, D. Langenkämper, C. Somsen, A. Ludwig, High-Throughput Structural and Functional Characterization of the Thin Film Materials System Ni–Co–Al, ACS Comb. Sci. 19 (2017) 618–624. doi:10.1021/acscombsci.6b00176.

[163] S. Borhani-Haghighi, M. Kieschnick, Y. Motemani, A. Savan, D. Rogalla, H.-W. Becker, J. Meijer, A. Ludwig, High-Throughput Compositional and Structural Evaluation of a Li a (Ni x Mn y Co z)O r Thin Film Battery Materials Library, ACS Comb. Sci. 15 (2013) 401–409. doi:10.1021/co4000166.

[164] V. Alexandrakis, W. Wallisch, S. Hamann, G. Varvaro, J. Fidler, A. Ludwig, Combinatorial Development of Fe–Co–Nb Thin Film Magnetic Nanocomposites, ACS Comb. Sci. 17 (2015) 698–703. doi:10.1021/acscombsci.5b00116.

[165] F. Pişkin, H. Akyıldız, T. Öztürk, Ti modified Pd–Ag membranes for hydrogen separation, Int. J. Hydrogen Energy. 40 (2015) 7553–7558. doi:10.1016/j.ijhydene.2014.11.049.

[166] F. Pişkin, T. Öztürk, Combinatorial screening of Pd-Ag-Ni membranes for hydrogen separation, J. Memb. Sci. 524 (2017) 631–636. doi:10.1016/j.memsci.2016.11.066.

[167] M. V. Mundschau, Hydrogen Separation Using Dense Composite Membranes: Part 1 Fundamentals, in: Inorg. Membr. Energy Environ. Appl., Springer New York, New York, NY, 2009: pp. 125–153. doi:10.1007/978-0-387-34526-0_8.

[168] K. Watanabe, Y. Fukai, Electrical resistivity due to interstitial hydrogen and deuterium in V, Nb, Ta and Pd, J. Phys. F Met. Phys. 10 (1980) 1795–1801. doi:10.1088/0305-4608/10/8/016.

[169] F.A. Lewis, S.G. McKee, Hydride Formation by Nickel, Palladium and Platinum, in: Met. Syst., Elsevier, 1982: pp. 423–436. doi:10.1016/B978-0-08-027311-2.50043-7.

[170] A. Pozio, Z. Jovanović, R. Lo Presti, M. De Francesco, S. Tosti, Pd–Ag hydrogen content and electrical resistivity: Temperature and pressure effect, Int. J. Hydrogen Energy. 37 (2012) 7925–7933. doi:10.1016/j.ijhydene.2012.01.108.

[171] V. Antonov, I. Belash, V. Malyshev, E. Ponyatovsky, The solubility of hydrogen in the platinum metals under high pressure☆, Int. J. Hydrogen Energy. 11 (1986) 193–197. doi:10.1016/0360-3199(86)90083-2.

[172] R. Chaubey, S. Sahu, O.O. James, S. Maity, A review on development of industrial processes and emerging techniques for production of hydrogen from renewable and sustainable sources, Renew. Sustain. Energy Rev. 23 (2013) 443–462. doi:10.1016/j.rser.2013.02.019.

[173] C. Wu, P.T. Williams, Pyrolysis-gasification of post-consumer municipal solid plastic waste for hydrogen production, Int. J. Hydrogen Energy. 35 (2010) 949–957. doi:10.1016/j.ijhydene.2009.11.045.

[174] D. Haeseldonckx, W. D’haeseleer, The use of the natural-gas pipeline infrastructure for hydrogen transport in a changing market structure, Int. J. Hydrogen Energy. 32 (2007) 1381–1386. doi:10.1016/j.ijhydene.2006.10.018.

[175] S. Tosti, L. Bettinali, V. Violante, Rolled thin Pd and Pd-Ag membranes for hydrogen separation and production, Int. J. Hydrogen Energy. 25 (2000) 319–325. doi:10.1016/S0360-3199(99)00044-0.

[176] A. Kulprathipanja, G. Alptekin, J. Falconer, J. Way, Pd and Pd–Cu membranes: inhibition of H permeation by HS, J. Memb. Sci. 254 (2005) 49–62. doi:10.1016/j.memsci.2004.11.031.

[177] D. Pizzi, R. Worth, M. Giacinti Baschetti, G.C. Sarti, K. Noda, Hydrogen permeability of 2.5μm palladium–silver membranes deposited on ceramic supports, J. Memb. Sci. 325 (2008) 446–453. doi:10.1016/j.memsci.2008.08.020.

[178] T.A. Peters, T. Kaleta, M. Stange, R. Bredesen, Development of thin binary and ternary Pd-based alloy membranes for use in hydrogen production, J. Memb. Sci. 383 (2011) 124–134. doi:10.1016/j.memsci.2011.08.050.

[179] A. De Ninno, Dynamics in Pd–H(D) Systems, Condens. Matter Nucl. Sci. 4 (2011) 291–303. http://www.iscmns.org/CMNS/JCMNS-Vol4.pdf.

[180] B.H. Howard, R.P. Killmeyer, K.S. Rothenberger, A.V. Cugini, B.D. Morreale, R.M. Enick, F. Bustamante, Hydrogen permeance of palladium-copper alloy membranes over a wide range of temperatures and pressures, J. Memb. Sci. 241 (2004) 207–218. doi:10.1016/j.memsci.2004.04.031.

[181] D.L. Mckinley, Metal alloy for hydrogen separation and purification, US3350845, 1967.

[182] P. Kamakoti, A comparison of hydrogen diffusivities in Pd and CuPd alloys using density functional theory, J. Memb. Sci. 225 (2003) 145–154. doi:10.1016/j.memsci.2003.07.008.

[183] D. Fort, J.P.G. Farr, I.R. Harris, A comparison of palladium-silver and palladium-yttrium alloys as hydrogen separation membranes, J. Less Common Met. 39 (1975) 293–308. doi:10.1016/0022-5088(75)90204-0.

[184] K. Bryden, Nanostructured palladium–iron membranes for hydrogen separation and membrane hydrogenation reactions, J. Memb. Sci. 203 (2002) 29–42. doi:10.1016/S0376-7388(01)00736-0.

[185] V.G. Litovchenko, A.A. Efremov, The enhanced catalytic dissociation of adsorbed hydrogen containing molecules, Condens. Matter Phys. 2 (1999) 561–576. http://www.icmp.lviv.ua/journal/zbirnyk.19/019/art19.pdf.

[186] W.-H. Chen, J.-J. Lu, Hydrogen production from water gas shift reactions in association with separation using a palladium membrane tube, Int. J. Energy Res. 36 (2012) 346–354. doi:10.1002/er.1801.

[187] A. Basile, A. Iulianelli, T. Longo, S. Liguori, M. De Falco, Pd-based Selective Membrane State-of-the-Art, in: Membr. React. Hydrog. Prod. Process., 2011: pp. 21–55. doi:10.1007/978-0-85729-151-6_2.

[188] B.A. McCool, Y.S. Lin, Nanostructured thin palladium-silver membranes: Effects of grain size on gas permeation properties, J. Mater. Sci. 36 (2001) 3221–3227. doi:10.1023/A:1017938403725.

[189] V. Jayaraman, Y.S.S. Lin, Synthesis and hydrogen permeation properties of ultrathin palladium-silver alloy membranes, J. Memb. Sci. 104 (1995) 251–262. doi:10.1016/0376-7388(95)00040-J.

[190] D.T. Hughes, I.R. Harris, A comparative study of hydrogen permeabilities and solubilities in some palladium solid solution alloys, J. Less-Common Met. 61 (1978). doi:10.1016/0022-5088(78)90229-1.

[191] C.G. Sonwane, J. Wilcox, Y.H. Ma, Solubility of hydrogen in PdAg and PdAu binary alloys using density functional theory., J. Phys. Chem. B. 110 (2006) 24549–24558. doi:10.1021/jp064507t.

[192] D. Fort, I.R. Harris, The physical properties of some palladium alloy hydrogen diffusion membrane material, J. Less-Common Met. 41 (1975) 313–327. doi:10.1016/0022-5088(75)90037-5.

[193] I.R. Harris, M. Norman, The electronic state of cerium in some palladium alloys, J. Less Common Met. 15 (1968) 285–298. doi:https://doi.org/10.1016/0022-5088(68)90187-2.

[194] X.L. Zhang, X.F. Xie, Y. Huang, Pure Ni and Pd-Ni Alloy Membranes Prepared by Electroless Plating for Hydrogen Separation, Adv. Mater. Res. 179–180 (2011) 1309–1313. doi:10.4028/www.scientific.net/AMR.179-180.1309.

[195] S. Tosti, F. Borgognoni, A. Santucci, Electrical resistivity, strain and permeability of Pd–Ag membrane tubes, Int. J. Hydrogen Energy. 35 (2010) 7796–7802. doi:10.1016/j.ijhydene.2010.05.088.

[196] R.J. Renka, Interpolation of data on the surface of a sphere, ACM Trans. Math. Softw. 10 (1984) 417–436. doi:10.1145/2701.2703.

[197] W.B. Pearson, A Handbook of Lattice Spacing and Structure of Metal and Alloys, Pergamon Press Ltd., 1958. doi:10.1524/zkri.1961.115.3-4.319.

[198] Y. Sakamoto, S. Hirata, H. Nishikawa, Diffusivity and solubility of hydrogen in Pd-Ag and Pd-Au alloys, J. Less Common Met. 88 (1982) 387–395. doi:10.1016/0022-5088(82)90247-8.

APPENDICES

A. PERMISSION LICENSES

ELSVEIR LICENSE

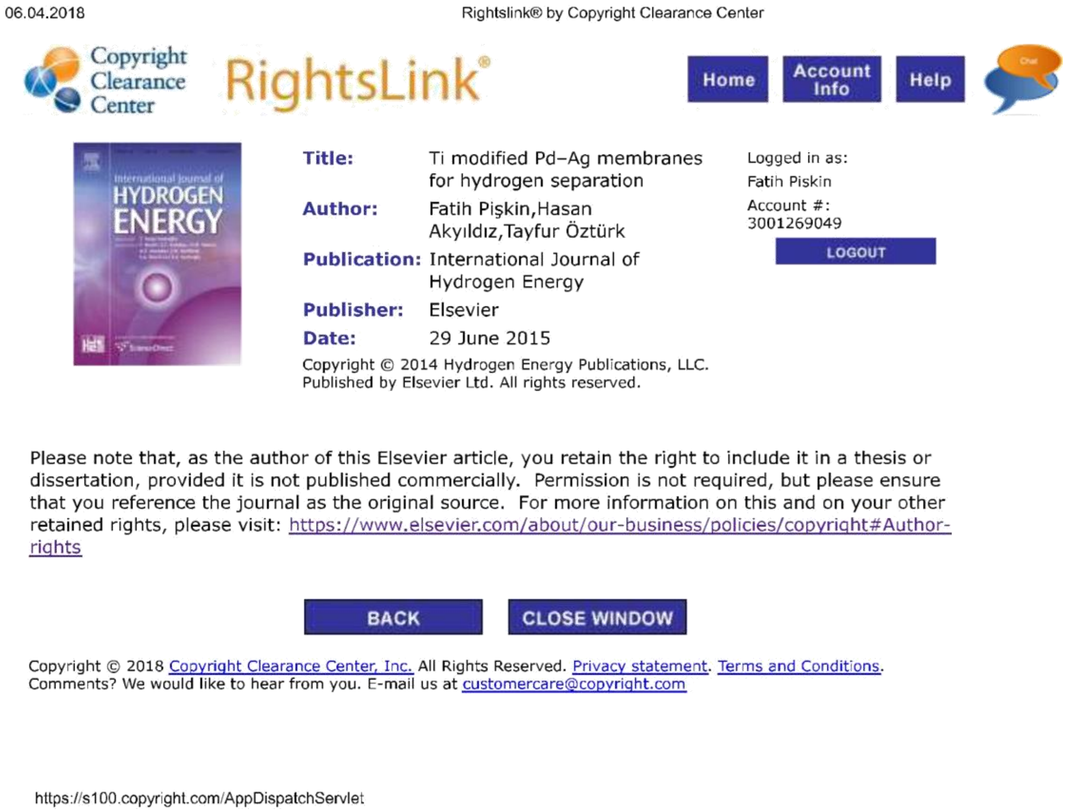

06.04.2018 Rightslink® by Copyright Clearance Center

Title: Ti modified Pd–Ag membranes for hydrogen separation

Author: Fatih Pişkin,Hasan Akyıldız,Tayfur Öztürk

Publication: International Journal of Hydrogen Energy

Publisher: Elsevier

Date: 29 June 2015

Copyright © 2014 Hydrogen Energy Publications, LLC. Published by Elsevier Ltd. All rights reserved.

Logged in as:
Fatih Piskin
Account #:
3001269049

Please note that, as the author of this Elsevier article, you retain the right to include it in a thesis or dissertation, provided it is not published commercially. Permission is not required, but please ensure that you reference the journal as the original source. For more information on this and on your other retained rights, please visit: https://www.elsevier.com/about/our-business/policies/copyright#Author-rights

Copyright © 2018 Copyright Clearance Center, Inc. All Rights Reserved. Privacy statement. Terms and Conditions.
Comments? We would like to hear from you. E-mail us at customercare@copyright.com

https://s100.copyright.com/AppDispatchServlet

ELSVEIR LICENSE

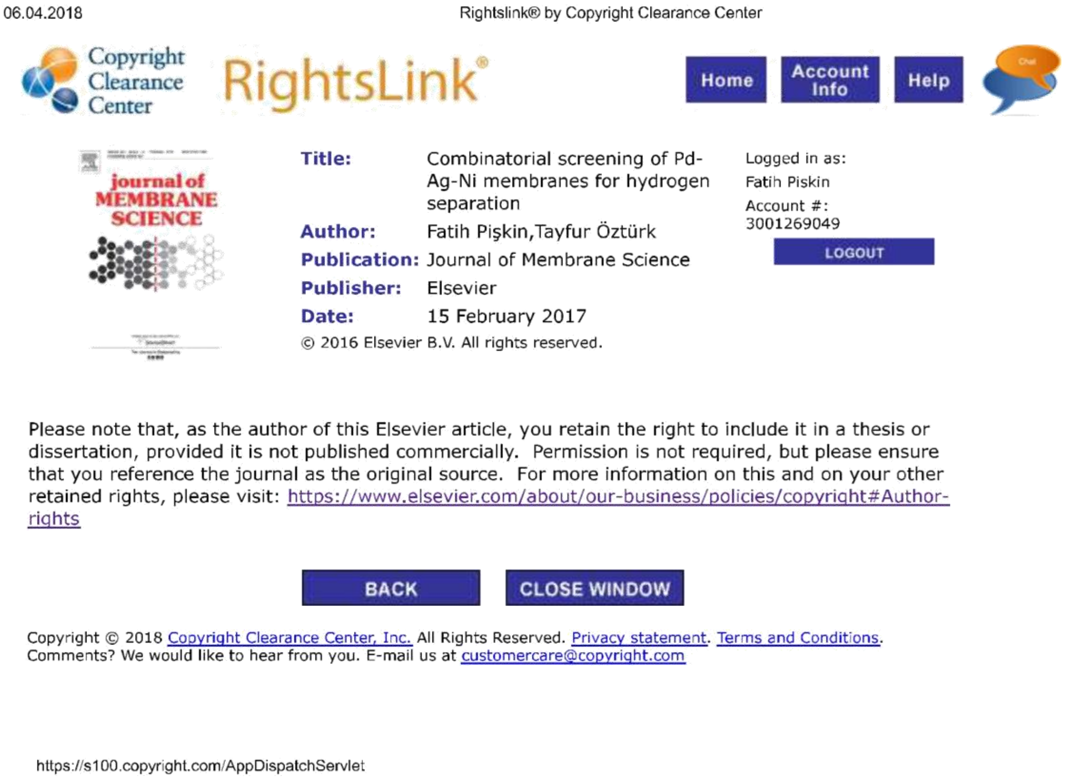

06.04.2018 Rightslink® by Copyright Clearance Center

Title:	Combinatorial screening of Pd-Ag-Ni membranes for hydrogen separation
Author:	Fatih Pişkin,Tayfur Öztürk
Publication:	Journal of Membrane Science
Publisher:	Elsevier
Date:	15 February 2017

© 2016 Elsevier B.V. All rights reserved.

Logged in as:
Fatih Piskin
Account #:
3001269049

Please note that, as the author of this Elsevier article, you retain the right to include it in a thesis or dissertation, provided it is not published commercially. Permission is not required, but please ensure that you reference the journal as the original source. For more information on this and on your other retained rights, please visit: https://www.elsevier.com/about/our-business/policies/copyright#Author-rights

Copyright © 2018 Copyright Clearance Center, Inc. All Rights Reserved. Privacy statement. Terms and Conditions.
Comments? We would like to hear from you. E-mail us at customercare@copyright.com

https://s100.copyright.com/AppDispatchServlet

CURRICULUM VITAE

PERSONAL INFORMATION

Surname, Name	: Pişkin, Fatih
Nationality	: Turkish (T.C.)
Date and Place of Birth	: 12 August 1985, Mersin
Marital Status	: Married
Phone	: +90 535-850 53 12
email	: fatihpiskin@mu.edu.tr

EDUCATION

Degree	**Institution**	**Year of Graduation**
M.Sc.	Middle East Technical University	2013
B.Sc.	Anadolu University	2009
High School	Mersin Tic. ve San. Odası Anatolian High School, Mersin	2003

WORK EXPERIENCE

Year	**Place**	**Enrollment**
2018-present	MSKU, Metallurgical and Materials Eng.	Research Assistant
2012-2018	METU, Metallurgical and Materials Eng.	Research Assistant
2016-2017	Massachusetts Institute of Technology (MIT), Nuclear Science and Eng.	Visiting Scholar
2011-2012	MSKU, Metallurgical and Materials Eng.	Research Assistant

PUBLICATIONS

F. Pişkin, R. Bliem, B. Yildiz, Effect of crystal orientation on the segregation of aliovalent dopants at the surface of $La_{0.6}Sr_{0.4}CoO_3$, *J. Mater. Chem. A.* (2018), submitted.

F. Pişkin, T. Öztürk, Nb-Pd-Ti BCC Thin Film for Hydrogen Separation: A Combinatorial Study, *ACS Combinatorial Science* (2018), submitted.

D. Sarı, **F. Pişkin**, Z. C. Torunoglu, B. Yasar, Y. Kalay, T. Öztürk, Combinatorial Development of $(La,Sr)CoO_3$-$(La,Sr)_2CoO_4$ Composite Cathodes for IT-SOFCs, *Solid State Ionics* (2018), submitted.

F. Pişkin, T. Öztürk, Combinatorial screening of Pd-Ag-Ni membranes for hydrogen separation, *J. Memb. Sci.* 524 (2017) 631-636. doi:10.1016/j.memsci.2016.11.066.

F. Pişkin, H. Akyıldız, T. Öztürk, Ti modified Pd-Ag membranes for hydrogen separation, *Int. J. Hydrogen Energy.* 40 (2015) 7553-7558. doi:10.1016/j.ijhydene.2014.11.049.